Doctoral Dissertation

博士論文

The search for fermionic thermal relic dark matter at future lepton colliders

(将来レプトン加速器におけるフェルミオン型熱的暗黒物質の探査に関する研究)

A Dissertation Submitted for the Degree of Doctor of Philosophy

December 2020

令和2年12月博士 (理学) 申請

Department of Physics, Graduate School of Science,

The University of Tokyo

東京大学大学院理学系研究科物理学専攻

Taisuke Katayose

片寄 泰佑

ABSTRACT

WIMP is one of the best dark matter (DM) candidates, and it is important to search WIMPs throughout various parameter space. We focused on standard model (SM) gauge singlet fermionic WIMP and figured out the role of future lepton colliders to search for such WIMPs. SM gauge singlet fermionic WIMP cannot have renormalizable interaction with SM particles, and we need mediator particles which connect WIMP and SM particles. We can separate the model by the properties of mediators, and there are several parameter regions which are difficult to search by LHC experiments or direct detection experiments, namely H-funnel region, Z-funnel region and Leptophilic region. H-funnel region is, however, almost searched by resent spin independent direct detection experiments (XENON 1T), and we just review about this region.

For Z-funnel region, the WIMP mass is almost half of Z-boson mass, and phenomenology is almost determined by dimension 6 operator $(\bar{\chi}\gamma^{\mu}\gamma_5\chi)(H^{\dagger}i\overleftrightarrow{D_{\mu}}H)$. There is small region remaining uncovered by spin dependent direct detection experiments. We discussed the detectability of Z-funnel WIMP by International Linear Collider (ILC) using mono-photon with missing energy process. Here the main back ground comes from the process of pair creation of neutrinos. ILC have the possibility to polarize electrons and positrons, and background can be reduced by setting electrons to be right-handed polarized, and positrons to be left-handed polarized. We also found that the effect of initial state radiation and beamsstrahlung are non-negligible, and we analyzed Z-funnel WIMP including these collider effects.

For Leptophilic region, WIMP mainly interact with SM leptons. We assumed Z_2 odd scalar mediator, which has same quantum numbers as sleptons. We also assumed lepton flavor universality for the coupling of WIMP, mediators and leptons. There are two types of mediators which couple with left-handed leptons and right-handed leptons. We analyzed left type mediators and right type mediators separately, and we found some parameter regions are detectable by future 250 GeV ILC using mono-photon signature. We also revealed that ILC detectable parameter region can explain $(g-2)_{\mu}$ anomaly by combining left and right type mediators.

Acknowledgements

First of all I would like to express my deep gratitude to my direct supervisor, Prof.Shigeki Matsumoto for teaching me about physics and taking care of my graduate course. He taught me a lot about the phenomenology of DM and new physics beyond SMs. I also would like to express my gratitude my supervisor, Prof.Hitoshi Murayama for concerning me at key points. I also would like to express my gratitude to Satoshi Shirai for teaching me the way to think physics and how to write papers. I would like to express my gratitude to Ipsita Saha, for helping me writing paper and having fruitful discussion. I would like to express my gratitude to Tomohiko Tanabe, for teaching me collider physics from the experimental aspect. I would like to express my gratitude to Shunichi Horigome for helping me with the parameter scanning. I would like to thank Asahi Kojima and Yu watanabe for having pleasant discussion. I would like to thank Yuko Enomoto for concerning me at important moment. Finally, I would like to express my heartfelt gratitude to my friends and family.

Contents

List of Figures

List of Tables

List of Acronyms

CDM	Cold Dark Matter
CEPC	Circular Electron Positron collider
CLIC	Compact Linear Collider
CMB	Cosmic Microwave Background
DM	Dark Matter
ISR	Initial State Radiation
LEP	Large Electron Positron Collider
LHC	Large Hadron Collider
NFW (profile)	Navarro-Frenk-White (profile)
SM	Standard Model
SUSY	Supersymmetry
WIMP	Weakly Interacting Massive Particle
VEV	Vacuum Expectation Value

Definition of notations

We use natural unit system as

$$c = \hbar = 1\,, \tag{1}$$

where c is the speed of light and $\hbar$ is Planck constant.

We define metric tensor as

$$g = \begin{pmatrix} 1 & 0 & 0 & 0 \\ 0 & -1 & 0 & 0 \\ 0 & 0 & -1 & 0 \\ 0 & 0 & 0 & -1 \end{pmatrix}\,. \tag{2}$$

Pauli matrices are

$$\sigma_1 = \begin{pmatrix} 0 & 1 \\ 1 & 0 \end{pmatrix} \tag{3}$$

$$\sigma_2 = \begin{pmatrix} 0 & -i \\ i & 0 \end{pmatrix} \tag{4}$$

$$\sigma_3 = \begin{pmatrix} 1 & 0 \\ 0 & -1 \end{pmatrix}\,. \tag{5}$$

Chapter 1

Introduction

Physicists have been making large effort to reveal the mysteries of universe, and we have gradually understood what the universe is made of. Our current understanding of universe is based on the standard model (SM) of particle physics, which is the chiral gauge theory and has $SU(3)_C \times SU(2)_L \times U(1)_Y$ gauge symmetry. The particle contents of SM were completed by the discovery of new 125 GeV Higgs like particle at CMS [2] and ATLAS [3] Collaborations at Large Hadron Collider (LHC) experiment. However, there are still unsolved problems remaining in particle physics, one of the most important problems is the dark matter (DM) problem.

DM is unknown gravity source in the universe and its existence is supported by various astrophysical observations and experiments. From the observation of cosmic microwave background (CMB) we have now understood that 27% of total energy of the universe is from DM, while ordinal matter (baryon) contribution is only 5% [4]. DM cannot be explained in the framework of SM and we need the extension of SM to explain DM problem. One of the most influential extension is supersymmetric theory (SUSY) [5], which impose the symmetry between fermion and boson. In SUSY, it is known that the lightest supersymmetric particle (LSP) becomes a stable particle because of R-parity, and it is one of the candidates of DM. The neutral components of supersymmetric partner of the electroweak gauge bosons and Higgs are called neutralino and it is a kind of so-called weakly interacting massive particles (WIMPs). WIMPs interact with SM particles in some degree and they are considered to have been in the thermal equilibrium with SM particles at the early hot universe. After a while, they become not able to maintain the equilibrium with SM particles because annihilation rate of DM becomes slower compared to the expansion rate of the universe, and some of them are left behind and remaining until today. DM created such mechanism is called thermal relic DM.

The relic abundance of WIMP can be calculated by solving Boltzmann equation, and we can predict the value of abundance with some extent of accuracy. If WIMP is interacting with SM particles at electroweak scale and the couplings are same order as that of SM, WIMP gives correct DM abundance observed today and it is called "WIMP miracle" [6]. New physics around electroweak scale is predicted by many models beyond SM in order to solve hierarchy problem [7],

and these facts make WIMPs more attractive candidates of DM.

The search for WIMP is largely divided in three types, which are direct detection experiments, indirect detection experiments and the collider experiments. At direct detection experiments, we search for local DM around the solar system using the detector placed at the underground, looking the scintillation caused by scattering of DM and nucleus. Indirect detection experiments are the search for DM in the galaxies, by looking for the cosmic ray emitted by the decay of DM or annihilation of DMs. Collider experiments are the search for new physics by colliding highly accelerated charged particles, represented by LHC experiments or Large Electron-Positron Collider (LEP) experiments. If the beam energy is larger than the mass of DM and interaction of DM and colliding particles is strong enough, we can create DM at the collider experiments. However, we cannot detect DM directly by the detectors, we must extract the information by looking at only SM particles. Now LHC experiments is ongoing, and the high luminosity upgrade is planned in near future. The next large collider experiments will be a lepton collider such as International Linear Collider (ILC) [8], Compact Linear Collider (CLIC) [9] or Circular Electron Positron Collider (CEPC) [10]. We will discuss the detectability of WIMP at these experiments, especially about the prospect from the future lepton colliders.

Many types of WIMP have been considered in the different contexts and models, such as SUSY, Kaluza–Klein theory [11] or little Higgs model [12]. In this thesis, we discuss the phenomenology of WIMP by model independent way, and focus on SM gauge singlet Majorana fermionic WIMP, which is represented by Bino in SUSY. Here we impose Z_2 symmetry on the model of SM+WIMP, as SM particles are Z_2 even and WIMP is Z_2 odd to make WIMP stable. If the additional particle is only SM gauge singlet Majorana fermionic WIMP, it cannot have renormalizable interaction with SM particles because of the gauge symmetry and Z_2 symmetry. Since WIMP must have some interactions with SM particles to maintain thermal equilibrium, we need other particles which couple with WIMP and SM particles. These particles are called mediators, and if the masses of mediator particles are heavy enough compared to electroweak scale and DM mass, we can integrate mediator fields out, and become able to discuss the phenomenology in the framework of effective field theory. The Lagrangian of effective field theory contains higher dimensional operator than mass dimension 5, and the analysis about the effective Lagrangian up to mass dimension 6 has been done in [13]. They have revealed that there are mainly 4 uncovered regions remaining, which are H-funnel region, Z-funnel region, Leptophilic region, and CP violating Higgs portal region. The former three regions conserve CP symmetry and we will focus on these CP conserving case. These regions are being classified by which annihilation channel works effectively in the early universe. At H-funnel region, the mass of DM is almost half of the mass of Higgs boson (125 GeV) and the annihilation cross section of WIMPs is largely enhanced because S-channel Higgs resonant process ($\chi\chi \to h \to XX$) works effectively. Here, χ is WIMP, h is SM Higgs and X is any SM particles. This resonant annihilation allows small coupling between WIMP and SM

particles, and it becomes difficult to search for such WIMP at direct detection because of the smallness of the coupling. At Z-funnel region, the mass of DM is almost half of the mass of Z boson (91 GeV), and the resonant annihilation via Z boson ($\chi\chi \to Z \to XX$) works effectively. It becomes also difficult to search this region by direct detection experiments for same reason. For Leptophilic region, the DM annihilation into two SM lepton pair ($\chi\chi \to \ell\bar{\ell}$) works most effectively at the early universe. Therefore, direct detection experiments do not work effectively because WIMP has little interaction with nucleus (quarks). In this thesis, we will discuss the future prospect for these regions, especially the prospect of future lepton colliders.

The structure of this thesis is as follows. In chapter 2 we will show the existence of DM and some properties of DM which we know currently. Next we will briefly review standard cosmology and thermal history of WIMP at chapter 3 and chapter 4. In chapter 5, we will introduce the principles and techniques of direct detection experiments, indirect detection experiments and collider experiments. In chapter 6, we will introduce effective field theory of SM gauge singlet Majorana fermionic WIMP and show current exclusion and surviving region by various experiments. In chapter 7, we will review previous studies about Higgs portal WIMP including H-funnel region. In chapter 8, we will discuss the detectability of Z-funnel WIMP based on actual performance of the future lepton colliders. In chapter 9, we will introduce specific mediators for Leptophilic WIMP and discuss future prospects and other physical implications including muon $(g-2)$. Finally in chapter 10, we will summarize our result from the analysis of Z-funnel WIMP and Leptophilic WIMP. The author contributed to the whole analysis of Z-funnel WIMP and Leptophilic WIMP.

Chapter 2

Dark matter

The DM has been suggested by many gravitational observations and experiments. The structure of this chapter is as follows. In Sec. 2.1, we will review some of important observations which suggest DM. In Sec. 2.2, we will show current knowledge about DM.

2.1 Existence of DM

The existence of DM is established by many observations of baryonic object which interact with DM thorough gravity. DM was firstly hypothesized in the late 19th century from the observation of the stars in the Milky Way [14], in order to explain the difference between mass of the galaxy which is estimated by the velocity dispersion of the stars in the galaxy and the mass of visible stars in the galaxy. Later, Jacobus Kapteyn and Jan Oort also suggested the existence of the DM by the observation of stellar motions in the local galactic neighborhood, here they found hidden gravity source in the galactic plane. In the following of this section we will review some important techniques and observations to prove the existence of DM.

2.1.1 Galaxy rotation curve

We can estimate the mass of galaxy in two ways. One way is using photonic observation of the object in the galaxy, and we can obtain the information of the mass of the object by applying the relationship between mass and luminosity. The second way is using the kinematics of the stellar object in the galaxy. When we accumulate the data of the velocity and position of the stellar objects, we can apply the Virial theorem to them, and we can estimate the amount of gravity source. If there is discrepancy between these two values, we can conclude that there is invisible gravity source, or DM. We show a plot for the relation between the distance of the stars from the galactic center and the velocity of them in Figure 2.1. Black dot is the observed data of stars, and there is discrepancy from the expected rotation curve only from the visible object (which is mentioned as Disk in the figure). Thus, we need another gravitational source to explain this,

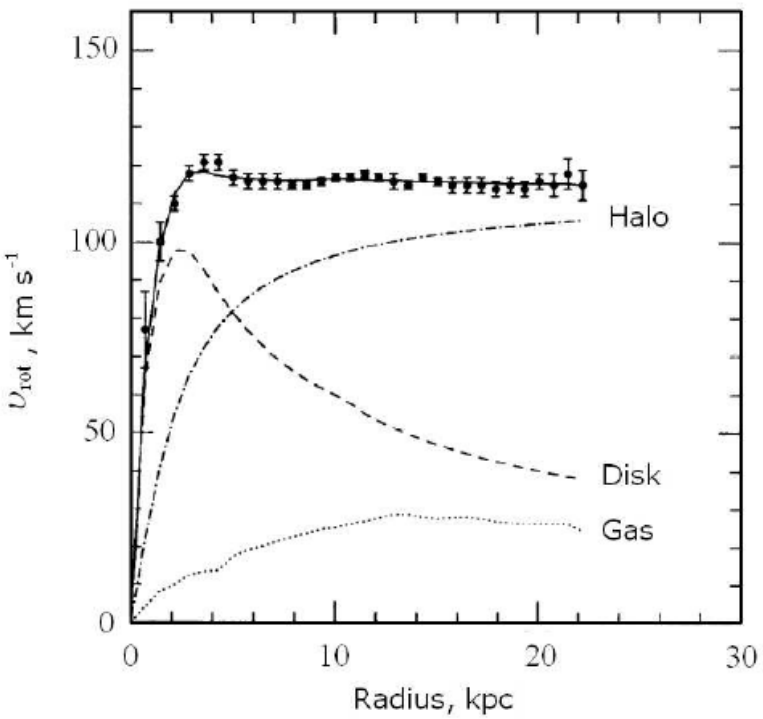

Figure 2.1: *Galactic rotation curve for NGC 6503 showing disk and gas contribution plus DM halo contribution needed to match the data. The figure is cited from [15].*

and we can conclude that there is DM halo in the galaxy.

2.1.2 Gravitational lensing

Einstein's general theory of relativity predict that the gravitational potential can bend the light, and this can be observed by gravitational lensing. Gravitational lensing is the effect that the image of the far stellar object is distorted or multiplied by the foreground massive object, and this is firstly reported as twin images of one quasar in 1979 [16]. This effect becomes stronger when the foreground object becomes more massive, thus we can estimate the mass of the object from the amount of the effect of gravitational lensing. Moreover, physicists are able to deduce the distribution on DM by accumulating the more images of gravitational lensing and analyzing them [17].

2.1.3 Cosmic microwave background

Cosmic microwave background (CMB) is the electromagnetic microwave radiation which is observed homogeneously and isotropic in the universe. This is considered as the remnant of early hot universe, and strong evidence of Big Bang cosmology [18]. Although CMB is almost homogeneous and isotropic, there is small fluctuation of the CMB [19] and Figure 2.2 shows the optical image of the fluctuation of the CMB.

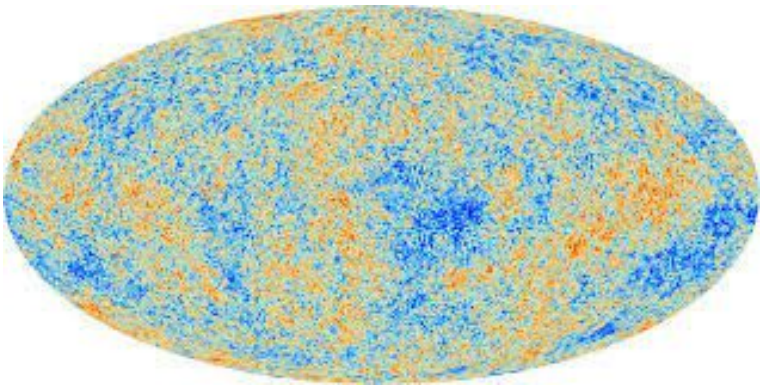

Figure 2.2: *All-sky map of the fluctuation of the CMB, created from 9 years of WMAP data [20]*

Though DM does not interact with photon because it has no electric charge, DM can modify the shape of CMB fluctuation by its gravitational potential. This fluctuation can be theoretically predicted by applying Λ-CDM model (c.f. Subsec. 2.2.2), and we can extract the information from the observation of the CMB using the expansion by spherical harmonics function. Figure 2.3 shows the best fit by ΛCDM model using these techniques and they obtained $\Omega_c h^2 = 0.120 \pm 0.001$ and $\Omega_b h^2 = 0.0224 \pm 0.0001$, where Ω_c is the ratio between the DM density and critical density of the universe, Ω_b is that of baryon density, and h is the scale factor of Hubble expansion rate.

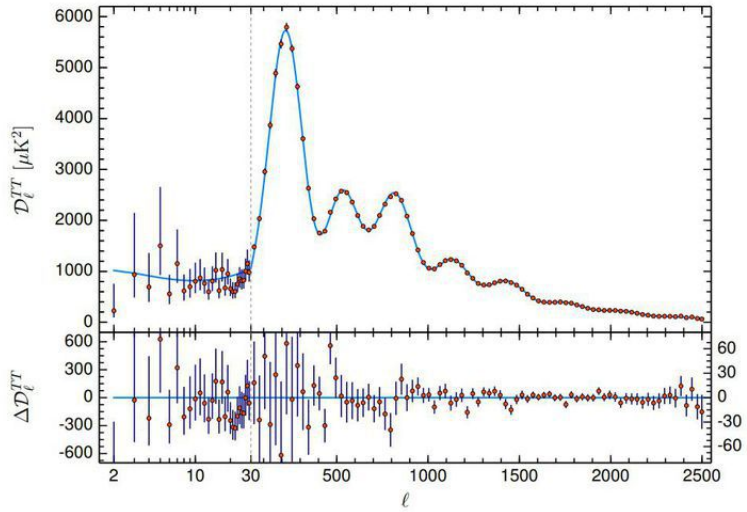

Figure 2.3: *Temperature power spectrum from Planck 2018 [4]. ℓ is the eigenvalue of spherical harmonics function. Blue line is the best fit from the theoretical prediction by Λ-CDM, and red point is the observed data with $\pm 1\sigma$ uncertainty.*

2.1.4 Structure formation

The temperature of the universe gradually decreased after the Big Bang and nucleosynthesis, and particles were gathered by their gravitational potential.

This leads to the formation of stars, galaxies, and cluster of galaxies. From n-body simulation result [21], only baryonic object cannot assemble by themselves because their gravity is weak, and we need to introduce DM to make additional gravity potential. Also, there arose new problems called small scale problems from this simulation. These problems point that there is discrepancy between the actual observation of the distribution of DM and the distribution obtained from the simulation. We do not have clear answer to this problem, and this can be derived from the nature of DM or the effect of the interaction between baryon.

2.2 Properties of DM

We have shown that many observations suggest the existence of DM. However, the knowledge about the properties of DM is very limited. We will review about a few things which we know about DM currently.

2.2.1 Darkness of DM

It is difficult to detect DM as mentioned "Dark" in its name. The constraint on the electromagnetic charge of the DM for GeV region is [22]

$$q_\chi < 10^{-4} \left(\frac{m_{\rm DM}}{\rm TeV} \right)^{1/2} , \tag{2.1}$$

where q_χ denotes DM charge and $m_{\rm DM}$ denotes DM mass. This is so small that we can assume that DM is neutral, moreover there might be the new physics which quantize electromagnetic charge such as Grand Unified Theory [23]. DM also does not have SM $SU(3)_C$ interaction, but can have $SU(2)_L$ interaction. Such DM with weak charge is one of the most motivated DM candidates (c.f. chapter 4).

2.2.2 Coldness of DM

DM is necessary for the structure formation of the universe, and DM have to be non-relativistic because it is trapped in the gravitational potential in the galaxy. The CMB observations also support cold DM in order to make small fluctuation. Λ-CDM model is the cosmology model which contain cold DM (CDM) and cosmological constant (Λ), and this is generally accepted model currently.

2.2.3 Stability of DM

The DM has been existing from the early stage of the universe until today. This means that DM is stable or has very long lifetime at least more than 13 Gyrs. In particle physics, the stability of the particle is often due to the

symmetries, and some DM candidates are protected by Z_2 symmetry (c.f. R-parity in Supersymmetric model, K-parity in Kaluza-Klein model [24])

2.2.4 Mass of DM

Although We do not have a clear information about DM mass, we have lower bound and upper bound for the mass as

$$10^{-22}\mathrm{eV} < m_{\mathrm{DM}} < M_{\mathrm{gal}}\,, \tag{2.2}$$

where M_{gal} is the mass of galaxy. The lower bound comes from the condition that the de Broglie wave length of DM must be shorter than the scale of galaxy, and this is given as

$$\frac{2\pi}{m_{\mathrm{DM}}v} < \mathcal{O}(100)\,\mathrm{pc}\,, \tag{2.3}$$

where v is the velocity of DM in the galaxy, which is estimated around 10^{-3} using Virial theorem.

Chapter 3

Standard cosmology

We refer to Ref. [25] in this chapter. To make large scale structure, DM is necessary components of the universe, and this fact assures that DM has been existing from the early stage of the universe. The evolution of the universe is closely related to the history of DM, and the knowledge of cosmology is necessary to understand the nature of DM. We will briefly review the basics of cosmology and the thermal history of the universe in this section.

3.1 Friedmann equation

The cosmological principle states that the universe is isotropic and homogeneous, and the Friedmann equation is derived from this principle using Einstein equations. Let us define the scale factor $a(t)$ as in the Robertson-Walker metric:

$$ds^2 = dt^2 - a^2(t)\left(\frac{1}{1-kr^2}dr^2 + r^2 d\theta^2 + r^2\sin^2\theta d\phi^2\right), \tag{3.1}$$

where k is the gaussian curvature of the space and takes (-1, 0, 1), and they correspond to open, flat, and closed universe respectively. Then the Friedmann equation is

$$\left(\frac{\dot{a}}{a}\right)^2 + \frac{k}{a^2} = \frac{8\pi G\rho}{3}, \tag{3.2}$$

where G is Newton's gravitational constant, ρ is mass density of universe and we denote $a(t)$ as a. The value of ρ which gives the curvature to be zero is called critical energy density, and it is given as

$$\rho_c = \frac{3H^2}{8\pi G}, \tag{3.3}$$

where $H \equiv \dot{a}/a$ is the Hubble parameter. Current observation gives $H_0 = 100\,h\,\mathrm{km\,s^{-1}\,Mpc^{-1}}$ where $h = 0.678(9)$ [26], and the index 0 indicates present value of the quantity.

The corresponding critical density is $\rho_c = 1.878 \times 10^{-29}\, h^2\, \mathrm{g\,cm^{-3}}$. Physicist usually use the ratio of the energy density of the species compared to this critical density as follows:

$$\Omega_i = \frac{\rho_i}{\rho_c}\,, \tag{3.4}$$

where i denotes each species (e.g. baryon, radiation, and DM).

3.2 Matter and radiation

From Friedmann equation we can derive the useful equation:

$$\frac{d\rho}{dt} + 3H(p+\rho) = 0\,, \tag{3.5}$$

where p is the pressure from the species. When the species in non-relativistic we can neglect the pressure compared to the energy density. Such species is called matter, and the energy density of matter scales as

$$\rho_m \simeq a^{-3}\,. \tag{3.6}$$

The mass less particle or very relativistic particle has the finite pressure as $p = \rho/3$. Such species is called radiation, and the energy density scale as

$$\rho_r \simeq a^{-4}\,. \tag{3.7}$$

These equations suggest that the early universe was firstly dominated by the radiation when $a \ll a_0$, and later dominated by matter. In the limit of matter dominant universe and $k = 0$, by using eq.(3.2) and eq.(3.6), we get

$$a(t) \simeq t^{2/3} \tag{3.8}$$

$$\rho_m = \frac{1}{6\pi G t^2}\,. \tag{3.9}$$

In the limit of radiation dominant universe and $k = 0$, by using eq.(3.2) and eq.(3.7), we get

$$a(t) \simeq t^{1/2} \tag{3.10}$$

$$\rho_r = \frac{3}{32\pi G t^2}\,. \tag{3.11}$$

3.3 Thermal equilibrium

In the present universe, the radiation, or relativistic particles, consists of photon and 3 neutrinos whose temperature are 2.75 K and 1.96 K respectively. In the early universe, the temperature of the particles is much higher than today, and other particles can be relativistic. When particles have some interaction each other, we can assume particles are in the thermal equilibrium. The number

density n, energy density ρ, and the pressure p of these particles can be given by the function of temperature T as

$$n = \begin{cases} \frac{\zeta(3)}{\pi^2} g T^3 & \text{(boson)} \\ \frac{3\zeta(3)}{4\pi^2} g T^3 & \text{(fermion)} \end{cases} \tag{3.12}$$

$$\rho = \begin{cases} \frac{\pi^2}{30} g T^4 & \text{(boson)} \\ \frac{7\pi^2}{240} g T^4 & \text{(fermion)} \end{cases} \tag{3.13}$$

$$p = \frac{\rho}{3}, \tag{3.14}$$

where $\zeta(3) = 1.20206\ldots$ is the Riemann zeta function of three, g is internal degrees of freedom, when T is much larger than mass of the particles ($T \gg m$). In the non-relativistic limit ($m \gg T$), the same values are given as

$$n = g\left(\frac{mT}{2\pi}\right)^{3/2} \exp\left[-\frac{m-\mu}{T}\right] \tag{3.15}$$

$$\rho = mn \tag{3.16}$$

$$p = nT, \tag{3.17}$$

where m is the mass of particle and μ is the chemical potential of the particle. It is good approximation to consider only relativistic particles because the energy density and pressure of non-relativistic particles are exponentially suppressed compared to that of relativistic particles. We can write the total energy density of the relativistic particles (ρ_r) and the total pressure of the relativistic particles (p_r) as follows:

$$\rho_r = \frac{\pi^2}{30} g_* T_\gamma^4 \tag{3.18}$$

$$p_r = \frac{\pi^2}{90} g_* T_\gamma^4, \tag{3.19}$$

where T_γ is the temperature of photon and g_* is the total number of effective degrees of freedom for relativistic particles ($m_i \ll T_\gamma$), and

$$g_* = \sum_{i=\text{bosons}} g_i \left(\frac{T_i}{T_\gamma}\right)^4 + \frac{7}{8} \sum_{i=\text{fermions}} g_i \left(\frac{T_i}{T_\gamma}\right)^4, \tag{3.20}$$

where subscript i denotes each species of particle. The time evolution of g_* is shown in Figure 3.1.

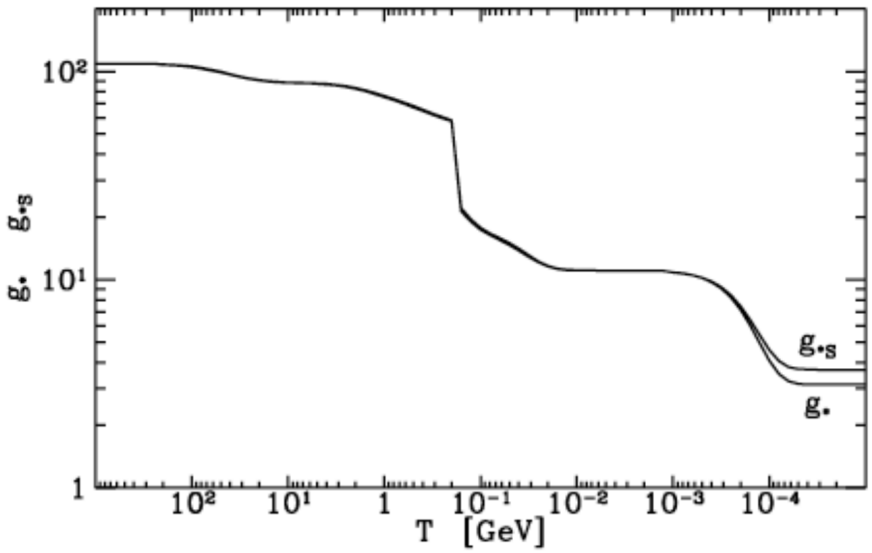

Figure 3.1: *The evolution of g_* as the function of temperature in particle SM. The figure is cited from [25]*

In the early universe, the reaction rates of the particles in the thermal bath were much greater than the expansion rate of the universe, or H, and local thermal equilibrium was maintained. In this case we can prove that entropy per unit comoving volume (S) is conserved from the thermodynamics. The proof is following. Applying the second law of thermodynamics to the unit comoving volume, we get

$$TdS = d(\rho V) + pdV = d[(\rho + p)V] - Vdp\,, \tag{3.21}$$

where V denotes physical volume. Then, the integrability condition,

$$\frac{\partial^2 S}{\partial T \partial V} = \frac{\partial^2 S}{\partial V \partial T}\,, \tag{3.22}$$

lead to the relation of temperature, energy density and pressure,

$$dp = \frac{\rho + p}{T} dT\,. \tag{3.23}$$

Using eq.(3.21) and eq.(3.23), we find

$$dS = \frac{1}{T} - d[(\rho + p)V] - (\rho + p)V\frac{dT}{T^2} = d\left[\frac{(\rho + p)}{T} + \text{const}\right]\,. \tag{3.24}$$

Then using the energy conservation law, we get

$$d[(\rho + p)V] = Vdp\,. \tag{3.25}$$

From eq.(3.23), we can conclude

$$d\left[\frac{(\rho + p)V}{T}\right] = 0\,. \tag{3.26}$$

This result mean that the entropy per comoving volume is conserved. It is useful to define the entropy density s as

$$s \equiv \frac{S}{V}, \tag{3.27}$$

where V denote the physical volume. As already mentioned it is good approximation to consider only relativistic particles, then we get

$$s = \frac{2\pi^2}{45} g_{*s} T_\gamma^3, \tag{3.28}$$

where

$$g_{*s} = \sum_{i=\text{bosons}} g_i \left(\frac{T_i}{T_\gamma}\right)^3 + \frac{7}{8} \sum_{i=\text{fermions}} g_i \left(\frac{T_i}{T_\gamma}\right)^3. \tag{3.29}$$

The evolution of g_{*s} is also shown in Figure 3.1. In the very early universe, the temperature of all particles are common because they were in same thermal bath, and we can replace g_{*s} to g_*. The conservation of S implies $s \propto a^{-3}$, and we define the number of some species in a comoving volume by $Y \equiv n/s$, where n is number density of that species.

Chapter 4

Thermal DM

Thermal DM, often called as WIMP (weakly interacting massive particle), is one of the best motivated DM candidates. WIMP hypothesis is that DM is in the thermal equilibrium with SM particles in the early universe and some WIMP remained until today through freeze out mechanism. In this chapter, we will review the Boltzmann equation from which we can calculate the number density of WIMP. Then we will show the solution of Boltzmann equation.

4.1 Freeze out of WIMP

Let us denote WIMP field as χ, WIMP mass as m_χ and any SM particles as X. When thermal equilibrium was accomplished, the inelastic scattering ($\chi\chi \leftrightarrow XX$) and elastic scattering ($\chi X \to \chi X$) should have happened faster enough than Hubble expansion rate (we show the illustration of these process in Figure 4.1). When ($\chi\chi \leftrightarrow XX$) process works effectively in the thermal equilibrium, the WIMP constantly repeat pair creation and annihilation. For ($\chi\chi \to XX$) process, the annihilation rate can be expressed as

$$\Gamma_{\text{inelastic}} = n_\chi \langle \sigma v \rangle \,, \tag{4.1}$$

where n_χ is the number density of WIMP, and $\langle \sigma v \rangle$ is the thermal averaged cross section. n_χ denpend on temperature as $n_\chi \propto T^{3/2} \exp[-m_\chi/T]$ (c.f. eq 3.15) and $\Gamma_{\text{inelastic}}$ can be same order or lower than Hubble expansion rate H as temperature goes down. At this moment, this annihilation process does not occur effectively, and the number of the WIMP is almost fixed. This is called freeze out of WIMP and the temperature at which freeze out occur is called freeze out temperature. As the freeze out temperature is much lower than WIMP mass, we do not need to consider about creation process of WIMP ($XX \to \chi\chi$). On the other hand, the elastic interaction ($\chi X \to \chi X$) rate is expressed as

$$\Gamma_{\text{elastic}} = n_X \langle \sigma v \rangle \,, \tag{4.2}$$

where n_X is the number density of SM particle X, and $n_X \propto T^3$ (c.f. eq 3.12) because SM particles are light and relativistic at freeze out temperature. Then

Γ_{elastic} can be enough larger than Hubble expansion rate and the temperature of WIMP maintained same as that of SM particles.

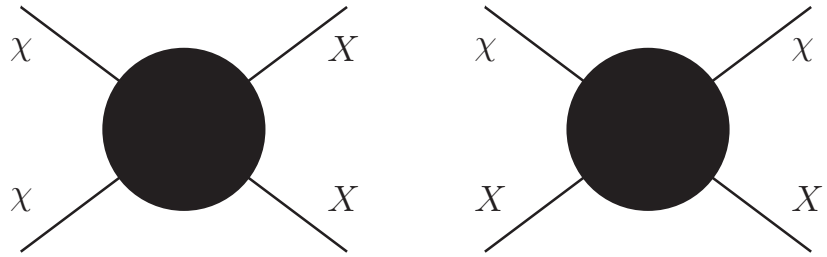

Figure 4.1: *An illustration of inelastic (left) and elastic (right) scattering. The time flows from left to right.*

4.2 Boltzmann equation

In this section we refer to the discussions in Ref. [27]. In order to follow the time evolution of the number density of WIMP, we need to solve Boltzmann equation for WIMP. The general Boltzmann equation can be written in the form as follows:

$$L[f(x,\vec{p})] = C[f(x,\vec{p})]\,, \tag{4.3}$$

where L is Liouville operator, C is collision operator which describes the interaction of the particles, and $f(x,\vec{p})$ is the phase space density of WIMP which is the function of four dimensional coordinate x and momentum $\vec{p}$. Considering that the universe is isotropic and homogeneous, $f(x,\vec{p})$ becomes the function of only two variables; energy of the particle E and time t. Then the number density of WIMP is given as

$$n_\chi \;=\; g\int f(E,t)\frac{d^3p}{(2\pi)^3}\,, \tag{4.4}$$

where g is inner degrees of freedom of WIMP. The time evolution of the number density of WIMP occurs in the expanding universe, and we need to consider covariant form of Liouville operator,

$$L[f(E,t)] \;=\; E\frac{\partial f(E,t)}{\partial t} - H|\vec{p}|^2\frac{\partial f(E,t)}{\partial E}\,, \tag{4.5}$$

where H is Hubble expansion rate. Using this equation and eq.(4.4), we get

$$g\int\frac{L[f(E,t)]}{E}\frac{d^3p}{(2\pi)^3} = \frac{dn_\chi}{dt} + 3Hn_\chi = \frac{1}{a^3}\frac{d}{dt}(n_\chi a^3)\,. \tag{4.6}$$

When there is no collision term, $C[f] = L[f] = 0$, and this means n_χ stays constant in time. The collision term includes many processes, let us consider

the process $(1+2 \leftrightarrow 3+4)$, where (1,2,3,4) denote the species of particles. The collision term is given as

$$\begin{aligned} g\int \frac{C[f]}{E}\frac{d^3p}{(2\pi)^3} &= -\int \frac{d^3p_1}{(2\pi)^3 2E_1}\int \frac{d^3p_2}{(2\pi)^3 2E_2}\int \frac{d^3p_3}{(2\pi)^3 2E_3}\int \frac{d^3p_4}{(2\pi)^3 2E_4} \\ &\times (2\pi)^4\delta^3(p_1+p_2-p_3-p_4)\delta(E_1+E_2-E_3-E_4) \\ &\times [f_1 f_2(1\pm f_3)(1\pm f_4)|\mathcal{M}_{12\to 34}|^2 \\ &\quad -f_3 f_4(1\pm f_1)(1\pm f_2)|\mathcal{M}_{34\to 12}|^2]\,, \end{aligned} \tag{4.7}$$

where $\mathcal{M}$ is the amplitude of each process and $(1 \pm f)$ represent Pauli blocking for fermions, Bose enhancement for bosons. Assuming $T \ll E - \mu$ phase space distribution f follows Maxwell-Boltzmann distribution, and f becomes so small that we can set $(1 + f) = 1$. Then this equation becomes easier form as

$$g\int \frac{C[f]}{E}\frac{d^3p}{(2\pi)^3} = -\langle\sigma v\rangle_{12\to 34} n_1 n_2 + \langle\sigma v\rangle_{34\to 12} n_3 n_4\,, \tag{4.8}$$

where $\langle\sigma v\rangle$ is thermal averaged cross section for each process. Let us assume particles (1, 2) are WIMP, and particles (3, 4) are SM particles. Then n_3 and n_4 are maintained in thermal equilibrium and

$$\langle\sigma v\rangle_{34\to\chi\chi} n_3 n_4 = \langle\sigma v\rangle_{34\to\chi\chi} n_3^{\rm eq} n_4^{\rm eq} = \langle\sigma v\rangle_{\chi\chi\to 34}(n_\chi^{\rm eq})^2\,, \tag{4.9}$$

where the subscription $n^{\rm eq}$ denote the number density of the particle in the thermal equilibrium with the temperature of SM particles. Using equations (4.3), (4.6), (4.8) and (4.9), we get the Boltzmann equation for WIMP as

$$\frac{dn}{dt} + 3Hn = \langle\sigma v\rangle(n_{\rm eq}^2 - n^2) \tag{4.10}$$

where we omitted the subscription χ for n and $\langle\sigma v\rangle$ is the thermal averaged annihilation cross section of $\chi\chi \to XX$ where X is any of SM particles. It is useful to rewrite the equation using $Y = n/s$ (c.f. Sec. 3.3) and $x = m_\chi/T$ instead of n and t, then we find

$$\frac{dY}{dx} = \frac{s\langle\sigma v\rangle}{xH(x)}(Y_{\rm eq}^2 - Y^2)\,. \tag{4.11}$$

4.3 Solution for Boltzmann equation

Let us consider the time evolution of the number density of WIMP which follows eq.(4.10). When $\langle\sigma v\rangle n_{\rm eq} \gg H$, the right side of the equation dominate the term $3Hn$, and the time evolution is almost determined by $\langle\sigma v\rangle(n_{\rm eq}^2 - n^2)$. Suppose that n is more than $n_{\rm eq}$, then right side become negative and the number density decrease and finally $n \simeq n_{\rm eq}$ achieved. Similarly, for the case when n is less than $n_{\rm eq}$, $n \simeq n_{\rm eq}$ achieved. These processes proceed very rapidly, and that means the Boltzmann equation is stable and it does not depend on the initial condition of the number density of WIMP. Next, when $\langle\sigma v\rangle n_{\rm eq} \ll H$, WIMP decouples from

the thermal bath of SM particles (freeze out), and the number density decrease according to the expansion of the universe. Thus, WIMP has been remaining until today, and it is called relic density. We show the numerical solution of Boltzmann equation in Figure 4.2 in the plane of x and Y, here the solid line represents the case that WIMP is in the thermal equilibrium, and dotted lines represent the decoupling of the WIMP from the thermal equilibrium. If $\langle \sigma v \rangle$ get larger, WIMP remains in the thermal equilibrium longer, and the relic density will decrease.

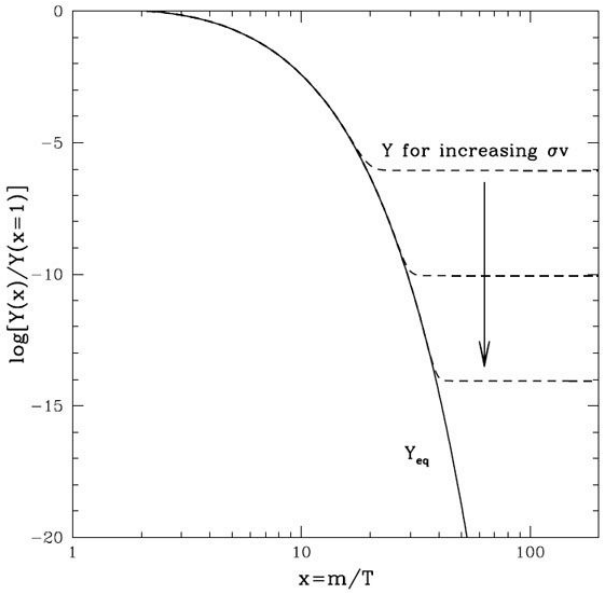

Figure 4.2: *Numerical solution for the Boltzmann equation. Solid line represent the time evolution in thermal equilibrium, dotted lines represent after freeze out. The figure is cited from [25].*

Then let us estimate relic abundance. Y decreases exponentially before freeze-out. After freeze-out, the abundance can be written as

$$\frac{dY}{dx} \simeq -\frac{\lambda}{x^{-n+2}}\,, \tag{4.12}$$

where

$$\lambda = \frac{\langle \sigma v \rangle_0 s_0}{x^2 H(x)} \tag{4.13}$$

and we assume $\langle \sigma v \rangle = \langle \sigma v \rangle_0 x^{-n}$ and $s = s_0 x^{-3}$ here. If we take $n = 0$ as an example, the DM abundance can be solved as

$$Y_{\rm today} \simeq \frac{x_f}{\lambda}\,, \tag{4.14}$$

where the subscript 'today' denotes the current value. From this equation and the relation

$$\Omega = \frac{m s_{\rm today} Y_{\rm today}}{\rho_{\rm c}}\,, \tag{4.15}$$

we get

$$\Omega h^2 \simeq \frac{10^{-26}\mathrm{cm}^3/\mathrm{s}}{\langle \sigma v \rangle} \,. \tag{4.16}$$

Consequently, the typical cross section of weak scale $\langle \sigma v \rangle \sim 10^{-26}\mathrm{cm}^3\mathrm{s}^{-1}$ explains observed DM density, and it is known as "WIMP miracle".

Chapter 5

Detection of WIMP DM

The WIMP is well motivated DM, and physicists have been making large effort to search for such particles. It is difficult to search WIMP optically because WIMP does not have electric charge. However, WIMP at least has certain amount of interaction with SM particles because WIMP was in thermal equilibrium with SM particles, and we can use this interaction to detect them. Suppose that X is SM particles, we use $(\chi X \to \chi X)$ process at direct detection experiments, $(\chi\chi \to XX)$ process at indirect detection experiments, and $(XX \to \chi\chi)$ process at collider experiments. We show this situation as an illustration in Figure 5.1. We will review the principle of each experiment in the following section.

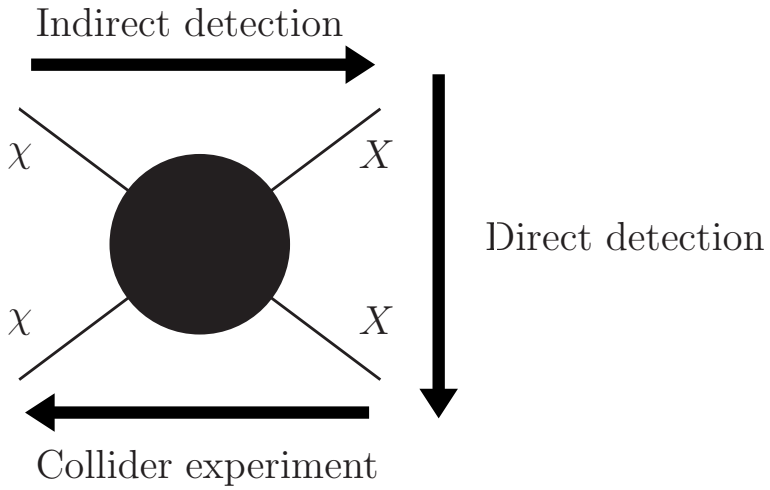

Figure 5.1: *The illustration of the relation between the interaction and each experiment.*

5.1 Direct detection

Direct detection is one of the most effective detection of DM, and in this experiment, we search for the WIMP at laboratory by looking the recoil of the

nucleus and DM. The laboratory is usually located in the underground to avoid the effect from cosmic ray, and it detect the DM which is moving in the Milky Way. We will see the kinematics of the direct detection in the following.

5.1.1 Recoil of DM and nucleus

The recoil energy of the nucleus is given as

$$E_R = \frac{(m_\chi v)^2}{2m_N} \simeq 50\text{keV}\left(\frac{m_\chi}{100\text{GeV}}\right)^2\left(\frac{100\text{GeV}}{m_N}\right), \tag{5.1}$$

where m_N is the mass of nucleus, n_χ is the density of dark matter and $v \simeq 10^{-3}$ is the velocity of DM around the earth. DM is almost collision less in the Milky Way and we can determine the velocity of DM using Virial theorem. The LUX experiment [28] or XENON experiment [29] use xenon for the nucleus and $m_N \simeq 100\text{GeV}$ and the detectable energy threshold is few keV. Therefore the threshold for m_χ becomes around 10 GeV.

5.1.2 Scattering rate

When considering the detectability of DM, the scattering rate is also important quantity. The differential scattering rate for recoil energy per unit detector mass is given as follows:

$$\frac{dR}{dE_R} = \frac{n_\chi}{m_N}\int dv^3 v f_{\text{lab}}(\vec{v})\frac{d\sigma}{dE_R}, \tag{5.2}$$

where $\vec{v}$ is the velocity of DM and $f_{\text{lab}}(\vec{v})$ is the distribution function of DM by the velocity from the rest system at the laboratory. We can calculate $f_{\text{lab}}(\vec{v})$ as

$$f_{\text{lab}}(\vec{v}) = f(\vec{v}+\vec{v}_{\text{lab}}), \tag{5.3}$$

where $f(\vec{v})$ is the distribution function of DM at rest system of the Milky Way, and $\vec{v}_{\text{lab}}$ is the velocity of the earth in the Milky Way. There also direct detection experiments to search for annual modulation by $\vec{v}_{\text{lab}}$ such as DAMA experiment [30].

5.1.3 Scattering cross section

The differential cross section can be separated in two part as follows

$$\frac{d\sigma}{dE_R} = \frac{d\sigma_{\text{SD}}}{dE_R}, + \frac{d\sigma_{\text{SI}}}{dE_R} \tag{5.4}$$

where σ_{SD} is the spin dependent cross section and σ_{SI} is the spin independent cross section. We will easily review these two types of cross section, which is important for the implication of particle physics. Let us consider the effective Lagrangian of axial vector coupling between DM and quarks as

$$\mathcal{L}_{\text{axial}} = d_q^A \bar{\chi}\gamma^\mu\gamma_5\chi\bar{q}\gamma_\mu\gamma_5 q, \tag{5.5}$$

where d_q^A is the coupling for axial vector interaction, χ is fermionic DM field and q is the SM quark field. To calculate the matrix element for the elastic scattering of DM and nucleus, let us start from calculating the matrix element of the quark axial vector current in nucleon. It is given as

$$\langle n|\bar{q}\gamma_\mu\gamma_5 q|n\rangle \;=\; 2s_\mu^n \Delta q^n \,, \tag{5.6}$$

where n denotes a proton or neutron, s_μ^n is the spin of nucleon and Δq^n is the quantity extracted by experiments. Then we can write the effective interaction of DM and nucleons as

$$\mathcal{L}_{\text{axial}} \;=\; \bar{\chi}\gamma^\mu\gamma_5\chi\bar{n}s_\mu n \sum_{q=u,d,s} 2d_q^A \Delta q^n \,, \tag{5.7}$$

where we summed only for light quarks. For the DM with $v \sim 10^{-3}$ and $m_\chi \sim 100\,\text{GeV}$, the de Broglie wave length is longer than the radius of nucleus, and this operator acts on the state of nucleus coherently. Therefore, the scattering cross section of the DM and nucleus depends on the total spin of the nucleus, and it is called spin dependent interaction. Then let us consider scalar type interaction as

$$\mathcal{L}_{\text{scalar}} = f_q \bar{\chi}\chi\bar{q}q \,. \tag{5.8}$$

Then the matrix element of the current of light quarks in nucleon is

$$\langle n|\bar{q}q|n\rangle \;=\; \frac{m_n}{m_q} f_{Tq}^n \,, \tag{5.9}$$

where f_{Tq} is also the parameter determined by experiments. Thus we get the effective operator for nucleon as

$$\mathcal{L}_{\text{scalar}} = \bar{\chi}\chi\bar{n}n \sum_{q=u,d,s} \frac{m_n}{m_q} f_{Tq}^n \,. \tag{5.10}$$

This operator works as a number operator of the nucleon in the nucleus, and the cross section is enhanced by the factor $\sim A^2$ where A is atomic mass number of the nucleus. This is called spin independent interaction, and this put stronger constraint than spin dependent one, because of the enhancement by A. We show the result of Xenon 1T experiment for spin independent case [31] in Figure 5.2 and spin dependent case [32] in Figure 5.3. These are shown in the plane of DM mass m_χ and the cross section of DM and nucleon.

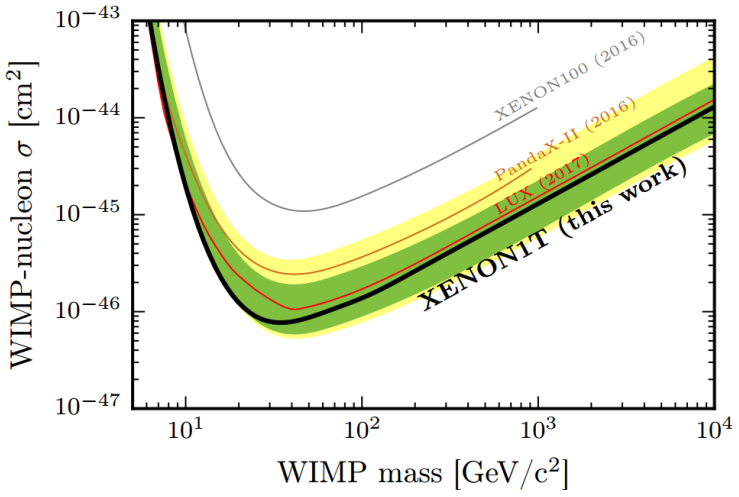

Figure 5.2: *The constraints for the cross section of WIMP and nucleon at spin independent interaction. 2σ and 1σ contours are shown in yellow and green respectively. The figure is cited from [31].*

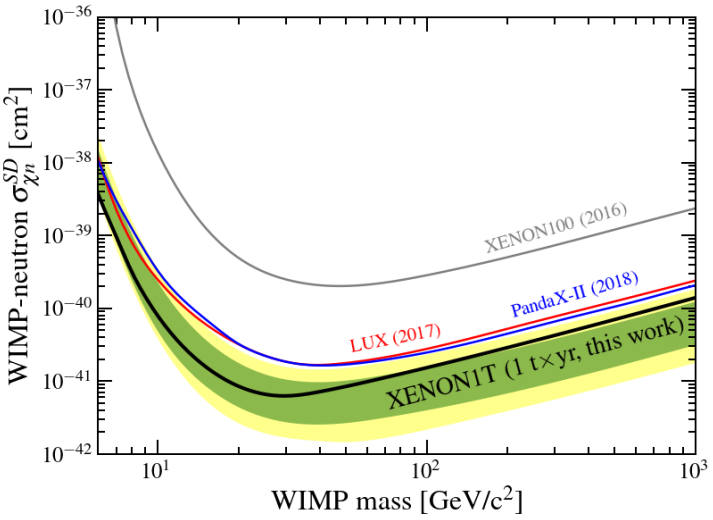

Figure 5.3: *The constraints for the cross section of WIMP and nucleon at spin dependent interaction. 2σ and 1σ contours are shown in yellow and green respectively. The figure is cited from [32]*

5.2 Indirect detection

Indirect detection is the search for DM using the observation of cosmic ray. If DM is very long-lived particle, some of DMs can decay into SM particles and these particles might come to the earth as cosmic ray. The other case, if DM is a stable particle, it can annihilate with other DM and emit SM particles.

5.2.1 Distribution of DM in the galaxy

If the cosmic ray is charged particle, it is bent by the magnetic field in the galaxy or the solar system, and we cannot guess the place where the cosmic ray came from. On the other hand, neutral particles move straight in the magnetic field, and we can get the information of the direction of origin from the observation. Therefore, it is important to know the distribution of DM for the neutral cosmic ray, and this distribution is also important for estimating the annihilation rate of DM.

The estimation of the distribution includes one of the largest uncertainty in the prediction of indirect detection. DM halo is not just spherical [33] and often contain substructure in it. The DM density profile used today is inspired by numerical simulation results, and the study in 1990's [34] showed the universal profile called Navarro-Frenk-White (NFW) profile, which is

$$\rho_{\mathrm{NFW}}(r) = \frac{\rho_0}{\left(\frac{r}{r_s}\right)\left[1+\left(\frac{r}{r_s}\right)\right]^2}, \tag{5.11}$$

where ρ_0 is the constant which has the dimension of density, r is the distance from the center of galaxy and r_s is a scale radius. Some simulations and observations suggest that profile at the inner part of the galaxy is more gentle compared to that of NFW profile as shown in Figure 5.4. In order to describe this modification, generalized NFW profile [35] is also commonly used, which is

$$\rho_{\mathrm{GNFW}}(r) = \frac{\rho_0}{\left(\frac{r}{r_s}\right)^{\gamma}\left[1+\left(\frac{r}{r_s}\right)\right]^{3-\gamma}}, \tag{5.12}$$

where the case with $\gamma = 1$ corresponds to NFW profile.

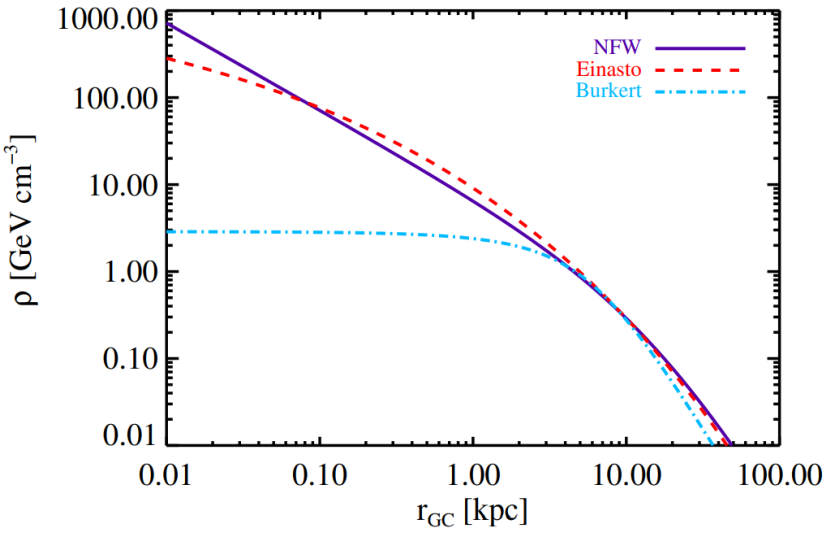

Figure 5.4: *DM density profile at Milky Way for selected cases. The figure is cited from [36].*

5.2.2 Signal of DM annihilation and decay

To estimate the flux of cosmic ray from DM, we need to take into account the property of DM in particle physics and also distribution of DM. The observed flux per area, time, solid angle, and energy is given as

$$\frac{dN_{\rm ann}}{dA\,dt\,d\Omega\,dE} = \frac{\langle\sigma v\rangle}{2m_\chi^2}\frac{dN_X}{dE}\frac{1}{4\pi}J_{\rm ann}(\psi) \tag{5.13}$$

for the annihilation of DM and

$$\frac{dN_{\rm dec}}{dA\,dt\,d\Omega\,dE} = \frac{1}{m_\chi\tau}\frac{dN_X}{dE}\frac{1}{4\pi}J_{\rm dec}(\psi) \tag{5.14}$$

for the decay of DM. Here N_X is the spectrum of SM particle X emitted by annihilation or decay of DM, τ is the lifetime of DM, and $J_{\rm ann/dec}(\psi)$ is the J-factor for annihilation/decay at the angle of line of sight ψ. J-factor include the information of DM distribution, and they are given as

$$J_{\rm ann}(\psi) = \int \rho^2(\psi, l)dl \tag{5.15}$$

$$J_{\rm dec}(\psi) = \int \rho(\psi, l)dl\,, \tag{5.16}$$

where l is the distance along the line of sight, and integration is executed along this line.

5.2.3 Examples of indirect detection

There are several particles detected as cosmic ray, and they have advantages and disadvantages. Photons are observed as Gamma-ray or X-ray, and they are searched by the experiments such as Fermi LAT [37] or H.E.S.S experiment [38]. Using photon has the advantage to be able to point back to the source because photon moves straight, on the other hand there are backgrounds from action of stars. Neutrinos are also neutral particles and they are observed by the experiments such as IceCube [39]. Neutrinos have very small cross section, and the low statics is remaining as a challenge. Other charged particles, such as positron or proton, are observed by PAMELA [40] or AMS [41]. There is a difficulty that we cannot point back to the source because they are charged, but there is an advantage that there are low backgrounds.

5.3 Collider search

WIMP DMs have some amount of interaction with SM particles, and we can create and search for WIMP using collider. However, WIMP is stable and neutral, and it is difficult to detect WIMP directly. In this section we will review some ways how we detect WIMP at collider.

5.3.1 Mono jet/photon search

One of the most effective way to search WIMP is search for some SM particles with missing energy. WIMP usually has Z_2 symmetry to make WIMP stable, and WIMPs are always pair created. For hadron colliders, the process ($qq \to g\chi\chi$) have the largest cross section among the process which include WIMP pair creation and other SM particles. The gluon emitted in the elementary process becomes jet and we detect this jet as a signal. We show the Feynman diagram in Figure 5.5. For lepton colliders, the mono photon search ($e^-e^+ \to \gamma\chi\chi$) is effective for same reason, and the Feynman diagram is shown in Figure 5.6. These processes have large SM back grounds coming from ($qq \to g\nu\nu$) or ($e^-e^+ \to \gamma\nu\nu$) process, here neutrinos are also not detected, and these processes give same signal.

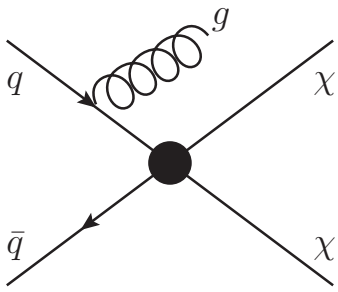

Figure 5.5: *Feynman diagram for mono jet process*

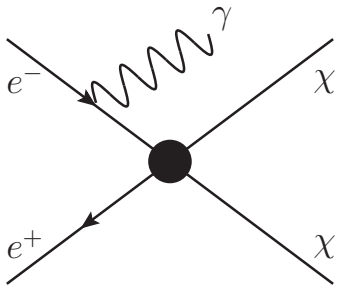

Figure 5.6: *Feynman diagram for mono photon process*

5.3.2 Invisible width

The properties of Higgs boson and Z-boson are searched by Large Electron-Positron collider (LEP) experiments or Large Hadron Collider (LHC) experiments. They are massive boson, and decay into SM particles. Considering the decay into missing particles such as neutrinos, this decay cannot be detected by collider experiment, and they contribute to invisible decay. Suppose that WIMP couple with SM particles such as Higgs or Z-boson and $2m_\chi < m_{h/Z}$, where $m_{h/Z}$ is the mass of Higgs/Z-boson. In this case Higgs and Z-boson decay into two WIMPs also contribute to their invisible width because WIMP cannot be detected. The property of Z-boson was measured precisely by Large Electron-Positron collider (LEP) experiment, and the total width is given as [42]

$$\Gamma_{Z\to\text{any}} \quad = \quad 2.4952 \pm 0.0023\,\text{GeV}\,. \tag{5.17}$$

The invisible width of Z-boson was measured in two methods at LEP experiments. The first method is using the process (e^+e^- $to\gamma Z$), here by measuring the distribution of photon, invisible width of Z-boson can be searched. The other method is considering the difference between total width and measured visible width. By these methods, Z-boson invisible width is given as [43]

$$\Gamma_{Z\to\text{inv}} \quad = \quad 499.0 \pm 1.5\text{MeV}\,. \tag{5.18}$$

The properties Higgs is being measured by LHC experiments, and constraint on the branching ratio to invisible mode is given as [44]

$$B_{h\to\text{inv}} < 0.22\,. \tag{5.19}$$

5.3.3 Associated particle search

The extension of SM with WIMP usually includes other particles. If WIMP is $SU(2)_L$ charged particle, there must be charged partners of this WIMP. Such particles usually decay into WIMP and SM particles, and if they are created by collider experiments, it gives characteristic signals. There can be other type of associated particles called mediator particle which interact with both of SM particles and WIMP. In some case it is easier to search mediator particles than search WIMP directly because mediator particles directly couple with SM particles.

Chapter 6

SM gauge singlet Majorana fermionic WIMP

Many physics beyond the SM include WIMP DM in its model, such as lightest supersymmetric particle in SUSY [6], lightest Kaluza-Klein paricle in Kalza-Klein theory [24] or lightest T-odd particle in little Higgs model [12]. However current LHC experiments reports null signals of these new physics beyond SM, and we should consider other possibilities for new physics and DM. In this chapter, we will divide WIMPs by SM gauge representation and focus on SM gauge singlet Majorana fermionic WIMP.

6.1 Classification of WIMP

To discuss WIMP model independently, it is convenient to classify WIMP by the quantum number of SM. From the condition that WIMP does not have electric charge and strong interaction (c.f. Sec. 2.2), quantum numbers of WIMP are limited. WIMP must be singlet under $SU(3)_C$ and if WIMP is singlet under $SU(2)_L$, $U(1)_Y$ hypercharge must be 0, if WIMP is doublet under $SU(2)_L$, $U(1)_Y$ hypercharge must be -1/2 or +1/2, and so on. We summarize possible SM gauge representations of WIMP at Tabletab:representaion. There is other possibility that WIMP is a mixed state of the neutral components of different $SU(2)_L$ representations. In the following section we will focus on SM gauge singlet fermionic WIMP. From the view point of minimality, we also assume this WIMP as Majorana fermion[1].

6.2 $SU(2)_L$ singlet Majorana fermionic WIMP

WIMP must be stable particle and this stability is usually supported by Z_2 symmetry. WIMP field appear quadratically by this symmetry, and this feature forbid WIMP to have gauge invariant interaction with SM particles by

[1]For Majorana fermion, please refer to Appendix.B

Lorentz	$SU(3)_C$	$SU(2)_L$	$U(1)_Y$
scalar		**1**	0
or		**2**	$-1/2, +1/2$
fermion	**1**	**3**	$-1, 0, +1$
or		**4**	$-3/2, -1/2, +1/2, +3/2$
vector		**5**	$-2, -1, 0, +1, +2$
		$\vdots$	$\vdots$

Table 6.1: *Possible combinations of SM gauge representations of WIMP*

renormalizable operator[2]. If we allow non-renormalizable operators, we can write gauge invariant effective Lagrangian as

$$\mathcal{L}_{\text{eff}} = \mathcal{L}_{\text{SM}} + \frac{1}{2}\bar{\chi}(i\partial\!\!\!/ - m_\chi)\chi + \frac{1}{2}\sum_{a,n} C_a \frac{\mathcal{O}_a}{\Lambda^{n-4}}\,, \tag{6.1}$$

where $\mathcal{L}_{\text{SM}}$ is the Lagrangian of the SM[3], m_χ is mass of the WIMP, $\mathcal{O}_a$ is non-renormalizable operator which contain WIMP fields, C_a is the coupling of each operator, n denotes the dimension of the non-renormalizable operator, and Λ is the cut off scale. The factor $1/2$ is for the normalization of Majorana fermion. This effective Lagrangian is valid only for the lower energy scale than Λ. We show the non-renormalizable operators up to dimension 6 at Table 6.2. Here We treated SM Weyl fermions as Dirac fermions, that correspond to the notation as follows:

$$F_L = \begin{pmatrix} 0 \\ f_L \end{pmatrix} \tag{6.2}$$

$$F_R = \begin{pmatrix} f_R \\ 0 \end{pmatrix}, \tag{6.3}$$

where F_L is left handed fermions which correspond to (Q, L) and F_R is right handed fermions which correspond to (U, D, E). Here we can also think axial vector interaction $(\bar{\chi}\gamma^\mu\gamma_5\chi)(\bar{F}_{Li}\gamma_\mu\gamma_5 F_{Lj})$ or $(\bar{\chi}\gamma^\mu\gamma_5\chi)(\bar{F}_{Ri}\gamma_\mu\gamma_5 F_{Rj})$. However, there is relationship with vector interaction such as

$$(\bar{\chi}\gamma^\mu\gamma_5\chi)(\bar{F}_{Ri}\gamma_\mu F_{Rj}) = (\bar{\chi}\gamma^\mu\gamma_5\chi)(\bar{F}_{Ri}\gamma_\mu\gamma_5 F_{Rj}) \tag{6.4}$$

$$(\bar{\chi}\gamma^\mu\gamma_5\chi)(\bar{F}_{Ri}\gamma_\mu F_{Rj}) = -(\bar{\chi}\gamma^\mu\gamma_5\chi)(\bar{F}_{Li}\gamma_\mu\gamma_5 F_{Lj}) \tag{6.5}$$

and we can identify these operators by changing coupling. Other operators such as vector interactions are prohibited by Majorana nature of DM.

The operator whose dimension is greater than 6 is highly suppressed by the cut off scale and the contribution from such operator is small. These effective operators are obtained by integrating out the fields of heavy particles which are contained in ultra-violet complete models. If we assume perturbativity at

[2]The mass dimension of renormalizable operator is under 4. The operator whose dimension is greater than 4 is called non-renormalizable operator.

[3]For the SM contents, please refer to Appendix.A

the high energy scale, the couplings of the heavy particle and WIMP or SM particles must be less than $\mathcal{O}(1)$. In that case, we can set Λ as the mass scale of the heavy particles and C_a as less than $\mathcal{O}(1)$.

6.3 Surviving parameter region

Specifically, WIMPs with a mass of the order of the electroweak scale have been studied intensively, since such a WIMP can be the key to solve naturalness problem of the electroweak scale. The observed relic abundance for such a WIMP with a mass between $\mathcal{O}(1)$ MeV [45, 46] and $\mathcal{O}(100)$ TeV [47–54] can be realized via the standard thermal freeze-out mechanism [55, 56]. In the freeze-out scenario, the DM abundance is strongly related to the annihilation rate of WIMPs in the early Universe with the relic density being approximately proportional to the inverse of the annihilation rate. Therefore, negligible interaction between the DM and the SM particles leads to too large DM relic abundance and conflicts with the current observation. Thus, for this mechanism to work, the DM should have sufficiently large interaction with the SM particles. One can further advantageously probe the WIMP in the collider, direct and indirect detection experiments due to the interactions. Today LHC experiments and several direct detection experiments are ongoing, and wide parameter regions of SM gauge singlet WIMP are explored due to this sufficiently large interaction. There are, however, several exceptions cases where it is difficult to search by LHC experiments or direct detection experiments. One possibility is that WIMP has very small interaction with quarks or Higgs and DM abundance is determined by the interaction with Leptons. Second possibility is that DM annihilation takes place near the pole mass of a mediator particle or SM particle, and becomes resonant annihilation. In such a case, the annihilation rate is drastically enhanced and the coupling between the WIMP and the SM particles can be adequately small and can even account for the correct DM abundance observed today. Such an example is when the WIMP mass is half of the Higgs boson mass (H-funnel region) [1] or the Z boson mass (Z-funnel region). For both cases, the cross section of the process ($q\bar{q} \to \chi\chi X$) or ($N\chi \to N\chi$) become very small and we need to consider other processes or experiments to search such regions. Consequently, there are three uncharted parameter regions for CP conserving case [13]:

Dim.5	$\mathcal{O}_S = (\bar{\chi}\chi)\lvert H\rvert^2$	$\mathcal{O}_{PS} = (\bar{\chi}i\gamma_5\chi)\lvert H\rvert^2$
Dim.6	$\mathcal{O}_Q = (\bar{\chi}\gamma^\mu\gamma_5\chi)(\bar{Q}_i\gamma_\mu Q_j)$	$\mathcal{O}_U = (\bar{\chi}\gamma^\mu\gamma_5\chi)(\bar{U}_i\gamma_\mu U_j)$
	$\mathcal{O}_D = (\bar{\chi}\gamma^\mu\gamma_5\chi)(\bar{D}_i\gamma_\mu D_j)$	$\mathcal{O}_L = (\bar{\chi}\gamma^\mu\gamma_5\chi)(\bar{L}_i\gamma_\mu L_j)$
	$\mathcal{O}_E = (\bar{\chi}\gamma^\mu\gamma_5\chi)(\bar{E}_i\gamma_\mu E_j)$	$\mathcal{O}_H = (\bar{\chi}\gamma^\mu\gamma_5\chi)(H^\dagger i\overleftrightarrow{D_\mu}H)$

Table 6.2: *SM gauge invariant interaction between WIMP and SM particles [13]. Here Q denote quark doublet, U denote up type quark singlet, D denote down type quark singlet, L denote lepton doublet, E denote lepton singlet, and H denote Higgs doublet.*

(1) *H-funnel region*
In this region $\mathcal{O}_S$ mainly contributes to the physics and DM mass is near the half of Higgs mass.

(2) *Z-funnel region*
In this region $\mathcal{O}_H$ mainly contribute to the physics and DM mass is near the half of Z-boson mass.

(3) *Leptophilic region*
In this region $\mathcal{O}_{L,E}$ mainly contribute to the physics.

We will discuss the future prospect of these regions by direct detection experiments or collider experiments. We will review about the study including H-funnel region at the next chapter, then move on to the analysis of Z-funnel region and Leptophilic region, which are our study.

Chapter 7

CP conserving Higgs portal DM

As we mentioned in chapter 6, when DM annihilation take place at the pole mass of Higgs boson, the coupling constant between Higgs boson and DM can be adequately small to give correct DM abundance observed today. As a result, experimental signature become weaker and it becomes difficult to search such DM. This occurs when DM mass is the half of Higgs boson mass and this region is called H-funnel region. In this chapter we will focus on SM gauge singlet Majorana fermion DM in the CP conserving Higgs portal scenario [57], where the DM couples solely to the Higgs boson. We will review about the status of Higgs portal DM.

7.1 Lagrangian

We focus on the Higgs portal DM, where the DM interacts with the SM particles through the Higgs boson and the other interactions are suppressed. The effective Lagrangian can be written as

$$\mathcal{L}_{\text{eff}} = \mathcal{L}_{\text{SM}} + \frac{1}{2}\bar{\chi}(i\partial\!\!\!/ - M_\chi)\chi + \frac{1}{2\Lambda}(\bar{\chi}\chi)(H^\dagger H)\,, \tag{7.1}$$

where M_χ is the DM mass and H is SM Higgs doublet field. By taking unitary gauge $H = (0, v+h)^T/\sqrt{2}$ with $v \simeq 246\,\text{GeV}$ being the vacuum expectation value of the Higgs doublet field and h being the physical Higgs particle, and the physical mass of DM is modified after electroweak symmetry breaking, which is,

$$m_\chi = M_\chi - \frac{1}{2\Lambda}v^2\,. \tag{7.2}$$

Then the Lagrangian becomes

$$\mathcal{L}_{\text{eff}} = \mathcal{L}_{\text{SM}} + \frac{1}{2}\bar{\chi}(i\partial\!\!\!/ - m_\chi)\chi + \frac{1}{2\Lambda}(\bar{\chi}\chi)(vh + \frac{1}{2}h^2)\,. \tag{7.3}$$

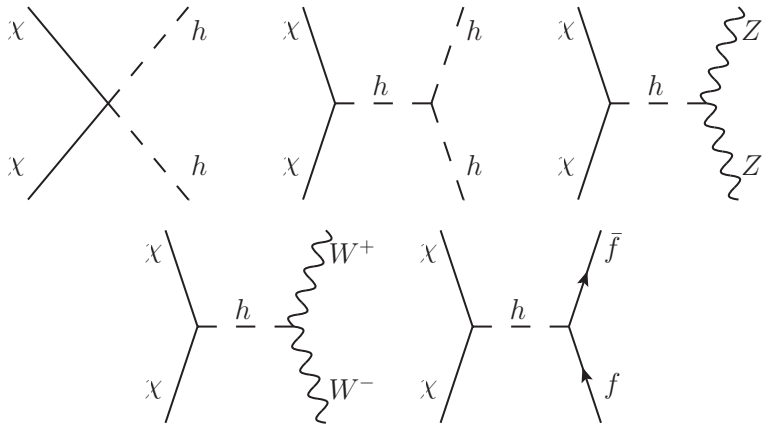

Figure 7.1: *Tree level annihilation of Higgs portal DM into SM particles*

7.2 Relic abundance condition

We will discuss relic abundance condition in this section. The annihilation of DM in Higgs portal occurs through several processes which are annihilation into Higgs pair, Z-boson pair, W-boson pair, and SM fermion pair. We show these processes diagrammatically in Figure 7.1 and there are two different types of diagrams for annihilation into Higgs pair. The analytical formulae of these annihilation cross section can be given as [58, 59]

$$\sigma_f(s; m_\chi, m_f) = \frac{1}{32\pi m_\chi^2}\sqrt{\frac{4m_\chi^2}{s}}\sqrt{\frac{m_\chi^2}{s-4m_\chi^2}}\sqrt{1-\frac{4m_f^2}{s}}\Sigma_f(s; m_\chi, m_f)\,, \quad (7.4)$$

where f denote the SM particle pair into which DM annihilate, s is the center of mass energy, and

$$\Sigma_f(s; m_\chi, m_f) \equiv \frac{1}{4}\sum_{\text{spins}}\frac{1}{4\pi}\int d\Omega|\mathcal{M}_f|^2 \quad (7.5)$$

$$= \frac{s}{8\Lambda^2}\frac{1-4m_\chi^2/s}{(1-m_h^2/s)^2+(m_h\Gamma_h/s)^2} \quad (7.6)$$

$$\times \begin{cases} [(1+2m_h^2/s)^2+(m_h\Gamma_h/s)^2] & (\chi\chi\to hh) \\ (1-4m_Z^2/s+12m_Z^4/s^2) & (ZZ) \\ 2(1-4m_W^2/s+12m_W^4/s^2) & (W^+W^-) \\ (1-4m_f^2/s)(4m_f^2/s) & (f\bar{f})\,, \end{cases} \quad (7.7)$$

where Γ_h is the decay with of Higgs boson. For the hh final state, although there are additional t-channel and u-channel diagrams, we have ignored them because we are interested in H-funnel region and s-channel diagram mainly contribute for this region.

7.3 Invisible width of the Higgs

When $2m_\chi < m_h$, Higgs can decay into DM pair and the total width will be different from that of SM. We have nontrivial constraint from this exotic invisible decay mode by measuring the total decay width of Higgs boson. The DM contribution to the invisible decay of Higgs can be calculated as

$$\Gamma_{h\to\chi\chi} = \frac{m_h}{16\pi}\frac{v^2}{\Lambda^2}\left(1-\frac{4m_\chi^2}{m_h^2}\right)^{\frac{3}{2}} . \tag{7.8}$$

The CMS and ATLAS experiment [60, 61] have set constraints on total decay width of Higgs boson as $\Gamma_h < 13$ MeV at 95% confidence level using Higgs decaying into 4 leptons via off shell ZZ. Although we have constraint on the coupling of DM and Higgs from this value, we have stronger constraint using invisible branching ratio. The DM contribution to the invisible branching ratio of Higgs boson is given as,

$$\mathcal{B}_{\rm inv} = \frac{\Gamma_{h\to\chi\chi}}{\Gamma_{\rm SM}+\Gamma_{h\to\chi\chi}} , \tag{7.9}$$

where $\Gamma_{\rm SM} = 4.21$ MeV is theoretical prediction of the total decay width of Higgs boson from SM. The best limit on the invisible branching ratio comes from the best fit to Higgs data, and this is given as $\mathcal{B}_{\rm inv} < 24\%$ at 95% confidence level.

7.4 Direct detection

Direct detection sets the strongest constraint on Higgs portal DM even for the H-funnel region. The t-channel diagram with the exchange of the Higgs boson gives relevant contribution to the elastic scattering of DM and nucleus, and the Feynman diagram is shown in Figure 7.2, where N denote nucleus.

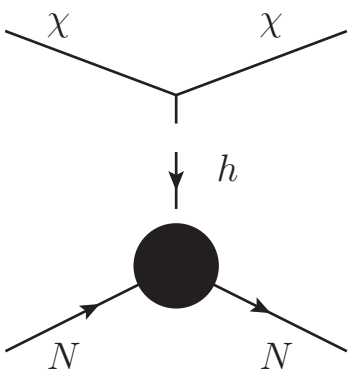

Figure 7.2: The diagram for the elastic scattering of DM and nucleus

The operators which are relevant to this process are given as

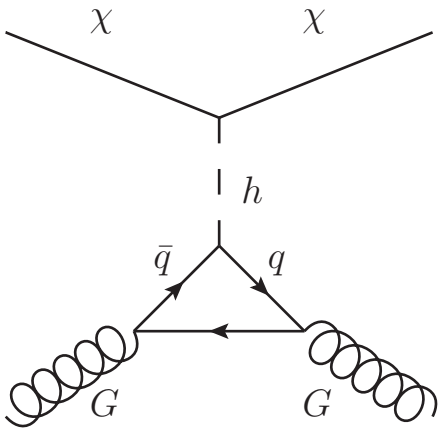

Figure 7.3: Interaction of DM and gluon via quark loop

$$\mathcal{L} \supset \frac{v}{2\Lambda}(\bar{\chi}\chi)h - \sum_q \frac{m_q}{v}\bar{q}qh\,, \tag{7.10}$$

where q denotes SM quarks and m_q is its mass. The typical momentum transfer of this process is calculated as $m_\mu v_{\rm DM} \lesssim \mathcal{O}(\mathrm{MeV})$, where $m_\mu = (m_N m_\chi)/(m_N + m_\chi)$ is the reduced mass, and $v_{\rm DM}$ is the velocity of DM in our galaxy. As this value is very small compared to the mass of Higgs boson, we can integrate out the Higgs field from the Lagrangian, and we get the effective Lagrangian as

$$\mathcal{L}_{\rm eff} \supset -\sum_q \frac{1}{m_h^2}\frac{m_q}{2\Lambda}(\bar{q}q)(\bar{\chi}\chi)\,. \tag{7.11}$$

We have also heavy quarks in the summation, and they induce the coupling of DM and gluons in the nucleon through the triangle diagram, which is shown in Figure 7.3. The scattering of DM and nucleus occurs spin independently, and the cross section of DM and nucleons are given as

$$\sigma_{\rm SI}^{\chi n} = \frac{1}{2\pi}\left(\frac{m_\mu}{m_h^2}\right)^2\left(\frac{f_n}{\Lambda}\right)^2\,, \tag{7.12}$$

where n denote the species of nucleons (proton or neutron) and

$$f_n \equiv m_n\left(\sum_{q=u,d,s} f_{Tq}^n + \frac{2}{9}f_{TG}^n\right) \tag{7.13}$$

is the nucleon matrix element (c.f. Sec 5.1). Previous study [1] gives current constraints and future prospect of the Higgs portal DM including H-funnel region, which is shown in Figure 7.4. Here $\lambda_{H\chi\chi}$ corresponds to v/λ for our model, the solid black contour line gives correct relic abundance which agree with PLANCK experiment, and shaded region is excluded region from Higgs invisible decay and Xenon 1T direct detection experiment, while other colored

dotted lines give future prospects by LZ/Xenon nT and DARWIN [62] direct detection experiment. The black dotted lines correspond to $\mathcal{B}_{\rm inv}$ =10%, 5% and 1% respectively. The sharp peak of black line at $m_\chi \simeq 60\,\mathrm{GeV}$ correspond to the H-funnel region, and they are almost excluded by current direct detection experiment. Small region is remaining uncovered at H-funnel region, but this region can be totally explored by LZ/Xenon nT direct detection experiments in the near future.

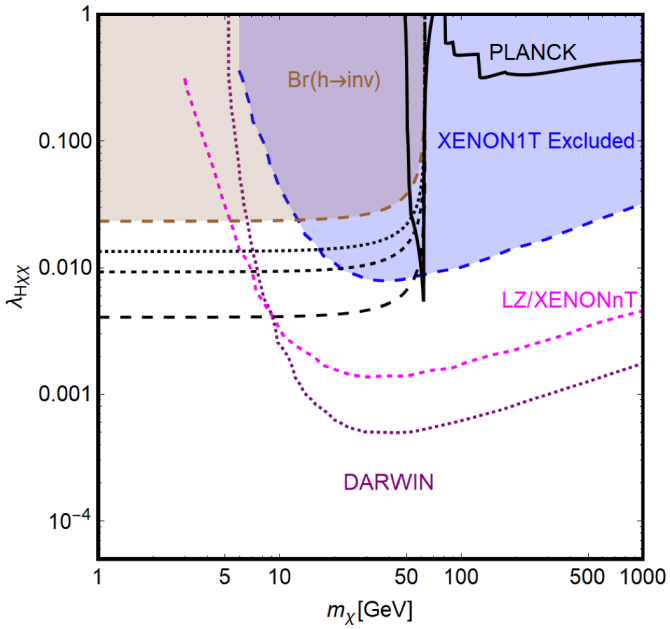

Figure 7.4: Current constraint and future prospect for Higgs portal DM. The figure is cited from [1].

Chapter 8

Z-funnel WIMP

In this chapter, we will consider the SM gauge singlet Majorana fermion DM (χ) in the Z-portal model [63], where the DM couples only to the Z boson. There are only two new physics parameters in the model: the DM mass (m_χ) and the coupling constant between the DM and the Z boson ($g_{\chi\chi Z}$). The observed DM abundance and the constraint from spin-dependent direct DM detection experiments have already excluded the most of the parameter space, except for the Z-funnel region, namely $m_\chi \simeq m_Z/2$. In the Z-funnel region, the coupling between the DM and Z boson can be small in order to explain the DM abundance in the present universe, and thus the constraint from the DM direct detection experiments is still weak [64]. The main goal of this chapter is to figure out what kind of role the future lepton colliders can play to probe the Z-funnel DM.

The rest of this chapter is organized as follows. In Sec. 8.1, we briefly discuss the framework of the effective Lagrangian for the SM gauge singlet Majorana fermionic WIMP in order to introduce the Z-funnel WIMP. In Sec. 8.2, we will discuss the current status of the Z-funnel WIMP by the relic abundance condition, direct DM detection, indirect DM detection, and collider experiments. For the analysis of the LEP experiments, we consider the mono-photon and invisible Z decay width searches. For the mono-photon signature, we reproduce the background data obtained by the previous study, and then put the constraint on the Z-funnel WIMP using the same data. In Sec. 8.3, we discuss the sensitivity of future experiments, namely the future lepton collider (ILC) and direct detection experiments. The sensitivity of the future lepton collider has not been obtained by any previous studies. In Sec. 8.4, we summarize our findings and conclude.

8.1 The Z-funnel WIMP model

We focus on the Majorana fermionic WIMP DM that is singlet under the SM gauge symmetry. To make the WIMP stable, we impose the discrete Z_2 symmetry under which the WIMP is odd, while all the SM particles are even. In this case, the WIMP cannot have any renormalizable interaction with the SM par-

ticles due to the symmetries. In order to introduce a renormalizable interaction between the WIMP and the SM particles, we have to introduce an additional new particle called the mediator. Physics of the WIMP strongly depends on the nature of the mediator. On the other hand, if the mediator is heavier enough than the WIMP and the electroweak (EW) scale, we can integrate out the mediator from the original renormalizable Lagrangian, and physics of the WIMP can be described by the effective Lagrangian with the cutoff scale Λ as long as we discuss WIMP dynamics at an energy scale sufficiently lower than Λ:

$$\mathcal{L}_{\rm EFT} = \mathcal{L}_{\rm SM} + \frac{1}{2}\bar{\chi}(i\partial\!\!\!/ - m_\chi)\chi + \mathcal{L}_5 + \mathcal{L}_6 + \mathcal{L}_{\geq 7}, \tag{8.1}$$

where χ is the WIMP Majorana fermion field with m_χ being its mass, and $\mathcal{L}_{\rm SM}$ is the SM Lagrangian. Interactions between the WIMP and the SM particles are described by higher dimensional operators in $\mathcal{L}_5$, $\mathcal{L}_6$ and $\mathcal{L}_{\geq 7}$, which involve operators of dimension five, six, and seven or higher, respectively, which are suppressed by Λ [65], where Λ represents a typical mass scale of the mediator.

As we are considering the singlet Majorana WIMP that interacts with the Z boson, its interaction originates in the dimension-six operator in $\mathcal{L}_{\rm EFT}$:

$$\mathcal{O}_H \equiv (\bar{\chi}\gamma_\mu\gamma_5\chi)(H^\dagger i D^\mu H)/2 + \text{h.c.}, \tag{8.2}$$

where H is the SM Higgs doublet field and D^μ is the covariant derivative acting on the Higgs field [13]. By taking the unitary gauge $H = (0, v+h)^T/\sqrt{2}$ with $v \simeq 246\,\text{GeV}$ being the vacuum expectation value of H and h being the physical Higgs particle after the EW symmetry breaking, this operator is expanded as

$$\mathcal{L}_6 \supset \frac{g_D}{\Lambda^2}\mathcal{O}_H = \frac{g_D}{4\Lambda^2}(\bar{\chi}\gamma_\mu\gamma_5\chi)\left(g_Z v^2 Z^\mu + 2g_Z v h Z^\mu + g_Z h^2 Z^\mu\right), \tag{8.3}$$

where Z is the Z boson field, g_D is a dimensionless coupling, and $g_Z \equiv g/\cos\theta_W$ with g and θ_W being the $\mathrm{SU}(2)_L$ gauge coupling constant and the weak mixing angle, respectively. The last three interactions on the right-hand side play negligible roles compared to the first one in the Z-funnel region, namely the region $m_\chi \sim m_Z/2$ with m_Z being the Z boson mass. Hence, we adopt the following simple Z-portal model to discuss the Z-funnel WIMP DM quantitatively:

$$\mathcal{L} = \mathcal{L}_{\rm SM} + \frac{1}{2}\bar{\chi}(i\partial\!\!\!/ - m_\chi)\chi + \frac{g_{\chi\chi Z}}{2}\,\bar{\chi}Z\!\!\!/\gamma_5\chi. \tag{8.4}$$

The dimensionless coupling constant $g_{\chi\chi Z}$ is given by $g_{\chi\chi Z} = g_D g_Z v^2/(2\Lambda^2)$, so that its range is expected to be $g_{\chi\chi Z} \lesssim 0.02\,(1\,\text{TeV}/\Lambda)^2$. Here, we assume that the underlying model behind the interaction in eq. (8.3) is weak-interacting, $g_D \lesssim 1$. It is also worth pointing out here that the above simplified model involves two new physics parameters m_χ and $g_{\chi\chi Z}$, so that all the results of our discussion can be cast onto the plane spanned by the two parameters.

A concrete example of the UV theory behind the Z-portal DM is the neutralino DM in the so-called "blind spot" region [66]. With an appropriate choice of neutralino mixing parameters as well as sfermion masses, dimension-five and dimension-six four-Fermi operators can be suppressed except the one in eq. (8.3).

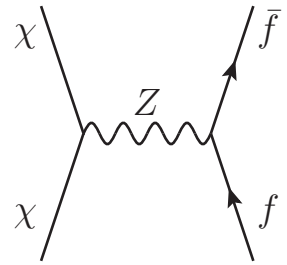

Figure 8.1: *Dominant process contributing to the Z-funnel WIMP annihilation.*

8.2 Present status of the Z-funnel WIMP

We discuss various constraints on the Z-funnel WIMP obtained by experiments and observations performed so far, and figure out which parameter region of the WIMP is still uncharted in the plane spanned by the parameters m_χ and $g_{\chi\chi Z}$.

8.2.1 Relic abundance condition

The annihilation of the Z-funnel WIMP is dominated by the process in Fig. 8.1, namely $\chi\chi \to Z \to \bar{f}f$ with f being a SM fermion. Since the WIMP is non-relativistic at the freeze-out temperature and $m_\chi \simeq m_Z/2$, this process is enhanced by the Z boson pole. The annihilation cross section is given by [63],

$$\begin{aligned}\sigma &= \frac{n_c^f}{24\pi\cos^2\theta_W}\frac{g_{\chi\chi Z}^2 g^2 s}{(s-m_Z^2)^2+m_Z\Gamma_Z^2}\frac{\sqrt{1-4\mu_f^2}}{\sqrt{1-4\mu_\chi^2}}\Bigg\{|V_f|^2\beta^2(1+2\mu_f^2)\\ &+ |A_f|^2\left[\beta^2+28\mu_f^2\mu_\chi^2+12\mu_f^2\mu_\chi^2\frac{s^2}{m_Z^2}-4\mu_f^2\left(1+6\mu_\chi^2\frac{s}{m_Z}\right)\right]\Bigg\}, \quad (8.5)\end{aligned}$$

where we suppose the interaction between the Z boson and the fermion f as

$$\mathcal{L}_{\rm int} = \frac{g}{4\cos\theta_W}\bar{f}\gamma^\mu(V_f - A_f\gamma^5)fZ_\mu\,, \quad (8.6)$$

and n_c^f is the color degree of freedom of the fermion f, θ_W is the Weinberg angle, s is the square of center of mass energy, $\mu_{f,\chi} = m_{f,\chi}/\sqrt{s}$ and $\beta = \sqrt{1-4\mu_\chi^2}$.

We have numerically solved the Boltzmann equation by implementing the interaction of the Z-portal DM, adopting the result in Ref. [67] for the massless degrees of freedom in the early universe (see Fig. 8.2), and using the MicrOMEGAs code [68, 69]. The result of the calculation is shown in Fig. 8.3, where three contours correspond to the cases that the Z-funnel WIMP contributes to 1 % (blue), 10 % (purple), and 100 % (red) of the dark matter abundance observed today, $\Omega_{\rm obs}h^2 = 0.12$ [4]. The region where the Z-funnel WIMP abundance is more than the observed one is shaded by red, and it is thus not favored.

8.2.2 Constraint from the direct DM detection

The direct detection of the scattering between the DM and a nucleon mediated by the Z boson at underground experiments gives the most promising signature of the Z-funnel WIMP. Since the Majorana fermionic DM does not have a vector but an axial-vector interaction with a nucleon, the scattering takes place in a spin-dependent way, and the corresponding cross section is severely constrained by the null results of the underground experiments. The spin-dependent scattering cross section between the DM and a proton (neutron) is given by

$$\sigma_{p\,(n)} = \frac{12}{\pi}\mu^2_{\chi p\,(n)}\, a^2_{p\,(n)}, \tag{8.7}$$

where $\mu_{\chi p\,(n)}$ is the reduced mass of the DM and a proton (neutron), while $a_{p\,(n)}$ is the scattering amplitude. A concrete expression of the amplitude is [6]

$$a_{p\,(n)} = \frac{g_{\chi\chi Z}\, g}{8 m_Z^2 \cos\theta_W}\left(\Delta_u^{p\,(n)} - \Delta_d^{p\,(n)} - \Delta_s^{p\,(n)}\right). \tag{8.8}$$

Here, $\Delta_q^{p\,(n)}$ is so-called the spin nucleon parameter, and we take the default values, namely $\Delta_u^p = \Delta_d^n = 0.842$, $\Delta_d^p = \Delta_u^n = -0.427$, $\Delta_s^p = \Delta_s^n = -0.085$, adopted in the MicrOMEGAs code [68, 69]. When the DM becomes much heavier than the nucleon, the above cross section is approximately estimated to be

$$\sigma_{p\,(n)} \simeq g^2_{\chi\chi Z}\,\left[3.0\,(2.3)\times 10^{-37}\right]\ \mathrm{cm}^2. \tag{8.9}$$

At present, XENON1T [32] experiment observing the scattering with a neutron gives the strongest constraint on the Z-funnel WIMP. When the Z-funnel WIMP occupies 100 % of the observed DM density, the constraint on the scattering cross section is given by $\sigma_n < 1.0\times 10^{-41}\,\mathrm{cm}^2$. On the other hand, the constraint depends on the fraction of total DM density when the DM does

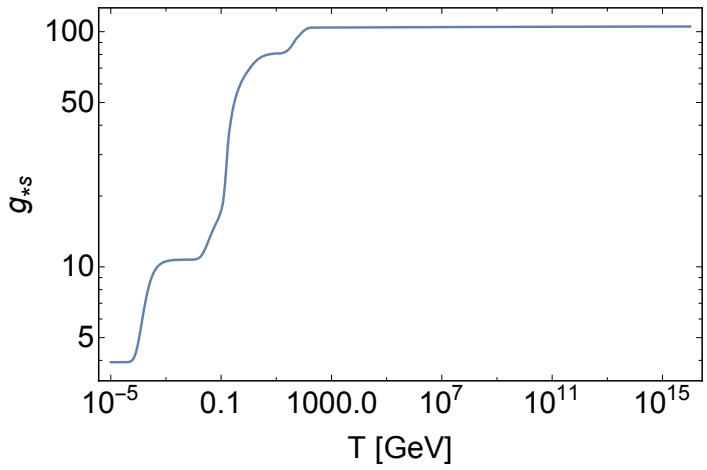

Figure 8.2: *Massless d.o.f. in the early universe as a function of the temperature.*

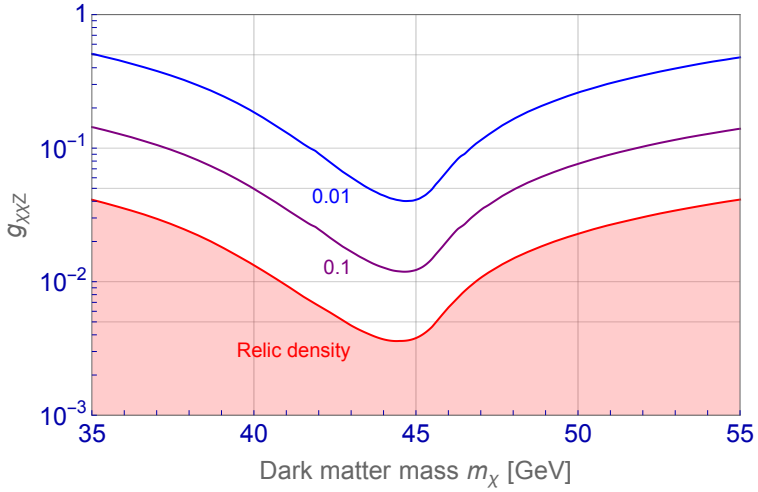

Figure 8.3: *The contribution of the Z-funnel WIMP in the DM density observed today. Blue, purple and red lines correspond to 1%, 10% and 100%, respectively.*

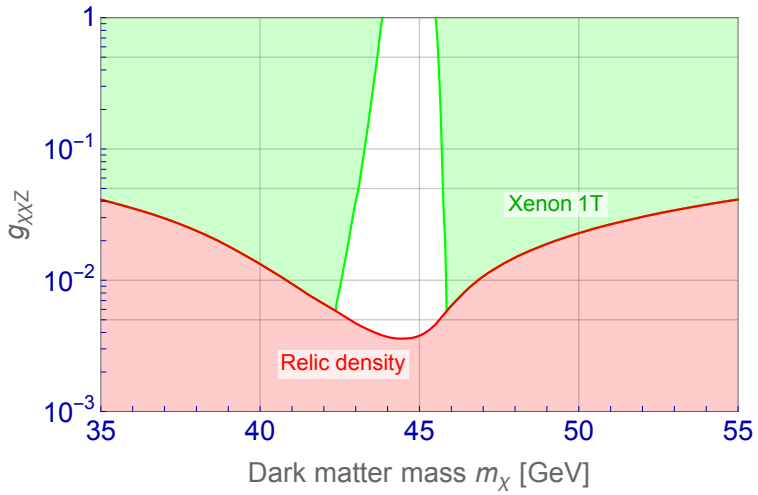

Figure 8.4: *Constraint from the direct detection. Green shaded region is not favored by the XENON1T experiment. The red shaded region is the same as that in Fig. 8.3.*

not occupy 100 % of the observed DM density, and the constraint will only be applied to the scaled scattering cross section between the DM and a nucleon as

$$\sigma^{\rm eff}_{p\,(n)} \equiv \frac{\Omega_{\rm th}\, h^2}{\Omega_{\rm obs}\, h^2}\, \sigma_{p\,(n)}\,, \tag{8.10}$$

where $\Omega_{\rm th}$ is the thermal relic abundance of the Z-funnel WIMP at given m_χ and $g_{\chi\chi Z}$. The constraint from the XENON1T experiment on the (m_χ, $g_{\chi\chi Z}$)-plane is shown in Fig. 8.4, which is obtained by considering $\sigma^{\rm eff}_n \leq 1.0 \times 10^{-41}\,{\rm cm}^2$.

Here, it is important to note that the thermal contribution $\Omega_{\rm th}\, h^2$ is inversely proportional to the annihilation cross section to a good approximation and hence $\Omega_{\rm th}\, h^2 \propto 1/g^2_{\chi\chi Z}$, while the un-scaled scattering cross section is proportional to the coupling constant squared as $\sigma_{p\,(n)} \propto g^2_{\chi\chi Z}$, the scaled scattering cross section $\sigma^{\rm eff}_{p\,(n)}$ is weakly dependent of the coupling $g_{\chi\chi Z}$. Such an interesting behavior of

the scaled scattering cross section originates in the fact that the relic abundance and the un-scaled scattering cross section are governed by a single interaction.

8.2.3 Constraint from the indirect DM detection

Let us briefly discuss the indirect detection signature from the DM annihilation at present universe. It is to be noted that being a Majorana fermion, the DM candidate in our Z-portal model has a significantly suppressed annihilation rate in the present universe. The DM annihilation will take place through s-wave and/or p-wave modes. Between these two possibilities, the s-wave annihilation rate of the DM is suppressed by factors of m_f/m_χ, while the p-wave annihilation rate is suppressed by the relative velocity of the DM, $v_{\rm rel}^2$. In the s-wave case, the Breit-Wigner enhancement of the DM annihilation will not work. Consequently, unlike the p-wave annihilation case, the velocity averaged DM annihilation rate becomes negligibly small. Quantitatively, the velocity averaged DM annihilation rate is around $(10^{-27}\,{\rm cm}^3/{\rm s})$ at least below one order of magnitude compared to the annihilation cross section limit put by the Fermi-LAT dwarf spheroidal galaxy searches [70][1]. In passing, we would like to mention that the small propagator width effect may play a role in the Z-funnel mass region and the p-wave annihilation becomes dominant. However, due to the low relative DM velocity of $\mathcal{O}(10^{-3}c)$ in the present galactic objects, the p-wave annihilation is also strongly suppressed and confirmed to be even lower than the s-wave contribution even for the DM mass of $m_\chi \sim M_Z/2$. Hence, there is no significant constraint on the Z-funnel WIMP from the indirect dark matter detection experiment.

8.2.4 Constraint from the LHC experiment

At the LHC experiment, the WIMP search has been performed through processes where WIMPs are pair produced in association with the SM particles, like photons (γ), gluons (g), $W^\pm$, Z, h and quarks. These processes lead to large missing transverse energy in association with mono-photon, jet(s), charged leptons signal at the detector. The theoretical formulation of the DM interaction with the SM sector is often based on the assumptions of the effective field theory (EFT) with the cut-off scale Λ, where Λ is the relevant scale of the process obtained after integrating out the heavy mediator particle, as we mentioned at Sec. 8.1. On the other hand, in an alternative approach, the so-called simplified scenario is assumed where the mass of the mediator particle is well within the kinematic reach of the LHC experiment and the WIMP interaction with the ordinary matter is determined by the WIMP mass, mediator mass along with the couplings of the mediator with the WIMP (g_χ) and the SM particles (g_q).

At the LHC, while looking for the signature of the WIMPs, it is generally assumed that the WIMP mass is relatively small compared to the the mass of the mediator. The exclusion limit from null observation is usually given in

[1]This limit should further be relaxed by an order due to the uncertainty in the J-factor.

terms of the mediator mass and the WIMP mass assuming particular values of g_χ and g_q in a simplified model. This exclusion limit can be easily translated in the EFT analysis in terms of the WIMP mass and the cut-off scale. Latest constraints from the Run-II LHC experiment at 13 TeV are given by the ATLAS collaboration from mono-photon search [71] and mono-jet searches [72].

The LHC constraint on the Z-funnel WIMP is obtained by applying the constraints mentioned above. It has been, however, shown that the new physics coupling, $g_{\chi\chi Z}$, greater than $\mathcal{O}(1)$ is excluded at 95 % C.L. for the Z-funnel WIMP mass region [73]. Since this limit is less stringent than the LEP constraint that will be discussed next, and shall not be further discussed in our analysis.

8.2.5 Constraints from the LEP experiment

Since the signature of the Z-funnel WIMP is one of the main topics of this thesis, we describe it in some details. There are two important search channels: one is the mono-photon and the other is the invisible Z decay width searches.

8.2.5.1 Mono-photon search

Since DM cannot be directly captured by collider detectors, we search for it indirectly through, for instance, the observation of a recoiled SM particle against the DM pair production. Among various channels to search for the DM, the mono-photon process ($e^-e^+ \to \chi\chi\gamma$) is known to be one of the most efficient channels at the lepton colliders. **The mono-photon signal** in the framework of the Z-funnel WIMP in eq. (8.4) is from Feynman diagrams shown in Fig. 8.5 (the top-left diagram), where the photon line which is not directly touched onto other lines means that it can be from either initial electron or positron line.

On the other hand, there are several SM processes contributing to the mono-photon channel as **backgrounds against the signal**. One of such backgrounds is an irreducible one from the neutrino pair production associated with a photon ($e^-e^+ \to \nu\,\bar{\nu}\,\gamma$), whose diagrams are also shown in Fig. 8.5. The Bhabha scattering process with a photon emission ($e^-e^+ \to e^-e^+\gamma$) can also be a background if both electron and positron at the final state go to the beam pipe direction. This background is, fortunately, reduced efficiently by considering only events with a large photon transverse momentum in the analysis. Other possible backgrounds come from the neutrino pair production associated with more than a photon ($e^-e^+ \to \nu\,\bar{\nu}\,\gamma$s). These contributions is taken into account as the initial state radiation effect, as will be discussed below. Finally, multi photon productions from the e^-e^+ annihilation ($e^-e^+ \to \gamma$s) can be backgrounds if some photons are failed to detect, though these are not significant compared to the irreducible background under an appropriate event selection [74]. We therefore only consider the irreducible background as the one against the mono-photon signal.

As mentioned above, we take the **Initial state radiation (ISR) effect** into account to evaluate the signal and the background. This is the effect that the incident electron and positron emit soft photons just before the collision so

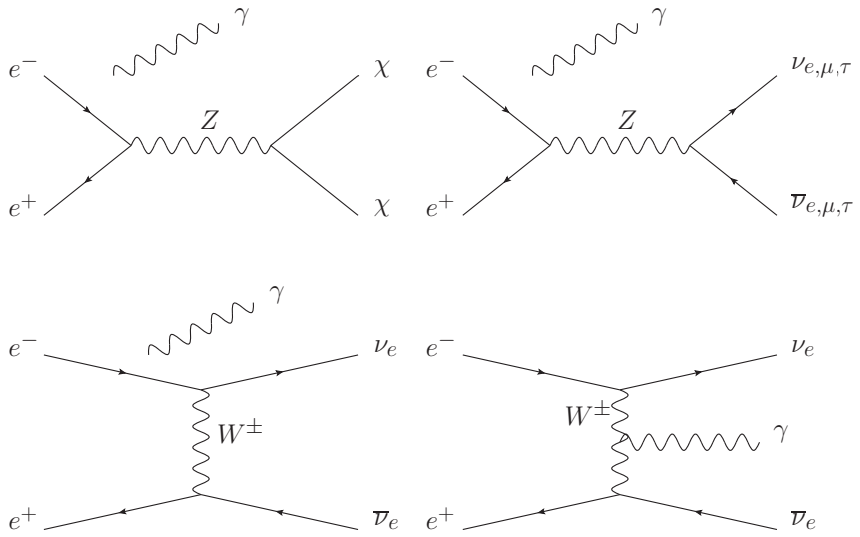

Figure 8.5: *Feynman diagrams for the signal process (top-left) and irreducible background processes (others) of the mono-photon search at lepton collider experiments. Here, the photon line which is not directly touched onto other lines indicate that the photon can be from either electron or positron line at the initial state.*

that the beam energy (thus, the collision energy) effectively diminishes. Among various methods to evaluate the effect, we adopt the one that was used for the mono-photon search at the LEP experiment [75]. Here, the ISR effect is involved through the function $F(x)$ with x being $x = E_{\rm out}/E_{\rm in}$, and the function $F(x)$ gives the energy ($E_{\rm out}$) distribution of the electron or positron (that originally has the energy of $E_{\rm in}$) after it experienced the ISR. Its explicit form is

$$F(x) = e^{\beta(3/4-\gamma_E)}\beta(1-x)^{\beta-1}\frac{4(1+x^2)-\beta\left[(1+3x^2)\ln x + 2(1-x)^2\right]}{8\Gamma(1+\beta)}, \quad (8.11)$$

where $\gamma_E \simeq 0.577$ is the Euler constant and $\beta = \alpha\left[2\log(E_{\rm in}/m_e) - 1\right]/\pi$. The ISR effect described by the function $F(x)$ is convoluted with the cross sections of the signal and the background processes that are discussed above.

We also take the **detector effect** into account to evaluate the signal and the background. A produced energetic photon is detected at the electromagnetic calorimeter, in which the photon causes an electromagnetic shower, creating a cascade of electron-positron pairs and bremsstrahlung photons. The electrons and positrons lose energy through ionization and are eventually stopped. The calorimeter measures this energy loss, which enables us to measure the energy of the original photon. Since the measurement owes to the stochastic process, it associates with an uncertainty caused by the number fluctuation in the development of cascade showers. This effect emerges as the stochastic term in the resolution of the calorimeter, and it is proportional to the square root of the photon energy due to the property of the fluctuation. In addition, there is another term in the resolution called the constant term, which is from the calibration. The resolution of the electromagnetic calorimeter is therefore given

by

$$\frac{\sigma(E_\gamma)}{E_\gamma} = \frac{a}{\sqrt{E_\gamma}} + b, \tag{8.12}$$

where E_γ is the photon energy coming into the calorimeter and $\sigma(E_\gamma)$ is the resolution which depends on E_γ. The values of a and b are shown in Table 8.1.

On the experimental data, in order to put a constraint on the Z-funnel WIMP, we consider the result of the Delphi collaboration based on the $650\,\mathrm{pb}^{-1}$ integrated luminosity data corrected during the running of 180–209 GeV, which is shown in Fig. 8.6 as black points [76]. On the other hand, on the theoretical prediction, we have analytically calculated the differential cross sections of the processes in Fig. 8.5, numerically integrated the cross sections with convoluting the ISR effect in eq. (8.11), and taking the detector effect summarized in Table 8.1 into account in order to evaluate the number of the signal and background events and compare them to the above experimental data. Here, we have used the observed total decay width of the Z boson ($\Gamma_Z = 2.4952 \pm 0.0023\,\mathrm{GeV}$ [43]) in the Z-boson propagator to calculate the cross sections and neglected the contribution to the width from the new physics process $Z \to \chi\chi$. This is because the new physics contribution is negligibly smaller than other SM contributions when the coupling is $g_{\chi\chi Z} \leq \mathcal{O}(1)$ due to the threshold suppression, $m_Z \simeq 2m_\chi$.[2] We have confirmed that the number of the background event obtained in the above method is well consistent with the one in Ref. [77] (blue histograms in Fig. 8.6), verifying our analysis method to put the constraint on the Z-funnel WIMP.

We have compared the theoretical prediction with the observed data of the single photon energy distribution, and set the upper limit on the Z-funnel

Polar angle	Energy threshold	Efficiency	Resolution
$45^\circ < \theta < 135^\circ$	$x_\gamma > 0.06$	(1)	$0.043 \oplus 0.32/\sqrt{E_\gamma}$
$12^\circ < \theta < 32^\circ$	$x_\gamma > 0.1$	(2)	$0.03 \oplus 0.12/\sqrt{E_\gamma} \oplus 0.11/E_\gamma$
$3.8^\circ < \theta < 8^\circ$	$x_\gamma > 0.3$	(3)	$0.0152 \oplus 0.135/\sqrt{E_\gamma}$

Table 8.1: *The simplified detector modeling. Here $x_\gamma \equiv E_\gamma/E_{\mathrm{beam}}$ with E_γ and E_{beam} being the photon and beam energies. For the resolution of detector E_γ is written in GeV unit. The efficiencies denoted by (1) to (3) are as follows: First, (1) Increasing linearly from 52 % at E_γ = 6 GeV to 77 % at 30 GeV and then to 84 % at 100 GeV, and then multiplied by the efficiency of the subsequent analysis which is increasing linearly from 41 % at 6 GeV to 78 % at 80 GeV and above. Next, (2) Increasing linearly from 93 % at 10 GeV to 100 % at 15 GeV and above, and the analysis efficiency is the product of a linear function , increasing from 57 % at 10 GeV to 75 % at 100 GeV, and a constant 89 %. In addition, imposing an energy dependent angular cut $\theta > (28 - 80x_\gamma)$. Last, (3) 48 % and imposing energy dependent angular cut $\theta > (9.2 - 9x_\gamma)$.*

[2] In fact, the new physics contribution to the total Z boson decay width is comparable to or even smaller than the experimental uncertainty of the total decay width when $g_{\chi\chi Z} \leq 1$.

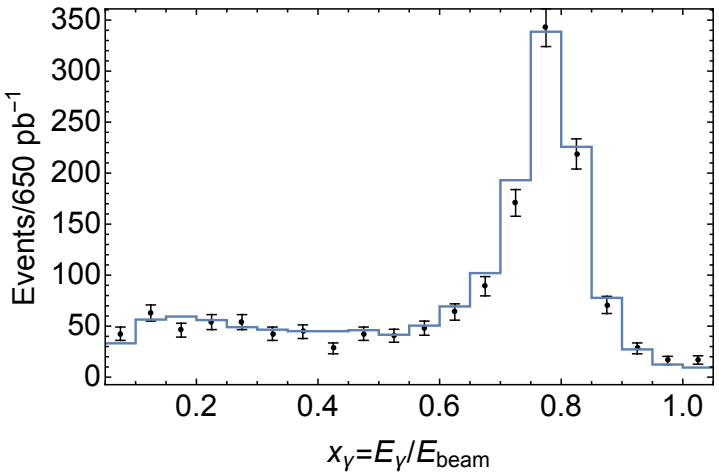

Figure 8.6: *The number of the mono-photon event at the LEP experiment. Black points are observed data, while blue histograms are simulated data shown in Ref. [77].*

WIMP signal at 90 % confidence level. We have included only the statistical uncertainty and neglected the systematic uncertainty, and thus the $\Delta\chi^2$ was defined as

$$\Delta\chi^2 \equiv \sum \frac{(N_i - N_i^{\text{Obs}})^2}{N_i^{\text{Obs}}}, \tag{8.13}$$

where i is the index of the energy bin, while N_i is the number of signal plus background events in the i-th energy bin, and N_i^{BG} is the number of the observed event in the same energy bin. Our analysis is performed assuming that this χ^2 follows the χ^2 distribution of one degree of freedom. The result of the analysis, namely the parameter space that is not favored by the mono-photon search at the LEP experiment, is shown in Fig. 8.6 as a blue shaded region.

8.2.5.2 Invisible Z decay

When the DM mass m_χ is less than half of the Z boson mass $m_Z/2$, the Z boson can decay into a pair of DMs in addition to ordinary decay channels into SM particles. Hence, it is possible to search for the DM by observing the invisible decay width of the Z boson. In the framework of the Z-funnel WIMP in eq. (8.4), this new physics contribution to the width is predicted as follows:

$$\Gamma(Z \to \chi\chi) = \frac{g_{\chi\chi Z}^2 m_Z}{24\pi}\left(1 - \frac{4m_\chi^2}{m_Z^2}\right)^{3/2}. \tag{8.14}$$

The SM process decaying into a neutrino pair also contributes to the invisible decay width, and it is proportional to the number of the neutrino flavors N_ν. The invisible decay width of the Z boson is experimentally determined using lepton collider experiments by comparing the total decay width and observable partial decay widths of the Z boson. At present, the invisible decay width is

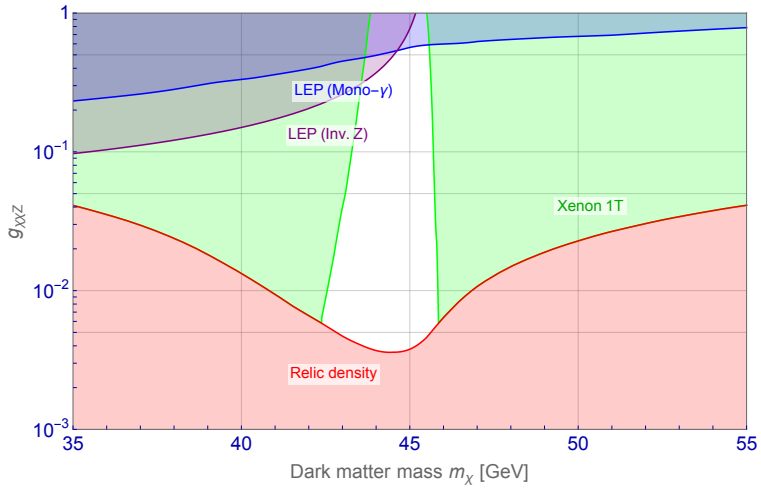

Figure 8.7: *The constraint from the LEP experiment. The blue shaded region is not favored by the mono-photon search at the experiment, while the purple one is not favored by the Z boson invisible width search. Other constraints from the DM relic abundance and direct DM detection are also shown as red and green shaded regions.*

observed to be $\Gamma_{\rm inv}^{(Z)} = 499.0 \pm 1.5\,{\rm MeV}$ at the LEP experiment [78], and this is equivalent to $N_\nu = 2.9840 \pm 0.0082$ [42]. Though this does not allow DM with $m_\chi \leq m_Z/2$, in order to get conservative limit on m_χ, we assume that the new physics contribution to the invisible decay width as $\Gamma(Z \to \chi\chi) \leq 1.5\,{\rm MeV}$, or in other words, $\Delta N_\nu \leq 8 \times 10^{-3}$ with ΔN_ν being the new physics contribution to the number of the neutrino flavors [79]. The constraint from the invisible Z decay width search at the LEP experiment is shown in Fig. 8.7 as a purple shaded region, where it is obtained by requiring the constraint $\Gamma(Z \to \chi\chi) \leq 1.5\,{\rm MeV}$.

8.2.6 Present status of the Z-funnel WIMP

Present status of the Z-funnel WIMP is summarized in Fig. 8.7, where all important constraints from the DM relic abundance, direct DM detection, and collider experiment are shown as various shaded regions. It is seen from the figure that the uncharted parameter space indeed exists at the Z-funnel WIMP region. We will quantitatively discuss in the next section that what kind of role the future lepton collider (ILC) experiment play to prove this uncharted parameter space.

8.3 Future prospect of the Z-funnel WIMP

We discuss how the future lepton collider (ILC) as well as direct dark matter detection (XENONnT, LZ, etc.) experiments play important roles to search for the Z-funnel WIMP by quantitatively figuring out the sensitivity of these experiments on the uncharted model parameter space spanned by m_χ and $g_{\chi\chi Z}$.

8.3.1 Search at the ILC experiment

At the ILC experiment, important research channels are again the mono-photon and the invisible Z decay width searches. Since the analysis at the ILC experiment has many overlaps with that of the LEP experiment in Sec. 8.2.5, we mainly discuss the difference between these two experiments in some details.

8.3.1.1 Mono-photon search

As the ILC is a high-luminosity linear lepton collider, the **Beamsstrahlung effect** becomes important in addition to the ISR one. This effect is explained as follows. When the electron and positron beams collide with each other, the energy distribution of each beam bunch is not monochromatic at the initial beam energy but described by the function having a long tail at the low energy region. This is because, when the electron and positron beams are closer, the beams come under the influence of the electromagnetic fields of each other and lose their energies through the bremsstrahlung process. We involve this effect using the formula developed in Refs. [80–82]. With $x \equiv E/E_{\rm in}$, where $E_{\rm in}$ is original beam energy and E is the energy of each particle after Beamsstrahlung, the the energy distribution function of the electrons and positrons can be written [82]

$$\psi_e(x) = e^{-N_\gamma}\left[\delta(x-1) + \frac{e^{-\eta_x}}{x(1-x)}\,h(N_\gamma \eta_x^{1/3})\right], \tag{8.15}$$

where the distribution function is normalized to be $\int_0^1 dx\,\psi_e(x) = 1$, and $N_\gamma = \sqrt{3}\sigma_z\nu_{cl}(1+\Upsilon^{2/3})$, $\eta_x = (1/x-1)\,\kappa$, $h(u) = \sum_{n=1}^{\infty} u^n/[n!\Gamma(n/3)]$, respectively. $\Gamma(x)$ is the gamma function, $\nu_{cl} = 5\alpha^2\Upsilon/(2\sqrt{3}\,r_e\gamma_0)$, $\Upsilon = 5r_e\gamma_0 N/\{6\alpha\sigma_z(\sigma_x+\sigma_y)\}$, and $\kappa = 2/(3\Upsilon)$. Here, α is the fine structure constant, $r_e \simeq 2.82\times10^{-15}\,\mathrm{m}$ is the classical electron radius, $\gamma_0 = E_{\rm in}/(m_e c^2)$ with m_e being the electron mass and N is the total number of electrons/positrons in a bunch, and $\sigma_{x,y,z}$ are the beam size. For the case of ILC, $N \simeq 2\times10^{10}$, $\sigma_x = 729\,\mathrm{nm}$, $\sigma_y = 7.7\,\mathrm{nm}$ and $\sigma_z = 0.3\,\mathrm{mm}$, respectively, referring to the values in the technical design report of the ILC experiment [8]. For the case of the circular collider experiment (LEP), we can ignore this effect, because the shape of the beam is broad enough.

The ILC experiment has the option to control the **Polarization of electron and positron beams**. The size of the beam polarization is defined as

$$P_i \equiv \frac{N_R^i - N_L^i}{N_R^i + N_L^i}, \tag{8.16}$$

where the subscript i denotes the species of the particle (electron or positron), and $N_{R/L}^i$ is the number of the right/left-handed particle. At the ILC experiment, the polarization can be as large as $P_{e^-} = \pm0.8$, $P_{e^+} = \pm0.3$ [8] at maximum.

The method to take the **Detector effect** into account at the ILC experiment is essentially the same as that adopted for the LEP experiment. At the ILC experiment, the parameters for the detector effect is summarized in Table 8.2.

Polar angle	Energy threshold	Efficiency	Resolution
$\lvert\cos\theta\rvert < 0.98$	10 GeV	100 %	$0.011 \oplus 0.166/\sqrt{E_\gamma}$

Table 8.2: *Parameters for the detector effect. E_γ is the photon energy in GeV unit.*

In order to estimate the capability (expected sensitivity) of the ILC experiment to explore the Z-funnel WIMP, we assume that the experiment accumulates $1\,\mathrm{ab}^{-1}$ data with the polarization of $(P_{e^-}, P_{e^+}) = (0.8, -0.3)$ and another $1\,\mathrm{ab}^{-1}$ data with $(P_{e^-}, P_{e^+}) = (-0.8, 0.3)$, thus $2\,\mathrm{ab}^{-1}$ in total, during the running of the 250 GeV center of mass energy. On the other hand, on the theoretical prediction, we take the same procedure as the one adopted in Sec. 8.2.5.1. Only the difference between the two procedures is that the Beamsstrahlung effect in addition to the ISR effect is also convoluted with the signal and background cross sections, and the detector effect is taken into account with the parameters shown in Table 8.2, to evaluate the number of the signal and background events and compare them to the experimental data. Resultant cross sections including all the ISR, Beamsstrahlung, detector effects are shown in Fig. 8.8, where both the signal ($m_\chi = 40\,\mathrm{GeV}$ & $m_\chi = 50\,\mathrm{GeV}$ with $g_{\chi\chi Z} = 1$) and the background cross sections are depicted with several choices of the beam polarization.

We have compared the theoretical prediction with the expected ILC data by the method different from the one adopted in Sec. 8.2.5.1 (LEP analysis). This is because the so-called systematic uncertainty (denoted by δ in this thesis) is expected to be important to evaluate the capability of the ILC experiment properly to explore the Z-funnel WIMP. Since it is difficult to evaluate the systematic uncertainty rigorously before the experiment start and the uncertainty may have a correlation among the bins, we use an appropriate single energy bin for the likelihood analysis with the systematic uncertainty being δ =0.1 % and 1 %. The target energy bin is selected so that the photon energy is in between 10 GeV to X GeV with X being determined to maximize the significance at each DM mass. Then, the likelihood is defined by the following equation:

$$\begin{aligned}\Delta\chi^2 = &\mathrm{Max}\left(\frac{\{N(X) - N^{\mathrm{BG}}(X)\}^2}{\delta N^{\mathrm{BG}}(X)^2 + N^{\mathrm{BG}}(X)} \middle| 10\,\mathrm{GeV} \le E_\gamma \le X\,\mathrm{GeV} \right)\Big|_{\mathrm{Right}} \\ &+\mathrm{Max}\left(\frac{\{N(X) - N^{\mathrm{BG}}(X)\}^2}{\delta N^{\mathrm{BG}}(X)^2 + N^{\mathrm{BG}}(X)} \middle| 10\,\mathrm{GeV} \le E_\gamma \le X\,\mathrm{GeV} \right)\Big|_{\mathrm{Left}}, \quad (8.17)\end{aligned}$$

where $N(X)$ is the expected number of signal plus background events in between 10 GeV to X GeV, while $N^{\mathrm{BG}}(X)$ is the expected number of the background event in the same energy range. $\delta N^{\mathrm{BG}}(X)$ concerns the systematic uncertainty, which will be estimated as a product of a given uncertainty (δ = 0.1 % or 1 %) and the number of background event ($N^{\mathrm{BG}}(X)$). The subscripts "Right" and "Left" denote the polarizations $(P_{e^-}, P_{e^+}) = (0.8, -0.3)$ and $(P_{e^-}, P_{e^+}) = (-0.8, 0.3)$, respectively. For reference, the value of X making $\Delta\chi^2$ maximum is shown in Fig. 8.9 as a function of the DM mass for the beam polarization $(P_{e^-}, P_{e^+}) = (-0.8, 0.3)$ and $(0.8, -0.3)$. The result of the analysis, namely the expected sensitivity of the ILC experiment to prove the uncharted Z-funnel

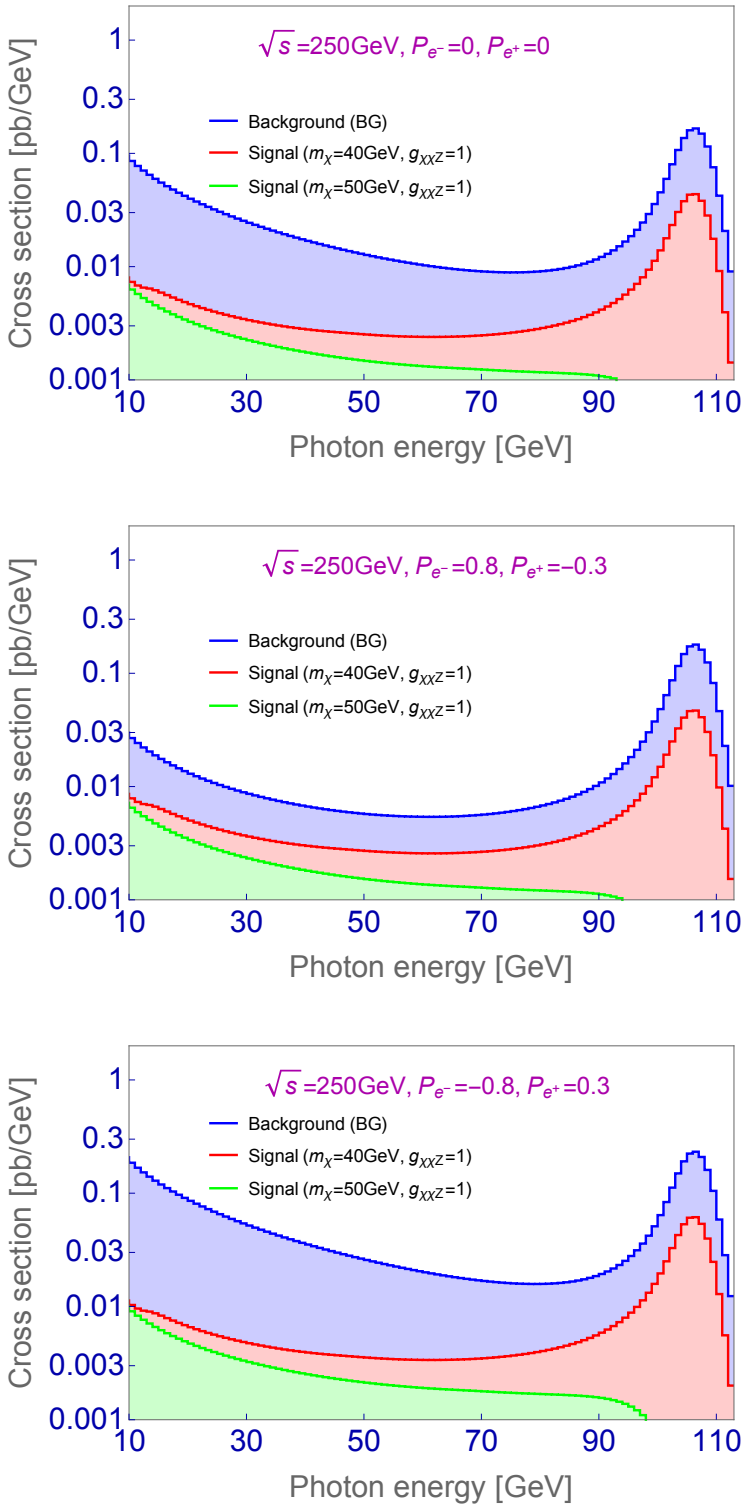

Figure 8.8: *Signal ($m_\chi = 40\,GeV$ & $m_\chi = 50\,GeV$ with $g_{\chi\chi Z} = 1$) and the background cross sections including all the ISR, Beamsstrahlung, detector effects with several choices of the beam polarization, $(P_{e^-}, P_{e^+}) = (0, 0)$, $(0.8, -0.3)$, and $(-0.8, 0.3)$.*

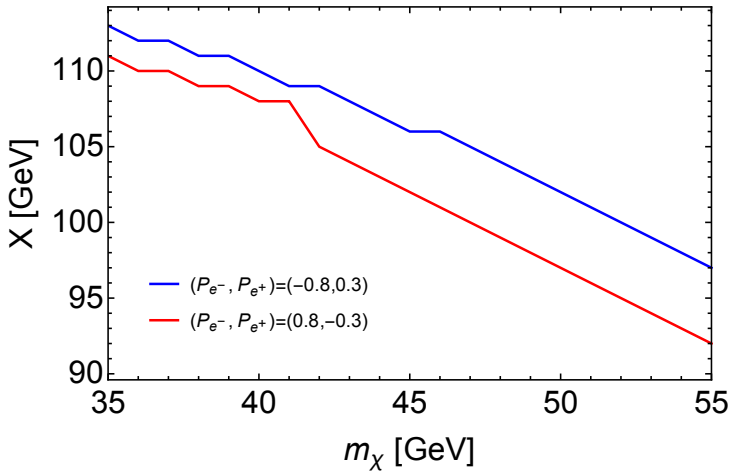

Figure 8.9: *The value of X making $\Delta\chi^2$ in eq. (8.17) maximum as a function of the DM mass m_χ for the beam polarization $(P_{e^-}, P_{e^+}) = (-0.8, 0.3)$ and $(0.8, -0.3)$.*

WIMP region by the mono-photon search is shown in Fig. 8.10 as orange dotted lines.

8.3.1.2 Invisible Z decay

At the ILC experiment, the precision of the Z boson width measurement could be improved if the so-called Giga-Z option is available. The expected sensitively of the measurement for the total Z boson decay width has been estimated to be $\delta\Gamma_Z = \pm 1\,\text{MeV}$ [83]. For reference, we also show the sensitivity of the measurement to search for the Z-funnel WIMP in Fig. 8.10 as a purple dotted line, which is obtained by requiring $\Gamma(Z \to \chi\chi) \leq 1\,\text{MeV}$. It is seen from the figure that the invisible Z boson width measurement covers the uncharted parameter region of the Z-funnel WIMP with the same magnitude as those of the above mono-photon search as long as the DM mass is less than half of the Z boson.

8.3.2 Search at future direct DM detection

The sensitivity of the direct DM detection to search for the Z-funnel WIMP is also improved in the near future. The LUX-ZEPLIN (LZ) experiment is one of such next-generation direct DM detection experiments, and it is possible to test the spin-dependent scattering cross section between the WIMP and a neutron down to $2.7 \times 10^{-43}\,\text{cm}^2$ when $m_\chi \simeq 45\,\text{GeV}$ [84]. The other next-generation experiment, the XENONnT experiment, has also very good sensitivity; the scattering cross section down to $2.2 \times 10^{-43}\,\text{cm}^2$ can be probed when $m_\chi = 50\,\text{GeV}$ [85]. Importantly, these experiments can cover the entire uncharted region of the Z-funnel WIMP shown in Fig. 8.7, as seen in Fig. 8.10 as dotted black lines.

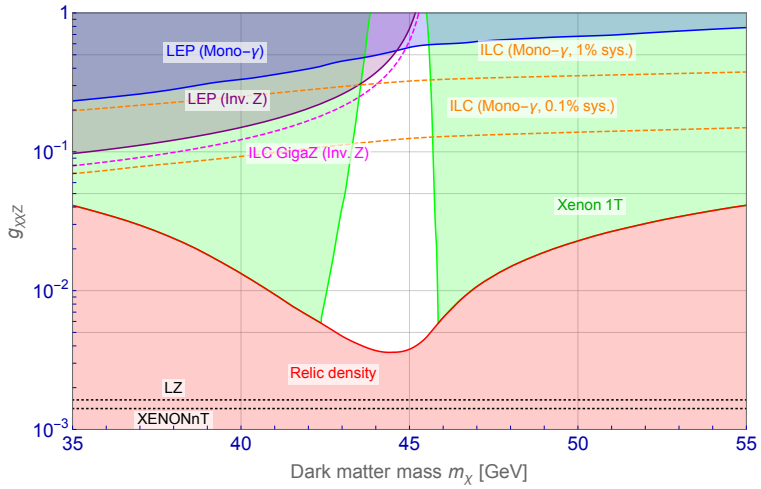

Figure 8.10: *The expected sensitivity of the ILC experiment through the mono-photon search (orange dotted lines) and the invisible decay width searches (purple dotted line). The expected sensitives of the direct DM detection experiments, XENONnT and LZ experiments, are also shown as black dotted lines. We concerned 90 % C.L here.*

8.3.3 Future prospects of the Z-funnel WIMP

Future prospects of the Z-funnel WIMP is summarized in Fig. 8.10, where expected sensitivities of future experiments to explore the WIMP, namely those by the mono-photon search and the invisible Z decay width search at the ILC experiment as well as the future direct DM detection experiments (XENONnT and LZ), are shown by various dotted lines. It is seen from the figure that all the future experiments are more or less probe the uncharted parameter region of the Z-funnel WIMP. We will discuss it in more details in the next section.

8.4 Summary of the Z-funnel WIMP

We have presented the expected sensitivity to search for the Z-funnel WIMP at the future lepton collider (ILC) experiment. We have adopted the effective operator method where the interaction between the singlet Majorana WIMP (χ) and the Z boson is interacted via the dimension-six operator $(\bar{\chi}\gamma_\mu\gamma_5\chi)(H^\dagger iD^\mu H)/2+h.c.$ The final result of our analysis thus is parametrized by only two new physics parameters; WIMP mass (m_χ) and effective WIMP-Z coupling ($g_{\chi\chi Z}$).

Through this study, we discussed the possibility of probing the Z-funnel WIMP with its mass region of $35-55$ GeV using the mono-photon plus missing energy signal at the future lepton collider (ILC) experiment. We have done a comprehensive signal-background analysis of the searches considering various collider features, such as the beam polarization, beamsstrahlung, initial-state-radiation and detector effects. While doing this analysis we have taken into account other important constraints on the parameters of this scenario coming from the mono-photon and Z-invisible width searches at the LEP experiment.

The 90 % C.L. expected limit is shown on the $(m_\chi, g_{\chi\chi Z})$-plane for the ILC experiment at the 250 GeV running with $2\,\mathrm{ab}^{-1}$ integrated luminosity. We have performed an analysis including the systematic uncertainty of the experiment by estimating $\Delta\chi^2$ with the 0.1 % and 1 % uncertainties, and presented the result on the plane. This limit is compared with those obtained by the Z invisible width measurement, direct DM detection and relic abundance of the WIMP.

It is important to mention that the direct DM detection experiments such as XENON1T have put a severe constraint on the Z-portal WIMP. In fact, if the WIMP is a dominant component of the DM in the present universe and thus we adopt the assumption of the standard local DM density $\rho_{\mathrm{DM}} = 0.3\,\mathrm{GeV/cm}^3$ for the WIMP, the current constraint from the XENON1T experiment has already excluded the reach of the future lepton collider. As discussed in Sec. 8.2.2, however, the direct DM search constraint critically depends on assumption. For instance, if the coupling $g_{\chi\chi Z}$ is larger and the WIMP is only a subdominant component of the DM in the present universe, the present direct DM detection cannot cover the mass range $m_\chi \in [42, 46]\,\mathrm{GeV}$. In addition, there is potentially a large astrophysical uncertainty in the local DM density, which also significantly affects the reach of the direct DM detection experiments. The future lepton colliders such as ILC can probe the WIMP DM without such uncertainties.

We have also studied the future prospect to search for the Z-funnel WIMP at the direct DM detection, and found that it is possible to discover the WIMP even if we assume conservative cosmological setup, namely the WIMP contributes to the DM density of the present universe in part according to its thermal relic abundance. If the future direct detection experiment discovers the WIMP, the role of the future lepton collider becomes particularly important, as it provides unique opportunity to identify the character of the WIMP. In conclusion, this study reveals the prospect of the Z-funnel WIMP detection in the future lepton collider, which is the most conservative test and confirmation of the WIMP.

Chapter 9

Leptophilic WIMP

In this chapter, we consider the SM gauge singlet Majorana fermion DM (χ) in Leptophilic models, where the DM couples only to the SM leptons. In the EFT framework, relevant operators for the Leptophilic WIMP are written as

$$\mathcal{O}_L = (\bar{\chi}\gamma^\mu\gamma_5\chi)(\bar{L}_i\gamma_\mu L_j) \tag{9.1}$$
$$\mathcal{O}_E = (\bar{\chi}\gamma^\mu\gamma_5\chi)(\bar{E}_i\gamma_\mu E_j). \tag{9.2}$$

Since DM and the SM leptons are fermionic, mediator particles that give the above interactions from renormalizable theory must be scalar or vector. In order to make vector mediators massive, we need another scalar field, and so we concentrate on the scalar mediator case from the viewpoint of minimality. The scalar mediator particle must be odd under the new Z_2 symmetry and must carry the exact quantum numbers of the SM leptons, as we will discuss later in more details. In the minimal renormalizable extension of the SM, one can either have three generations of the $SU(2)_L$ doublet scalar mediator corresponding to the left-handed leptons or three generations of the $SU(2)_L$ singlet ones corresponding to the right-handed SM leptons. It is to be mentioned that we will only consider lepton flavor blind interactions of the DM particle for sake of simplicity. The comprehensive analysis of such Leptophilic WIMP models including the future lepton collider analysis has not been done in any previous studies.

This chapter is organized as follows. In section 9.1, we describe the Lagrangian for the SM gauge singlet Majorana fermionic WIMP and its Leptophilic interaction via the scalar mediators by explaining all the relevant parameters of the potential. Next, in section 9.2, we discuss all the relevant constraints at present including the vacuum stability condition, the relic abundance condition and constraints from the LEP and LHC experiments. We show the allowed parameter space for each model that satisfy all the present constraints. In section 9.3, we show the sensitivity of future colliders to explore the presently surviving parameter space in each model with an emphasis on the mono-photon search at the ILC 250 GeV experiment. Finally, in section 9.4, we briefly discuss the combined model scenario consisting both the doublet and singlet mediators. Here, we present the calculation for anomalous muon magnetic moment and show the the allowed model parameter region that is capable of explaining the

Mediator Type	Spin	$SU(3)_C$	$SU(2)_L$	$U(1)_Y$	Z_2
Scalar	0	**1**	**1**	-1	-1
Scalar	0	**1**	**2**	$-1/2$	-1
Vector	1	**1**	**1**	-1	-1
Vector	1	**1**	**2**	$-1/2$	-1
Vector	1	**1**	**1**	0	$+1$

Table 9.1: *Possible quantum numbers of the mediator for the Leptophilic WIMP*

experimental anomaly, and discuss the role of the future lepton collider to test the region. Lastly, in section 9.5 we summarize our findings and conclude.

9.1 Minimal models of the Leptophilic WIMP

We consider minimal and renormalizable models to explore the interaction of a singlet Majorana fermion WIMP that only talks to the SM leptons. In the simplest system composed of the WIMP and the SM particles, no renormalizable interaction exists due to the presence of the SM gauge symmetry and the newly imposed Z_2 symmetry making the WIMP stable. The WIMP (SM particles) is charged odd (even) under the Z_2. Hence, an additional new particle (mediator) is introduced. Possible quantum numbers of the mediator for a renormalizable interaction between the WIMP and the SM leptons are shown in Fig.9.1.

Renormalizable models including a vector mediator are, however, complicated in general, for it should contain the "Higgs mechanism" to make the mediator massive and not a few new (chiral) fermions must be introduced to make the models anomaly free. We therefore focus on the models including a scalar mediator; the mediator particle is either a SU(2) scalar doublet with U(1) hypercharge $-1/2$ ($Q = T_3 + Y$) which we named left-(handed) mediator, or a SU(2) scalar singlet with U(1) hypercharge -1, namely right-mediator. Analogous to the three generation of the SM leptons, for each case, there are three scalar mediators corresponding to each lepton flavor. For the sake of simplicity, we consider a flavor-universal scenario and define the scalar masses by only one degenerate mass parameter. We will explain it later in more details.

In the following sections, we will discuss phenomenology of individual model perspective with left- or right-mediators. The effect of introducing both types of the mediators is also discussed in Sec. 9.4 including its motivation.

9.1.1 Left-mediator model

Left-mediator is the SU(2) scalar doublet that has charged and neutral components analogous to the left-handed charged-lepton and neutrino in the SM. The complete Lagrangian for the left-mediator consists of two additional parts besides the usual SM Lagrangian ($\mathcal{L}_{\rm SM}$) and the kinetic terms of the WIMP and the scalar mediator. These are respectively the interaction between the

WIMP and the mediator ($\mathcal{L}_{\mathrm{DM}\,L}$) and the scalar potential (V_L) describing the self-interaction of the new scalar doublet and its interaction with the Higgs boson:

$$\begin{aligned}
\mathcal{L}_L &= \mathcal{L}_{\mathrm{SM}} + \frac{1}{2}\bar{\chi}\left(i\partial\!\!\!/ - m_\chi\right)\chi + (D_L^\mu \tilde{L}_i)^\dagger (D_{L\,\mu}\tilde{L}_i) + \mathcal{L}_{\mathrm{DM}\,L} - V_L(H, \tilde{L}_i), \quad (9.3)\\
\mathcal{L}_{\mathrm{DM}\,L} &= -y_L \bar{L}_i \tilde{L}_i \chi + h.c,\\
V_L &= m_{\tilde{L}}^2 |\tilde{L}_i|^2 + \frac{\lambda_L}{4}|\tilde{L}_i|^4 + \lambda_{LH}|\tilde{L}_i|^2|H|^2\\
&\qquad + \lambda'_{LH}(\tilde{L}_i^\dagger \tau^a \tilde{L}_i)(H^\dagger \tau^a H) + [\frac{\lambda''_{LH}}{4}(\tilde{L}_i^\dagger H^c)^2 + h.c.].
\end{aligned}$$

where a summation over the repeated indices is implicitly assumed, and the index i spans lepton flavors (e, μ, τ). Additionally, χ describes the Leptophilic WIMP field, L_i is the SM lepton doublet, H is the Higgs doublet ($H^c \equiv i\sigma_2 H^*$), $\tilde{L}_i$ is the scalar mediator doublet whose quantum numbers matches with L_i, τ^a is Pauli matrices and D_L^μ is the covariant derivative acting on the mediator $\tilde{L}_i$.

Since we are assuming lepton flavor universality, the Lagrangian parameters y_L, $m_{\tilde{L}}$, λ_L, λ_{LH}, λ'_{LH} and λ''_{LH} are common in different flavors. To avoid sizable contribution to tiny neutrino masses, we impose the lepton number symmetry. This is equivalent to assign the lepton number to the mediator particle, and the term proportional to λ''_{LH} is prohibited. After the electroweak symmetry breaking with $v \simeq 246\,\mathrm{GeV}$ being the vacuum expectation value of the Higgs field, the physical mass of the each component of the scalar mediator is

$$m_{\tilde{e}_L}^2 = (\lambda_{LH} + \lambda'_{LH})\frac{v^2}{2} + m_{\tilde{L}}^2, \quad (9.4)$$

$$m_{\tilde{\nu}_L}^2 = (\lambda_{LH} - \lambda'_{LH})\frac{v^2}{2} + m_{\tilde{L}}^2, \quad (9.5)$$

with $\tilde{L}_i = (\tilde{\nu}_i, \tilde{e}_{L\,i})^T$. The nomenclature of the physical masses are done in analogy to the superpartners of the leptons in supersymmetric SMs (sleptons).

9.1.2 Right-mediator model

Akin to Left-mediator model, one can write down the full Lagrangian for the right-mediator where instead of a doublet the mediator is a SU(2) singlet with the same quantum number as the right-handed SM charged leptons:

$$\begin{aligned}
\mathcal{L}_R &= \mathcal{L}_{\mathrm{SM}} + \frac{1}{2}\bar{\chi}\left(i\partial\!\!\!/ - m_\chi\right)\chi + (D_R^\mu \tilde{R}_i)^\dagger (D_{R\,\mu}\tilde{R}_i) + \mathcal{L}_{\mathrm{DM}\,R} - V_L(H, \tilde{R}_i), \quad (9.6)\\
\mathcal{L}_{\mathrm{DM}\,R} &= -y_R \bar{E}_i \tilde{R}_i \chi + h.c,\\
V_R &= m_{\tilde{R}}^2 |\tilde{R}_i|^2 + \frac{\lambda_R}{4}|\tilde{R}_i|^4 + \lambda_{RH}|\tilde{R}_i|^2|H|^2,
\end{aligned}$$

where E_i describes the SM charged lepton singlet, $\tilde{R}_i$ is the scalar mediator singlet whose quantum numbers resembles E_i and D_R^μ is the covariant derivative acting on the mediator $\tilde{R}_i$. Here also, we consider all the parameters y_R,

$m_{\tilde{R}}$, λ_R and λ_{RH} to be the same for different lepton flavors. Taking the same nomenclature as above, the physical mass for the right-mediator is given by

$$m^2_{\tilde{e}_R} = \lambda_{RH}\,\frac{v^2}{2} + m^2_{\tilde{R}}. \tag{9.7}$$

9.2 Present status of the Leptophilic WIMP

In this section, we discuss all relevant theoretical and experimental constraints imposed to the Leptophilic models defined in the previous section, and figure out the present status of the Leptophilic WIMP by integrating all the constraints.

9.2.1 Theoretical constraint

Since we introduce new scalar fields (mediators) in the Leptophilic WIMP models, the stability of the scalar potential has to be ensured. The complete scalar potential for the model includes the SM Higgs potential in addition to V_L,

$$V_L^{\rm Full}(H,\,\tilde{L}) = \mu^2|H|^2 + \frac{\lambda}{4}|H|^4 + V_L(H,\,\tilde{L}), \tag{9.8}$$

where the explicit form of V_L is given in eq. (9.3). First, we obtain the following constraints because of the request that the potential is bounded from below:

$$\lambda > 0, \quad \lambda_L > 0, \quad \sqrt{\lambda\,\lambda_L} > 2\,(|\lambda'_{LH}| - \lambda_{LH}). \tag{9.9}$$

Next, since the Z_2 symmetry should not be broken after the electroweak symmetry breaking to make the WIMP stable at present universe, the scalar mediator should not develop any vacuum expectation value. Hence, we obtain the other constraint from the request that the masses in eq. (9.5) must be positive:

$$-\lambda\, m^2_{\tilde{L}}/(2\,\mu^2) > |\lambda'_{LH}| - \lambda_{LH}. \tag{9.10}$$

Here, v is replaced by $v = (-4\mu^2/\lambda)^{1/2}$. It is then possible to prove that our vacuum, namely the potential minimum with the vacuum expectation value of H being $\langle H\rangle = (0, v/\sqrt{2})^T$ and that of the scalar mediator being $\langle\tilde{L}\rangle = 0$, becomes a global one if the constraints written in eq.(9.9) and eq.(9.10) are satisfied.

Akin to the left-mediator model discussed above, the constraints making our vacuum stable in the right-mediator model is summarized as follows:

$$\lambda > 0, \quad \lambda_R > 0, \quad \sqrt{\lambda\,\lambda_R} > -\lambda_{RH}, \quad -\lambda\, m^2_{\tilde{R}}/(2\,\mu^2) > -\lambda_{RH}. \tag{9.11}$$

It makes our vacuum being stable, namely the global minimum of the potential.

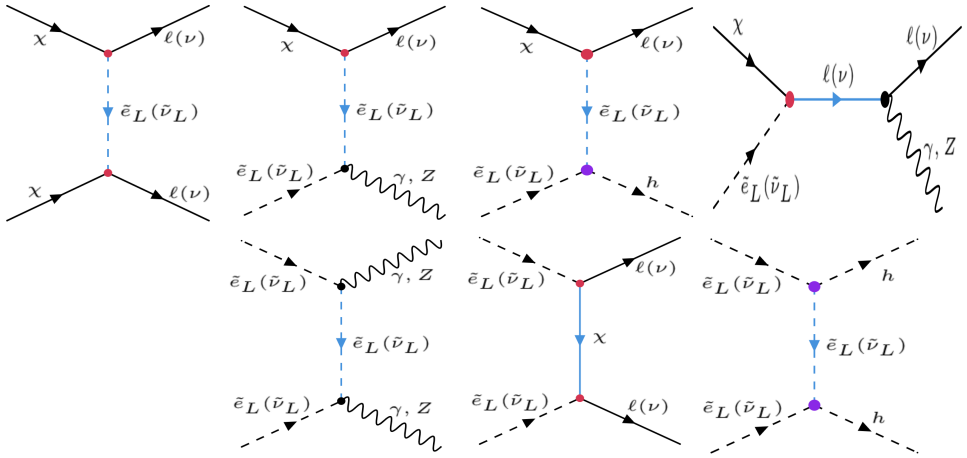

Figure 9.1: Some illustrative Feynman diagrams for self-annihilation and co-annihilation processes to calculate the relic abundance of the WIMP in the left-mediator model. Red colored vertices corresponds to Yukawa coupling y_L, while magenta vertices are proportional to the scalar coupling λ_{LH}. For the right mediator model, $\tilde{e}_L$ is replaced by $\tilde{e}_R$ and there is no neutral partner.

9.2.2 Relic abundance

In the Leptophilic WIMP models, when the scalar mediator is much heavier than the WIMP, the WIMP only annihilates into the SM leptons and contributes to the relic abundance, as shown by the top-left diagram in Fig. 9.1 for the left-mediator model. In this limit, the WIMP annihilation cross section only depends on the WIMP mass (m_χ), the mediator mass ($m_{\tilde{e}_L}$ & $m_{\tilde{\nu}_L}$ or $m_{\tilde{e}_R}$) and the Yukawa coupling (y_L or y_R) for the left- or right-mediator model, respectively. On the other hand, when the mediator mass and the WIMP mass are degenerate within 10%, the relic density is controlled by so-called co-annihilation processes [86], which is summarized in Appendix. C in more details. The scalar quartic couplings between the mediator and the SM Higgs also become important in this limit for the relic density calculation, as shown by several diagrams in Fig. 9.1 for the left-mediator model. In our analysis, we scanned over the model parameter space considering both the limits that yield the correct relic abundance by the WIMP self-annihilation and the co-annihilation processes. The relic density is calculated numerically using the code **micrOMEGAs-v5** [69].

Uncertainty at the relic density calculation due to the SM thermodynamics has recently been estimated in refs. [67, 87], where it shows that the uncertainty of the effective massless degrees of freedom can be as large as 10%, depending on the temperature of the universe. This in turn induces $\mathcal{O}(5\%)$ uncertainty of the WIMP density during the freeze-out. We have thus incorporated this uncertainty in the **micrOMEGAs** code using the data provided by ref. [87].

9.2.3 Direct and Indirect detections

Direct DM detection is known to be very powerful to search for various WIMP candidates. The detection, however, relies on the scattering between WIMP and nucleus, so that it is not efficient for the Leptophilic WIMPs. One might think that such a scattering emerges radiatively through one-loop diagrams where the SM leptons are propagating in the loop, and it still might enable us to search for the Leptophilic WIMP. The scattering cross section of such a process, however, turns out to be too small to be detected at the present and near future detectors when the Leptophilic WIMP is a Majorana fermion [88]. Hence, we do not include any constraints from the direct WIMP detection in our analysis.

On the other hand, the WIMP annihilation cross section for a singlet Majorana WIMP is p-wave suppressed, namely the annihilation cross section is suppressed by the incident WIMP. It is therefore insignificant at the present universe, and the indirect detection constraint is also irrelevant in the models.

9.2.4 Mediator production at the LEP and LHC experiments

It is difficult to directly probe the Leptophilic WIMP at the current Large Hadron Collider (LHC) since it only interacts with the SM lepton and it is a gauge singlet. However, the mediator particle is a charged scalar and thus it is accessible both at the lepton and hadron colliders. The LEP experiment [89] has searched for supersymmetric charged sleptons which decays dominantly to a SM lepton and a bino-like Lightest Supersymmetric (SUSY) Particle (LSP) neutralino. For the right-handed smuon pair-production, the LEP experiment excluded smuon masses below 94 GeV [90] for a neutralino-smuon mass gap above 10 GeV. This is a model-independent bound on leptonic charged scalars, and thus we impose this constraint on the right-mediators and as a conservative limit on the left-mediators. The excluded region is shown as the gray-shaded area in Fig. 9.2.

The LHC experiment has also looked for such a simplified scenario where charged sleptons with 100% branching ratio (BR) to its SM lepton partner and bino-like LSP are produced. After the run 2 of the LHC at 13 TeV center of mass energy, the ATLAS collaboration has reported the 95% exclusion limit on the left and right-handed sleptons at 139 fb^{-1} luminosity [91] for the slepton-neutralino mass difference more than 80 GeV. Dedicated search for compressed spectra where the slepton-neutralino mass difference become as low as 550 MeV for a slepton mass around 70 GeV has also been done [92] and the 95% C.L. exclusion limit is presented. In Fig. 9.2, we show this excluded region for the smuon pair production as yellow and green shaded region for the left and right-handed smuons respectively. The earlier limit from the 8 TeV run of the LHC experiment has also been included in the contours. Here, we would like to remind us that we only consider the degenerate, flavor universal case and therefore we use the most-sensitive smuon search limit on the models as the strongest one.

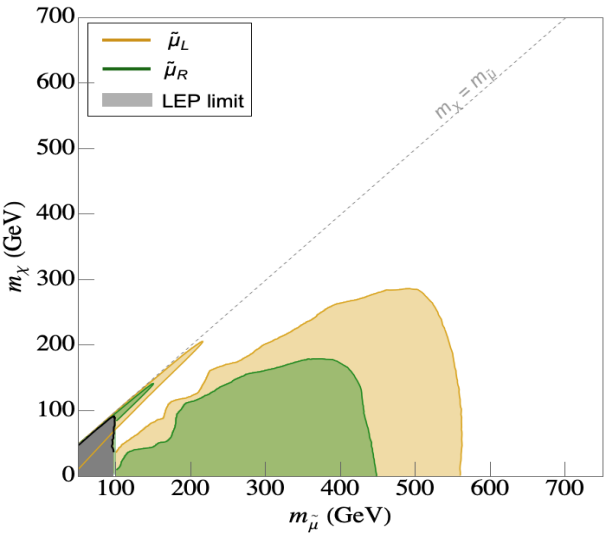

Figure 9.2: *The 95% C.L. exclusion limit on the smuon-neutralino mass plane from the smuon pair production at the LEP-II and LHC (8 and 13 TeV runs) experiments.*

9.2.5 Higgs to Diphoton

With the accumulation of more data, the LHC Higgs data has been updated with unprecedented accuracy and it shows an increasing affinity to the SM value. In our model, the tree-level Higgs decay branching will exactly follow the SM value. However, the left and right charged mediator can significantly contribute to the loop induced Higgs to diphoton decay mode [93–95]. The latest constraint on the Higgs to diphoton signal strength is given by the CMS collaboration as $\mu_{\gamma\gamma} = 1.18^{+0.17}_{-0.14}$ [96]. The signal strength is defined as the ratio of the Higgs production cross-section times its BR to the gamma gamma mode with the corresponding SM value. Since, the exotic charged mediator does not contribute to the production channel and considering that the total decay width only changes negligibly due to the diphoton mode, the signal strength in our case can be approximated as the ratio between the partial decay width of the Higgs to diphoton decay to its SM value. Now, the charged mediator coupling to the SM Higgs is given by the scalar quartic couplings $(\lambda_{LH} + \lambda'_{LH})$ for the left-mediator and λ_{RH} for the right-mediator. In fact, the partial decay width is be written as [97],

$$\Gamma(h \to \gamma\gamma) = \frac{G_F\, \alpha^2 m_h^3}{128\sqrt{2}\pi^3} \left| \sum_i A_i(\tau_i) \right|^2 , \tag{9.12}$$

where G_F is the Fermi constant, α is the fine structure constant, m_h is the mass of the Higgs boson, and τ_i is defined as $\tau_i = m_h^2/(4m_i^2)$ with m_i being the mass of a loop particle. The amplitude from various particles are given as follows:

$$\begin{aligned} A_W &= g_{hWW} F_1(\tau_W), \\ A_f &= N_c Q_f^2 g_{hff} F_{1/2}(\tau_f), \\ A_{\tilde{e}_L} &= (\lambda_{LH} + \lambda'_{LH})(m_Z^2/m_{\tilde{e}_L}) F_0(\tau_{\tilde{e}_L}), \\ A_{\tilde{e}_R} &= \lambda_{RH}(m_Z^2/m_{\tilde{e}_R}) F_0(\tau_{\tilde{e}_R}), \end{aligned} \tag{9.13}$$

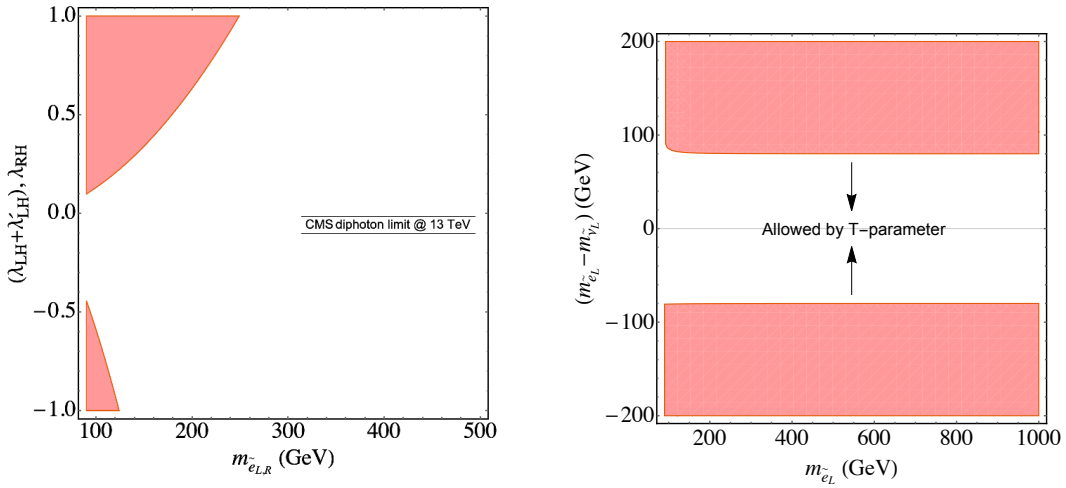

Figure 9.3: *The region region shaded by red color depicts the excluded parameter space at 95% C.L. limit from the present Higgs to di-photon decay width measurement (left) and the electroweak precision (oblique T-parameter) constraint (right).*

where g_{hii} denote the coupling between the particle i and the Higgs boson in the SM and N_c is the color charge degree of freedom. Functions $F_i(\tau)$ are written

$$\begin{aligned} F_1(\tau) &= [2\tau^2 + 3\tau + 3(2\tau-1)f(\tau)]/\tau^2, \\ F_{1/2}(\tau) &= -2[\tau + (\tau-1)f(\tau)]/\tau^2, \\ F_0(\tau) &= [\tau - f(\tau)]/\tau^2, \\ f(\tau) &= \arcsin^2(\tau^{1/2})\,\theta(1-\tau) \\ &- (1/4)\log^2\left(\frac{1+\sqrt{1-\tau^{-1}}}{1-\sqrt{1-\tau^{-1}}} - i\pi\right)\theta(\tau-1). \end{aligned} \tag{9.14}$$

In Fig. 9.3 (left), we show the excluded parameter space in the charged mediator mass vs its coupling to the Higgs boson at the 95% C.L. as a red-shaded region.

9.2.6 Oblique Parameter

In the left-mediator case, the scalar mediator is a doublet under the SM $\mathrm{SU}(2)_L$ gauge group. Therefore, it can significantly contribute to the self-energy correction of the SM gauge bosons. Hence, an additional constraint from the oblique T-parameter value that combines the electroweak precision data should be considered [98–100]. It is important to notice that unlike the usual inert Higgs doublet extensions, here the T-parameter puts a stringent constraint on the mass splitting between the charged and the neutral left-mediator due to the absence of the additional scalar quartic term proportional to λ''_{LH}. The latest value of T-parameter from new physics is restricted to be $\Delta T = 0.05 \pm 0.06$ [90]. The T-parameter is defined as $\alpha T = \Pi_{WW}(0)/m_W^2 - \Pi_{ZZ}(0)/m_Z^2$ with $\Pi_{WW}(0)$ and $\Pi_{ZZ}(0)$ being the self-energies of the W and Z bosons at zero momentum transfer. The contribution from each left mediator particle can be written

as [101]

$$\Delta T = \frac{1}{16\pi^2 \alpha v^2}\left(\frac{m^2_{\tilde{e_L}} + m^2_{\tilde{\nu}}}{2} - \frac{m^2_{\tilde{e_L}} m^2_{\tilde{\nu}}}{m^2_{\tilde{e_L}} - m^2_{\tilde{\nu}}} \log \frac{m^2_{\tilde{e_L}}}{m^2_{\tilde{\nu}}}\right) . \tag{9.15}$$

In Fig. 9.3 (right panel), we show the 95% exclusion limit on the charged vs the charged to neutral mass difference plane. As is evident from the figure that one can not get a mass gap larger than 80 GeV for all charged scalar mass value.

9.2.7 Present status of the Leptophilic WIMP

Following all the constraint on the previous subsections, we set the range of scan for the model parameters. First of all, we restrict that the mediator mass is greater than the WIMP mass, i.e. $m_\chi < \{m_{\tilde{e}_L,}, m_{\tilde{\nu}_L}, m_{\tilde{e}_R}\}$, and fix the quartic parameters λ_{LL}, $\lambda_{RR} = 1$ which do not contribute to any physical observables and only required to be positive from the vacuum stability conditions given in section 9.2.1. The other relevant parameters are varied in the scan as follows:

$$\begin{aligned} -1 \leq &\ \lambda_{LH} &\leq 1, \\ -1 \leq &\ \lambda'_{LH} &\leq 1, \\ 0 \leq &\ y_L &\leq 1, \\ 1\,\text{GeV} \leq &\ m_\chi &\leq 2\,\text{TeV}, \\ 90\,\text{GeV} \leq &\ m_{\tilde{e}_L} &\leq 2\,\text{TeV}, \end{aligned} \tag{9.16}$$

for the left-mediator model. On the other hand, in the right-mediator model, the relevant model parameters are varied in the scanning as follows:

$$\begin{aligned} -1 \leq &\ \lambda_{RH} &\leq 1, \\ 0 \leq &\ y_R &\leq 1, \\ 1\,\text{GeV} \leq &\ m_\chi &\leq 2\,\text{TeV}, \\ 90\,\text{GeV} \leq &\ m_{\tilde{e}_R} &\leq 2\,\text{TeV}. \end{aligned} \tag{9.17}$$

In order to figure out the present status of the Leptophilic WIMP, we have performed the parameter scanning in each model (according to the above scanning range) taking the relic abundance condition as well as constraints from the Higgs to diphoton and the oblique T-parameter measurements into account. For the Higgs to diphoton and the oblique T-parameter constraints, we have directly used the 95% C.L. exclusion contours on our scanned parameter space. For the relic abundance condition for the WIMP, because the experimental uncertainty of the dark matter relic abundance is much weaker than the uncertainty in the theoretical calculation that comes from the massless degrees of freedom in the early universe, we have considered the 2σ uncertainty in the theoretical calculation and choosing the central value of $\Omega h^2 = 0.120$ obtained by the PLANCK experimental data. Concerning constraints from the mediator production at the LEP and LHC experiments, we have directly applied their 95% C.L. exclusion contours on the result of the aforementioned scanning, as seen in Fig. 9.4.

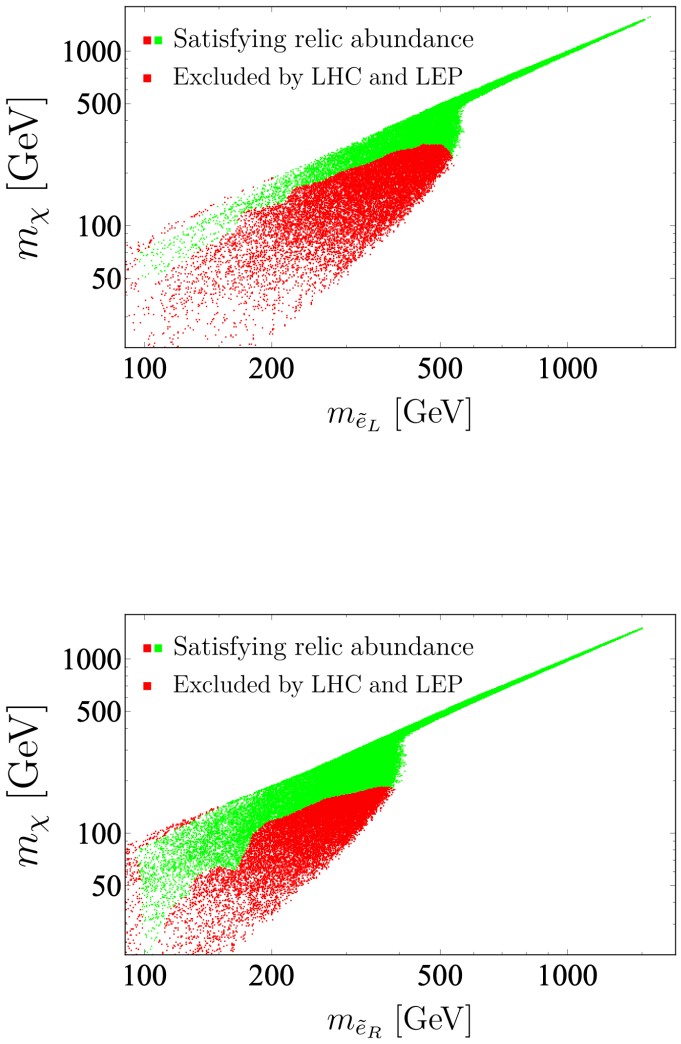

Figure 9.4: *Allowed parameter space at 95% C.L. from theoretical and experimental constraints on the* $(m_\chi, m_{\tilde{e}_L})$*- and* $(m_\chi, m_{\tilde{e}_R})$*-planes for the left-mediator (top panel) and right-mediator (bottom panel) models, respectively See text for more details.*

In Fig. 9.4, we show the allowed parameter space for the correct relic abundance in the $(m_{\tilde{e}_{L(\tilde{e}_R)}} - m_\chi)$ plane for both the left and right-mediator models. The region spread by points are allowed by the present relic abundance condition and constraints from the Higgs to diphoton and the oblique T-parameter measurements at 95% C.L. It is evident from the figure that at large WIMP mass, only degenerate masses for the WIMP and the mediator can satisfy the correct relic abundance via the co-annihilation mechanism. On the other hand, as the WIMP mass increases, the Yukawa coupling needs to be large enough to keep the annihilation cross-section around 1 pb since the annihilation cross-section is proportional to $y_L^4\ (y_R^4)/m_\chi^2$ unless the co-annihilation comes into play.

In the left-mediator model, the co-annihilation takes the dominant role when the WIMP mass is $m_\chi > 500\,\mathrm{GeV}$, while for the right-mediator case, it appears beyond 400 GeV. The presence of an additional degree of freedom ($\tilde{\nu}_L$) in the left-mediator case helps in allowing larger WIMP mass with the correct relic abundance via the self-annihilation mechanism of the WIMP. In the co-annihilating degenerate mass region, the scalar quartic coupling of the mediator become effective and the correct relic abundance for the large WIMP mass is achieved for the largest value of the scalar coupling $\lambda_{LH\,(RH)} \sim 1$ which renders an upper bound on the co-annihilating mass range at 1.5 TeV. Furthermore, the region spread by red points in the figure depicts the excluded region by the direct searches of the scalar mediator at the LHC experiment described in section 9.2.4. As expected, the self-annihilation region has largely been excluded by the direct searches, while the co-annihilation region survives and will become important to probe in future lepton colliders, as we show in the following section in details.

9.3 Future prospects of the Leptophilic WIMP

We discuss the prospect of probing the Leptophilic WIMP at future colliders, the High-luminosity LHC (HL-LHC) and the international linear collider (ILC).

First of all, the future projection of the **Higgs to diphoton decay** mode predicts that it will reach an accuracy at around 2% level at the HL-LHC [102]. Therefore, the coupling of the charged scalar mediators to the Higgs will be further constrained. In Fig. 9.5, we show the projected limit from the Higgs to diphoton searches at the HL-LHC experiment assuming that the uncertainty will be reduced to 2% while the central value being equal to the SM value. On the other hand, currently there are no projected reach that has been reported by the HL-LHC working group for the direct slepton production search.

When the WIMP mass is lower than half of the center of mass energy, the mono-γ channel works effectively because relatively large $y_{L/R}$ couplings are needed to achieve the observed relic density. However, when the WIMP mass and the mediators masses are degenerate, it become difficult to search for the WIMP using the mono-γ channel because $y_{L/R}$ can be small due to the coannihilation mechanism. In such a case, we can use the channel with the pair production of the mediator particles associated with an additional high energy photon. The mediator particles will finally decay into an electron/positron and a WIMP. If the masses of the WIMP and the mediator particles are highly degenerate, they emit soft electron/positron and that channel can be counted as a mono-photon event. Then, the cross section of this channel is not suppressed by $y_{L/R}$ anymore because of the existence of the Drell-Yan process, and we can obtain a severe constraint also for the co-annihilation region. The main background comes from the mono-photon associated with the pair production of neutrinos.

We have calculated the cross sections of the signal and the background events for each energy bin by integrating the analytic formula of the differential cross

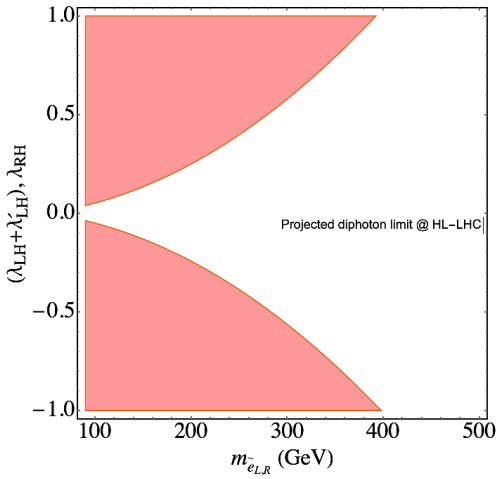

Figure 9.5: *The region shaded by red color depicts the projected reach of the parameter space at 95% C.L. from the future sensitivity of the Higgs to di-photon decay width measurement at the HL-LHC experiment. See text for details.*

section involving all the ISR, Beamsstrahlung, and detector effects discussed in Chapter 8. The result is shown in Fig. 9.6, where the region spread by points are the presently surviving parameter space at 95 % C.L., namely the same as the one spread by green points in Fig. 9.4, while the region spread by magenta points in the figure is the 95% C.L expected reach at the 250 GeV ILC experiment with 500 fb^{-1} luminosity obtained by the mono-photon search assuming 0.1 % systematic uncertainty. To perform the signal-background analysis for the ILC searches, we followed the approach in the previous chapter 8. It can be seen from the figure that the projected reach for the Leptophilic WIMP mass at 95% C.L from the mono-photon search analysis is around 110 GeV. Since the improvement of the Higgs to diphoton decay width measurement at the HL-LHC experiment unfortunately affects little about the model parameter region, in particular the one with the EW scale WIMP and mediator. If anything, the search of the direct mediator production will be more important than the Higgs decay width search at the HL-LHC experiment especially when the WIMP and mediator are well above the EW scale, playing a complementary role to the ILC search.

9.4 Combined model with left- and right-mediators

We briefly discuss the consequences of considering the combined mediator scenario in this section. The Lagrangian containing both the mediators is as fol-

lows:

$$\begin{aligned}
\mathcal{L} &= \mathcal{L}_{SM} + \mathcal{L}_{\rm DM} + (D_{\mu L}\tilde{L}_i)^\dagger (D_L^\mu \tilde{L}_i) \\
&\quad + (D_{\mu R}\tilde{E}_i)^\dagger (D_R^\mu \tilde{E}_i) - V(\phi, \tilde{L}_i, \tilde{E})\,. \qquad (9.18) \\
V(\phi, \tilde{L}, \tilde{E}) &= V_L(\phi, \tilde{L}_i) + V_R(\phi, \tilde{E}) + \lambda_{LR}(\tilde{L}_i^\dagger \tilde{L}_i)(\tilde{E}_i^\dagger \tilde{E}_i) \\
&\quad + (A m_i \tilde{E}_i \tilde{L}_i^\dagger \phi + h.c.) \qquad (9.19) \\
\mathcal{L}_{\rm DM} &= \frac{1}{2}\bar{\chi}\left(i\partial\!\!\!/ - m_\chi\right)\chi - (y_L \bar{\chi}\tilde{L}_i L_i + y_R \bar{\chi}\tilde{E}_i E_i + h.c)\,, \qquad (9.20)
\end{aligned}$$

where, 'A' is a dimensionless parameter contributing to the trilinear scalar coupling, m_i is the mass of the SM leptons (e, μ, τ), and the other parameters are the same as in Sec. 9.1. After the electroweak symmetry breaking, the 'A' term cause the mixing between the two mediators ($\tilde{\ell}_{iL}, \tilde{\ell}_{iR}$), ($\tilde{\ell}_i = \tilde{e}, \tilde{\mu}, \tilde{\tau}$). From the condition that the diagonalized mass of the mediators must be positive,

$$\left|\frac{A\, v\, m_\tau}{\sqrt{2}}\right| < m_{\tilde{\tau}_L} m_{\tilde{\tau}_R}. \qquad (9.21)$$

When $y_L/m_{\tilde{L}} \gg y_R/m_{\tilde{R}}$ or $y_L/m_{\tilde{L}} \ll y_R/m_{\tilde{R}}$ is satisfied, this combined model is nothing but the left- or right-mediator model, respectively, because the other mediator decouples from low energy physics. Even in the case where $y_L/m_{\tilde{L}} \simeq y_R/m_{\tilde{R}}$ is satisfied, we can conclude that the effect to left or right-mediator model is limited. This is explained as follows. We can roughly estimate $\langle\sigma v\rangle \propto 2(y_L/m_{\tilde{L}})^4 + (y_R/m_{\tilde{R}})^4$, and the deviation from the left or right-mediator model is maximized when $2(y_L/m_{\tilde{L}})^4 \simeq (y_R/m_{\tilde{R}})^4$ is satisfied. It means $y_L/m_{\tilde{L}}$ or $Y_R/m_{\tilde{R}}$ can be maximally 15% less than that of the left or right-mediator model.

Important motivation for going beyond the minimal single mediator models to the combined one is the explanation of the anomalous muon magnetic moment as addressed below. There is a long-standing discrepancy in the theoretical and experimental results of the $(g-2)_\mu$ that hints towards some new physics effect to the SM calculation. Currently, the discrepancy from the SM prediction is given by $\Delta a_\mu \equiv a_\mu^{\rm exp} - a_\mu^{\rm SM} = 261(63)(48) \times 10^{-11}$ [26], where the first error is from experiment, and the second is from theory. This difference is already at 3.3 σ level with a possible indication of new physics. If the discrepancy persists in the future experimental results which are currently being explored at the Fermilab and J-PARC, this will be a smoking-gun signature of the EW new physics.

The Leptophilic DM and the mediator couple to the SM leptons directly inducing the anomalous magnetic moment to them. The contribution from the Leptophilic DM with a single mediator comes from the diagrams shown in the upper panel of Fig. 9.7 (a) and (b). These can be calculated as follows [103]:

$$\begin{aligned}
\Delta a_\mu^{\rm L/R} &= -\frac{Y_{L/R}^2}{16\pi^2}\frac{m_\mu^2}{m_{\tilde{\mu}_{L/R}}^2} f(r) = -65 \times 10^{-11} \times Y_{L/R}^2 \left(\frac{90{\rm GeV}}{m_{\tilde{\mu}_{L/R}}}\right)^2 f(r), \\
f(r) &= \frac{1 - 6r + 3r^2 + 2r^3 - 6r^2 \log r}{6(1-r)^4}, \qquad (9.22)
\end{aligned}$$

where $r \equiv m_\chi^2/m_{\tilde{\mu}_{L/R}}^2$ and the function $f(r)$ takes a value in between zero and one when $0 < r < 1$. This, however, always gives a negative contribution to Δa_μ and thus it is difficult to explain the muon $(g-2)$ anomaly from the models.

On the other hand, the combined model involving both the mediators yields an additional contribution to Δa_μ through diagrams in Fig. 9.7 (c) and (d). By using the mass insertion approximation, these contribution is given by [104],

$$\begin{aligned} \Delta a_\mu^{\rm L+R} &= -\frac{Y_L Y_R A}{16\pi^2}\frac{v\, m_\chi m_\mu^2}{\sqrt{2} m_{\tilde{\mu}_L}^2 m_{\tilde{\mu}_R}^2} f(x,y), \qquad (9.23) \\ f(x,y) &= xy\left[\frac{-3+x+y+xy}{(x-1)^2(y-1)^2} + \frac{2x\log x}{(x-y)(x-1)^3} - \frac{2y\log y}{(x-y)(y-1)^3}\right], \end{aligned}$$

where $x \equiv m_{\tilde{\mu}_L}^2/m_\chi^2$ and $y \equiv m_{\tilde{\mu}_R}^2/m_\chi^2$. The function $f(x,y)$ takes a value in between zero and one when $1 < x, y$. $\Delta a_\mu^{\rm L+R}$ can be either positive or negative, and be much larger than those in the previous one in eq. (9.22) thanks to the existence of the 'A' term. We show the value of the parameter required to explain the present muon $(g-2)$ anomaly in Fig. 9.8. Here, we assume the relation $y_L/3 = y_R$ and $m_{\tilde{e}_L} = m_{\tilde{e}_R}$ (top panel) or $y_L = y_R/3$ and again $m_{\tilde{e}_L} = m_{\tilde{e}_R}$ (bottom panel). For the former case, considering that the contribution of the right mediator to the DM annihilation is limited, and thus we plot the contour of 'A' on the plot of the top panel in Fig. 9.4 (top panel). For the latter case, we plot the contour on the plot of the bottom panel of the same figure. We have confirmed numerically that if 'A' is $\mathcal{O}(10)$, the vacuum is always stable, and importantly such a region is in the reach of the ILC experiment.

9.5 Summary of the Leptophilic WIMP

Minimal and renormalizable models for a singlet Majorana fermion WIMP that interacts only with the SM leptons via the scalar mediator(s) have been considered. We have performed an extensive analysis taking all robust theoretical and present experimental constraints into account to show the feasibility of the models. To start with, we have considered two distinct models; each has one type of the single scalar mediator: one is a doublet and the other one is a singlet under the $\mathrm{SU}(2)_L$ symmetry of the SM. Our choice of a Majorana fermion WIMP makes it necessary for the mediators to carry the exact same quantum numbers as their SM lepton partners. We have considered the degenerate flavor-blind scenario for the sake of simplicity, so that a single mass and coupling parameters will define those of all the three generations of the scalar mediator.

The most important constraint comes from the relic abundance of the WIMP. We figure out the allowed parameter space at 95% C.L. to the experimental limit, including an additional theoretical uncertainty that comes from the SM thermodynamics in the early universe. The relic abundance constraint was further accompanied by a theoretical one, such as the vacuum stability, and electroweak precision data, the Higgs precision data, and all relevant direct search

limits from the LEP and LHC run-II experiments. Our analysis show that at the large WIMP mass only coannihilation mechanism with the mediator particle can survive the relic abundance constraint and the largest allowed mass for the WIMP and the mediator can be around 1.5 TeV. We have also showed that the direct search limit on the scalar mediators only discard a part of the parameter space that contributes to the relic abundance via the self-annihilation region for the WIMP mass below 300 GeV and WIMP-mediator mass gap above 80 GeV.

As a next step, we have discussed the possibility of probing the unexplored parameter region at future colliders, specifically at the ILC experiment. We have done a signal-background analysis for the mono-photon search at the ILC experiment, and showed that the ILC-250 GeV can indeed pin-down the WIMP mass around 110 GeV with almost degenerate WIMP-mediator mass. For the degenerate case, we have also included the pair production of the scalar mediators as well that will contribute non-negligibly to the mono-photon signal.

We have also considered the combined model scenario where both the doublet and the singlet scalar mediators contribute to the relic abundance of the WIMP. Introduction of a third degree of freedom to the WIMP co-annihilation decreases the largest allowed mass of the WIMP down to 1.2 TeV. In the light of the anomalous magnetic moment of the muon, this combined model should be considered as the minimal scenario. Since, without the presence of both the mediator particles, it is impossible to explain the present discrepancy on the muon $(g-2)$. We have shown that we have ample parameter space that can simultaneously explain both the relic abundance of the WIMP and the muon $(g-2)$ anomaly. Moreover, we have repeated the ILC mono-photon analysis for the combined model as well, and found that the ILC-250 will be able to probe the aforementioned parameter space favored by the relic abundance and the muon $(g-2)$ data. If the muon anomaly persists in the future experimental data, then the ILC experiment may confirm or discard the model hypothesis.

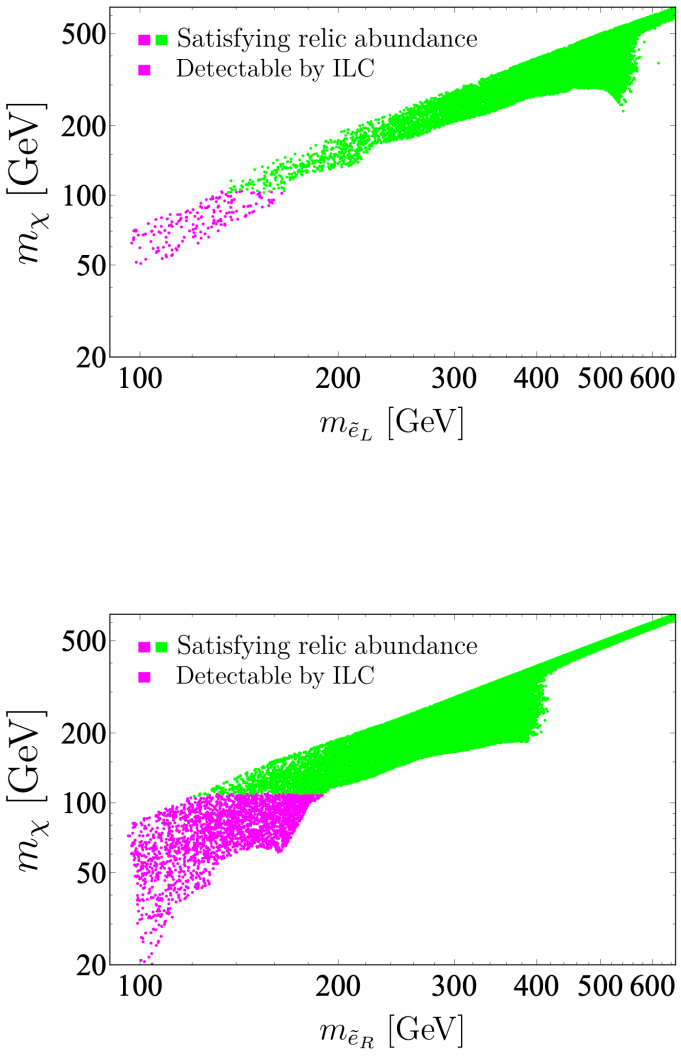

Figure 9.6: *The region spread by points are the presently surviving parameter space at 95 % C.L., the same as the one spread by green points in Fig. 9.4 for the left (top panel) and right (bottom panel) mediator models, respectively. The region spread by magenta points is the 95% C.L expected reach at the 250 GeV ILC experiment with 500 fb^{-1} luminosity by the mono-photon search assuming 0.1 % systematic uncertainty.*

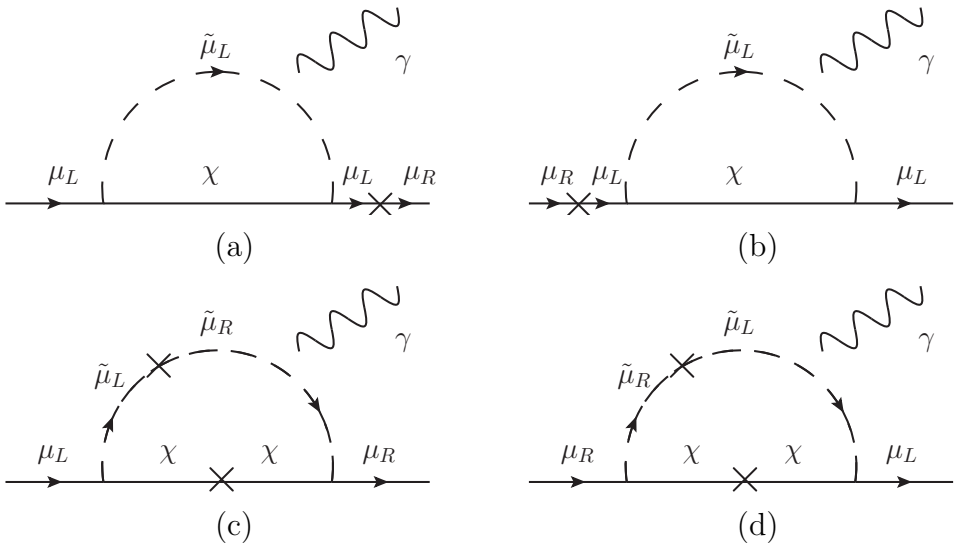

Figure 9.7: *Diagrams (a) and (b) contribute to the muon $(g-2)$ for the left-mediator model. Similar diagrams for the right-mediator model can be found by swapping L by R. Diagrams (c) and (d) contribute to the muon $(g-2)$ for the combined model.*

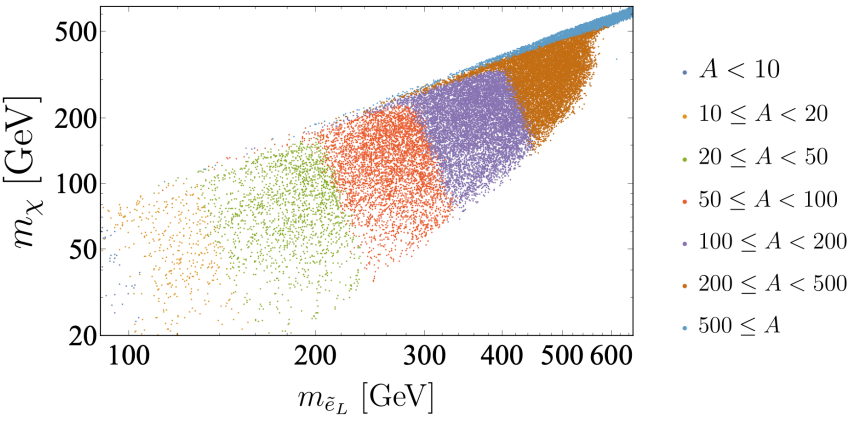

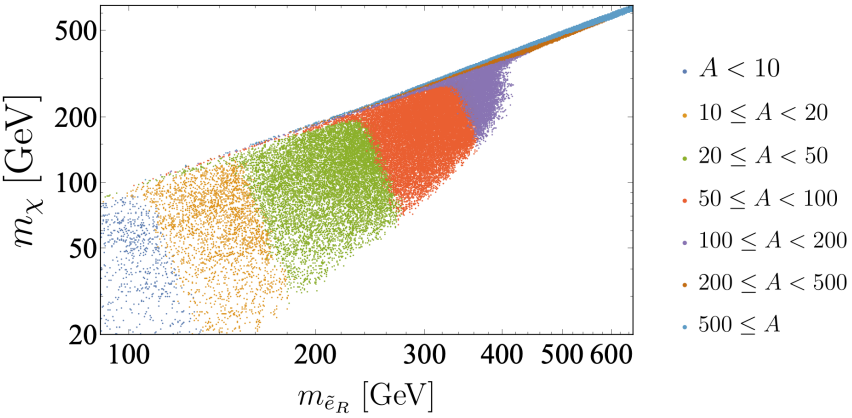

Figure 9.8: *The contour of the 'A' parameter required to explain the present muon* $(g-2)$ *anomaly assuming* $y_L/3 = y_R$ *and* $m_{\tilde{e}_L} = m_{\tilde{e}_R}$ *(top panel), or that assuming a differential coupling relation* $y_L = y_R/3$ *but the same mass relation* $m_{\tilde{e}_L} = m_{\tilde{e}_R}$.

Chapter 10

Conclusion

The existence of DM has been confirmed by various astrophysical observations, and physicist have been making large effort to search the identity of DM. WIMP is one of the best DM candidates, and it assures some interaction with SM particles from the assumption that WIMP was in thermal equilibrium with SM particles at the early universe. We can utilize this interaction to detect WIMP at indirect detection experiments, direct detection experiments, and collider experiments. Today we are in the situation where we cannot detect any signal of new physics beyond SM, and we analyzed WIMP by model independent way.

When considering WIMPs model independently, it is effective to classify WIMPs by its gauge representaion of SM, and we focused SM gauge singlet WIMP. Such WIMP cannot have renormalizable interaction with SM particles and we need to introduce mediator particles which connect WIMP and SM particles. If mediators are heavy enough compared to WIMP mass and electroweak scale, we can integrate out mediator fields and get effective Lagrangian which only contain WIMP and SM particles. There are unexplored region remaining for CP conserving effective operators, these are H-funnel region, Z-funnel region and Leptophilic region. It is difficult to search these regions by LHC experiments or direct detection experiments, we discussed about future prospect for these regions.

At Chapter 8, we have presented the expected sensitivity of the Z-portal WIMP at the future lepton colliders. We have adopted the effective operator method where the interaction between the singlet Majorana WIMP (χ) and the Z boson is mediated via the dimension-six operator $(\bar{\chi}\gamma_\mu\gamma_5\chi)(H^\dagger iD^\mu H)/2+h.c.$ The final result of our analysis is parametrized by only two parameters, the WIMP mass (m_χ) and the effective WIMP-Z coupling ($g_{\chi\chi Z}$). We discussed the possibility of probing the Z-funnel WIMP mass region (35-55 GeV) using the mono-photon plus missing energy signal at the future lepton colliders. We have done a comprehensive signal-background analysis of the mono-photon searches considering various collider features, such as beam polarization, beam breamsstrahlung, initial-state-radiation and detector effects. While doing this analysis we have considered other important constraints on the parameters of this scenario coming from the mono-photon searches, Z-invisible width obtained from the LEP data. This limit is combined with the ones obtained from the

Z-invisible width measurement, direct detection, and relic abundance of the WIMP. We have done a realistic estimation including the systematic uncertainties for the ILC beam. To do so, we estimate the $\Delta\chi^2$ with 0.1 % and 1 % systematic uncertainties. The collective 90 % C.L. bound for all the cases for a 250 GeV ILC beam with 0.1 % and 1 % systematic uncertainties has also been presented.

At chapter 9, we also presented the expected sensitivity of Leptophilic WIMP at future lepton colliders. We assumed specific mediators, namely Z_2 odd scalar mediators which couple to WIMP and SM leptons. There are two different type of mediators: left mediators which couple to WIMP and left-handed leptons, and right mediators which couple to WIMP and right-handed leptons. Here we introduced three generations of mediators for left and right mediators, and we imposed lepton flavor universality on the operators.

There are several parameters, which are couplings of the operators, WIMP mass (m_χ), left mediator mass ($m_{\tilde{e}_L}$) and right mediator mass ($m_{\tilde{e}_R}$). We scanned the parameter region where the perturbativity holds, by considering relic abundance condition and collider experiments. The results are shown in (m_χ,$m_{\tilde{e}_L}$)-plane for left mediator case, and (m_χ,$m_{\tilde{e}_R}$)-plane for right mediator case. There is lower limit and upper limit on WIMP mass from the condition that WIMP gives correct DM abundance observed today, and we found that the bulk region lies on $m_\chi < 500$ GeV and $m_{\tilde{e}_L} < 600$ GeV for left mediator case, and $m_\chi < 400$ GeV and $m_{\tilde{e}_R} < 400$ GeV for right mediator case. When $m_\chi \simeq m_{\tilde{e}_L}$ or $m_\chi \simeq m_{\tilde{e}_R}$ is satisfied, so-called co-annihilation mechanism works, and even higher mass region can explain current DM abundance.

The mediators has been searched in the context of slepton search at LEP or LHC experiments through pair production of sleptons via Drell-Yan process. LHC experiments put constraints on the large area of bulk region, but when WIMP and mediator particle have similar mass, it becomes difficult to search mediator particles. For the lepton colliders, WIMP directly couple with electron and positron, and we can search these WIMPs more effectively. We revealed that WIMP with $m_\chi < 110$GeV can be searched by 250 GeV ILC using mono-photon plus missing energy process.

We also analyzed Leptophilic WIMP introducing left and right mediator simultaneously, and in this case WIMP and mediators cause anomalous muon magnetic moment $(g-2)$ because of the existence of 'A' term. Recent studies report anomaly in muon $(g-2)$ and we find that for the most of bulk region can explain this anomaly with proper 'A' term. Importantly, we have shown that there are detectable parameter regions by ILC which can also explain muon $(g-2)$ anomaly.

Appendix A

Standard Model

A.1 SM contents

SM is a chiral gauge theory under $SU(3)_C \times SU(2)_L \times U(1)_Y$. It contains three generations of chiral fermions, three gauge bosons which mediate gauge interactions, and Higgs boson which generate the mass of SM felmions and $SU(2)_L$ gauge bosons. Left-handed charged lepton (e.g. electron) and neutrinos form the $SU(2)_L$ doublet and left-handed up-type quark and left-handed down-type quark form $SU(2)_L$ doublet. On the other hand right-handed fermions are $SU(2)_L$ singlets. $SU(3)_C$ interaction governs strong interaction, and all quarks are $SU(3)_C$ triplet. Electric charge is defined as $Q = Y + T^3$ where Y is the charge of $U(1)_Y$ interaction and T^3 is the isospin of $SU(2)_L$ interaction. We show the table of SM particles on Table A.1. Here, subscript L/R denote left/right-handed fermions and i denotes the flavor of fermions. W^a_μ is $SU(2)_L$ gauge bosons and a spans 1,2 and 3. W^1_μ and W^2_μ form charge eigenstates as follows:

$$W^\pm_\mu = \frac{1}{\sqrt{2}}(W^1_\mu \mp iW^2_\mu)\,. \tag{A.1}$$

The fields of photon and Z-boson can be written in the linear combination of B_μ and W^3_μ as

$$A_\mu = W^3_\mu \sin\theta_W + B_\mu \cos\theta_W \tag{A.2}$$
$$Z_\mu = W^3_\mu \cos\theta_W - B_\mu \sin\theta_W\,, \tag{A.3}$$

where θ_W is Weinberg angle which follows the equation:

$$e = g\,\sin\theta_W = g'\,\cos\theta_W = \frac{gg'}{\sqrt{g^2 + g'^2}}\,, \tag{A.4}$$

where e is electromagnetic coupling, g is $SU(2)_L$ coupling and g' is $U(1)_Y$ coupling.

Particle	Spin	$SU(3)_c$	$SU(2)_L$	$U(1)_Y$	Q
$L_i = \begin{pmatrix} \nu_i \\ e_{iL} \end{pmatrix}$	1/2	**1**	**2**	$-1/2$	$\begin{pmatrix} 0 \\ -1 \end{pmatrix}$
$E_i = e_{iR}$	1/2	**1**	**2**	-1	-1
$Q_i = \begin{pmatrix} u_{iL} \\ d_{iL} \end{pmatrix}$	1/2	**3**	**2**	1/6	$\begin{pmatrix} 2/3 \\ -1/3 \end{pmatrix}$
$U_i = u_{iR}$	1/2	**3**	**1**	2/3	2/3
$D_i = d_{iR}$	1/2	**3**	**1**	$-1/3$	$-1/3$
B_μ	1	**1**	**1**	0	0
W^a_μ	1	**1**	**3**	0	$(-1, 0, +1)$
G_μ	1	**8**	**1**	0	0
$H = \begin{pmatrix} H^+ \\ H^0 \end{pmatrix}$	0	**1**	**2**	1/2	$\begin{pmatrix} 1 \\ 0 \end{pmatrix}$

Table A.1: Particle contents of the SM

A.2 Electroweak symmetry breaking

The Lagrangian of Higgs sector can be written as

$$\mathcal{L}_H = |D_\mu H|^2 - V(H)\,, \tag{A.5}$$

where $D_\mu \equiv \partial_\mu + ig(1/2)\sigma_a W^a_\mu + ig'(1/2)B_\mu$ is covariant derivative, and $V(H)$ is the potential term, which is

$$V(H) \;=\; \mu^2|H|^2 + \lambda|H|^4\,. \tag{A.6}$$

If $\mu^2 < 0$, the global minimum point shift from $|H| = 0$. Then the Higgs field gain vacuum expectation value (VEV), such as

$$\langle H \rangle = \sqrt{\frac{-\mu^2}{2\lambda}} \equiv \frac{v}{\sqrt{2}}\,. \tag{A.7}$$

Taking unitary gauge, the Higgs field can be written as

$$H = \frac{1}{\sqrt{2}} \begin{pmatrix} 0 \\ v + h \end{pmatrix}\,, \tag{A.8}$$

where h is physical Higgs field. Then $SU(2)_L$ and $U(1)_Y$ gauge bosons gain the mass term from the kinetic term of Higgs field, as follows:

$$\begin{aligned} |D_\mu H|^2 \;&\supset\; \left| \left(\partial_\mu + \frac{i}{2} g \sigma_a W^a_\mu + \frac{i}{2} g' B_\mu \right) \frac{1}{\sqrt{2}} \begin{pmatrix} 0 \\ v \end{pmatrix} \right| \\ &=\; \frac{v^2}{8} \left| \begin{pmatrix} g W^1_\mu - i g W^2_\mu \\ -g W^3_\mu + g' B_\mu \end{pmatrix} \right|^2 \\ &=\; \frac{v^2}{8} [g^2 (W^1_\mu)^2 + g^2 (W^2_\mu)^2 + (g W^3_\mu - g' B_\mu)^2] \qquad \text{(A.9)} \\ &=\; m_W^2 W^+ W^- + \frac{m_Z^2}{2} Z_\mu Z^\mu\,, \qquad \text{(A.10)} \end{aligned}$$

where

$$m_W = \frac{gv}{2} \tag{A.11}$$

$$m_Z = \frac{\sqrt{g^2+g'^2}v}{2}\,. \tag{A.12}$$

As we can see from this derivation, photon field A_μ does not gain the mass from Higgs VEV and stays mass less. SM fermions gain their mass from Yukawa couplings with Higgs field, and these are follows

$$\mathcal{L}_{\text{Yukawa}} = \Gamma^u_{ij}\bar{Q}_i H^c U_j + \Gamma^d_{ij}\bar{Q}_i H D_j + \Gamma^e_{ij}\bar{L}_i H E_j + h.c.\,, \tag{A.13}$$

where $H^c \equiv i\sigma_2 H^*$ is charge conjugation of Higgs field, Γ denote each Yukawa coupling and subscript (i, j) means generations of fermion.

Appendix B

Majorana fermion

We can define 4 components Majorana fermion as

$$\psi = \begin{pmatrix} -i\sigma_2\eta^* \\ \eta \end{pmatrix} \tag{B.1}$$

where η is left handed weyl fermion. For Majorana fermion, following equation is satisfied:

$$\psi = \psi^c \equiv C\bar{\psi}^T\,, \tag{B.2}$$

where subscript c means charge conjugation, and $C \equiv i\gamma^2\gamma^0$ is charge conjugation matrix. C satisfies following equations:

$$C = -C^{-1} = -C^\dagger \tag{B.3}$$
$$C^{-1}\gamma^\mu C = -\gamma^{\mu T} \tag{B.4}$$

We can show vector current vanish for Majorana fermion as following:

$$\begin{aligned}
\bar{\psi}\gamma^\mu\psi &= \bar{\psi}^c\gamma^\mu\psi^c && \text{(B.5)}\\
&= \psi^T\gamma^0C^\dagger\gamma^0\gamma^\mu C\gamma^0\psi^* && \text{(B.6)}\\
&= -\left[\psi^T\gamma^0C^\dagger\gamma^0\gamma^\mu C\gamma^0\psi^*\right]^T && \text{(B.7)}\\
&= \bar{\psi}C^T\gamma^{\mu T}C\psi && \text{(B.8)}\\
&= -\bar{\psi}\gamma^\mu\psi && \text{(B.9)}\\
&= 0 && \text{(B.10)}
\end{aligned}$$

We can also show tensor current vanish for Majorana fermion as following:

$$\begin{aligned}
\bar{\psi}\sigma^{\mu\nu}\psi &= \bar{\psi}^c\sigma^{\mu\nu}\psi^c && \text{(B.11)}\\
&= \psi^T\gamma^0C^\dagger\gamma^0\sigma^{\mu\nu}C\gamma^0\psi^* && \text{(B.12)}\\
&= -\left[\psi^T\gamma^0C^\dagger\gamma^0\sigma^{\mu\nu}C\gamma^0\psi^*\right]^T && \text{(B.13)}\\
&= -\bar{\psi}C^T\sigma^{T\mu\nu}C\psi && \text{(B.14)}\\
&= -\bar{\psi}\sigma^{\mu\nu}\psi && \text{(B.15)}\\
&= 0 && \text{(B.16)}
\end{aligned}$$

where

$$\sigma^{T\mu\nu} \equiv \frac{i}{2}[\gamma^{\mu T}, \gamma^{\nu T}]\,. \tag{B.17}$$

We will show that neutral dirac fermion is equivalent to two Majorana fermions next. Suppose dirac fermion feild as ψ_D, then the Lagrangian can be written as

$$\mathcal{L} \;=\; \overline{\psi_D}(i\partial\!\!\!/ - m)\psi_D\,. \tag{B.18}$$

We can difine two Majorana fields as

$$\psi_1 = \frac{\psi_D + \psi_D^c}{\sqrt{2}} \tag{B.19}$$

$$\psi_2 = i\frac{\psi_D - \psi_D^c}{\sqrt{2}} \tag{B.20}$$

and they satisfy Majorana conditions

$$\psi_1 \;=\; \psi_1^c \tag{B.21}$$

$$\psi_2 \;=\; \psi_2^c \tag{B.22}$$

Then the Lagrangian can be written as

$$\mathcal{L} \;=\; \overline{\psi_D}(i\partial\!\!\!/ - m)\psi_D \tag{B.23}$$

$$\;=\; \frac{1}{2}\overline{\psi_D}(i\partial\!\!\!/ - m)\psi_D + \frac{1}{2}\overline{\psi_D^c}(i\partial\!\!\!/ - m)\psi_D^c \tag{B.24}$$

$$\;=\; \frac{1}{2}\overline{\psi_1}(i\partial\!\!\!/ - m)\psi_1 + \frac{1}{2}\overline{\psi_2}(i\partial\!\!\!/ - m)\psi_2 \tag{B.25}$$

Appendix C

Co-annihilation

There are some exception cases that standard calculation of relic abundance (c.f. Chapter 4) fails. One case is called co-annihilation, and it happens when the DM mass and mediator mass are nearly degenerated. Let us denote mediator particles as $\chi_{1,\cdots N}$ and DM as χ_0, and mass of WIMP as m_0 and mass of mediators as $m_{1,\cdots N}$. If the mass difference, $\delta m = m_{i>0} - m_0$ is large compared to freeze out temperature, mediator particles are not in thermal bath and play no significant role. However if δm is similar to freeze out temperature, mediators also appear in the thermal bath and other channel become important.

For standard calculation, the annihilation process of DM ($\chi_0\chi_0 \leftrightarrow XX$) determine the freeze out temperature, where X is any SM particle. If mediators are in thermal bath, following processes also happen:

$$\chi_i\chi_j \leftrightarrow XX \tag{C.1}$$
$$\chi_i X \leftrightarrow \chi_j X \tag{C.2}$$
$$\chi_i \leftrightarrow \chi_j XX\,, \tag{C.3}$$

where we also assume that mediator particles and WIMP are Z_2 odd under Z_2 symmetry. After the freeze out, these mediators decay into χ_0 and SM particles, and we can effectively consider these mediators as DM. The Boltzmann equation for DM and mediators can be written as [86]

$$\begin{aligned}\frac{dn_i}{dt} = -3Hn_i \;-\; &\sum_{j,X}[\langle\sigma_{ij}v\rangle(n_in_j - n_i^{eq}n_j^{eq}) \\ &-(\langle\sigma'_{ij}v\rangle n_in_X - \langle\sigma'_{ji}v\rangle n_in_X) \\ &-\Gamma_{ij}(n_i - n_i^{eq})]\,,\end{aligned} \tag{C.4}$$

where the cross sections are defined as

$$\sigma_{ij} = \sigma(\chi_i\chi_j \to XX) \tag{C.5}$$
$$\sigma'_{ij} = \sigma(\chi_iX \to \chi_jX) \tag{C.6}$$
$$\Gamma_{ij} = \sigma(\chi_i \to \chi_jXX)\,. \tag{C.7}$$

The current relic abundance is determined by the summation of n_i, because

mediators finally decay into DM. The effective Boltzmann equation can be obtained by taking summation of eq.(C.4)

$$\frac{dn}{dt} = -3Hn - \sum_{i,j=0} \langle \sigma_{ij} v \rangle (n_i n_j - n_i^{eq} n_j^{eq}) \tag{C.8}$$

where n is defined as

$$n \equiv \sum_i n_i \,. \tag{C.9}$$

For the Leptophilic WIMP case, WIMP and mediators are Z_2 odd particles, and if there masses are similar, they cause co-annihilation. In that case, there are additional annihilation process as we have shown in Fig.9.1, and DM can achieve observed relic abundance even with small couplings.

References

[1] Giorgio Arcadi, Abdelhak Djouadi, and Martti Raidal. Dark Matter through the Higgs portal. 2019.

[2] Serguei Chatrchyan et al. Observation of a New Boson at a Mass of 125 GeV with the CMS Experiment at the LHC. *Phys. Lett. B*, 716:30–61, 2012.

[3] Georges Aad et al. Observation of a new particle in the search for the Standard Model Higgs boson with the ATLAS detector at the LHC. *Phys. Lett. B*, 716:1–29, 2012.

[4] N. Aghanim et al. Planck 2018 results. VI. Cosmological parameters. *Astron. Astrophys.*, 641:A6, 2020.

[5] Stephen P. Martin. A Supersymmetry primer. *Adv. Ser. Direct. High Energy Phys.*, 21:1–153, 2010.

[6] Gerard Jungman, Marc Kamionkowski, and Kim Griest. Supersymmetric dark matter. *Phys. Rept.*, 267:195–373, 1996.

[7] Jonathan L. Feng, Konstantin T. Matchev, and Takeo Moroi. Focus points and naturalness in supersymmetry. *Phys. Rev. D*, 61:075005, 2000.

[8] The International Linear Collider Technical Design Report - Volume 1: Executive Summary. 6 2013.

[9] A Multi-TeV Linear Collider Based on CLIC Technology: CLIC Conceptual Design Report. 10 2012.

[10] CEPC Conceptual Design Report: Volume 1 - Accelerator. 9 2018.

[11] Geraldine Servant and Timothy M.P. Tait. Is the lightest Kaluza-Klein particle a viable dark matter candidate? *Nucl. Phys. B*, 650:391–419, 2003.

[12] Andreas Birkedal, Andrew Noble, Maxim Perelstein, and Andrew Spray. Little Higgs dark matter. *Phys. Rev. D*, 74:035002, 2006.

[13] Shigeki Matsumoto, Satyanarayan Mukhopadhyay, and Yue-Lin Sming Tsai. Effective Theory of WIMP Dark Matter supplemented by Simplified Models: Singlet-like Majorana fermion case. *Phys. Rev. D*, 94(6):065034, 2016.

[14] Gianfranco Bertone and Dan Hooper. History of dark matter. *Rev. Mod. Phys.*, 90(4):045002, 2018.

[15] Katherine Freese. Review of Observational Evidence for Dark Matter in the Universe and in upcoming searches for Dark Stars. *EAS Publ. Ser.*, 36:113–126, 2009.

[16] D. Walsh, R.F. Carswell, and R.J. Weymann. 0957 + 561 A, B - Twin quasistellar objects or gravitational lens. *Nature*, 279:381–384, 1979.

[17] Priyamvada Natarajan et al. Mapping substructure in the HST Frontier Fields cluster lenses and in cosmological simulations. *Mon. Not. Roy. Astron. Soc.*, 468(2):1962–1980, 2017.

[18] R.H. Dicke, P.J.E. Peebles, P.G. Roll, and D.T. Wilkinson. Cosmic Black-Body Radiation. *Astrophys. J.*, 142:414–419, 1965.

[19] George F. Smoot et al. Structure in the COBE differential microwave radiometer first year maps. *Astrophys. J. Lett.*, 396:L1–L5, 1992.

[20] G. Hinshaw et al. Nine-Year Wilkinson Microwave Anisotropy Probe (WMAP) Observations: Cosmological Parameter Results. *Astrophys. J. Suppl.*, 208:19, 2013.

[21] Volker Springel et al. Simulating the joint evolution of quasars, galaxies and their large-scale distribution. *Nature*, 435:629–636, 2005.

[22] Samuel D. McDermott, Hai-Bo Yu, and Kathryn M. Zurek. Turning off the Lights: How Dark is Dark Matter? *Phys. Rev. D*, 83:063509, 2011.

[23] H. Georgi and S.L. Glashow. Unity of All Elementary Particle Forces. *Phys. Rev. Lett.*, 32:438–441, 1974.

[24] Gianfranco Bertone, Dan Hooper, and Joseph Silk. Particle dark matter: Evidence, candidates and constraints. *Phys. Rept.*, 405:279–390, 2005.

[25] Edward W. Kolb and Michael S. Turner. *The Early Universe*, volume 69. 1990.

[26] P.A. Zyla et al. Review of Particle Physics. *PTEP*, 2020(8):083C01, 2020.

[27] Mariangela Lisanti. Lectures on Dark Matter Physics. In *Theoretical Advanced Study Institute in Elementary Particle Physics: New Frontiers in Fields and Strings*, pages 399–446, 2017.

[28] D.S. Akerib et al. Results from a search for dark matter in the complete LUX exposure. *Phys. Rev. Lett.*, 118(2):021303, 2017.

[29] E. Aprile et al. The XENON1T Dark Matter Experiment. *Eur. Phys. J. C*, 77(12):881, 2017.

[30] R. Bernabei et al. First results from DAMA/LIBRA and the combined results with DAMA/NaI. *Eur. Phys. J. C*, 56:333–355, 2008.

[31] E. Aprile et al. First Dark Matter Search Results from the XENON1T Experiment. *Phys. Rev. Lett.*, 119(18):181301, 2017.

[32] E. Aprile et al. Constraining the spin-dependent WIMP-nucleon cross sections with XENON1T. *Phys. Rev. Lett.*, 122(14):141301, 2019.

[33] Philip Bett, Vincent Eke, Carlos S. Frenk, Adrian Jenkins, John Helly, and Julio Navarro. The spin and shape of dark matter haloes in the Millennium simulation of a lambda-CDM universe. *Mon. Not. Roy. Astron. Soc.*, 376:215–232, 2007.

[34] Julio F. Navarro, Carlos S. Frenk, and Simon D.M. White. The Structure of cold dark matter halos. *Astrophys. J.*, 462:563–575, 1996.

[35] Toshiyuki Fukushige and Junichiro Makino. Structure of dark matter halos from hierarchical clustering. *Astrophys. J.*, 557:533, 2001.

[36] Jennifer M. Gaskins. A review of indirect searches for particle dark matter. *Contemp. Phys.*, 57(4):496–525, 2016.

[37] W.B. Atwood et al. The Large Area Telescope on the Fermi Gamma-ray Space Telescope Mission. *Astrophys. J.*, 697:1071–1102, 2009.

[38] F. Aharonian et al. The h.e.s.s. survey of the inner galaxy in very high-energy gamma-rays. *Astrophys. J.*, 636:777–797, 2006.

[39] M.G. Aartsen et al. Observation of High-Energy Astrophysical Neutrinos in Three Years of IceCube Data. *Phys. Rev. Lett.*, 113:101101, 2014.

[40] Oscar Adriani et al. An anomalous positron abundance in cosmic rays with energies 1.5-100 GeV. *Nature*, 458:607–609, 2009.

[41] M. Aguilar et al. First Result from the Alpha Magnetic Spectrometer on the International Space Station: Precision Measurement of the Positron Fraction in Primary Cosmic Rays of 0.5–350 GeV. *Phys. Rev. Lett.*, 110:141102, 2013.

[42] S. Schael et al. Precision electroweak measurements on the Z resonance. *Phys. Rept.*, 427:257–454, 2006.

[43] M. Tanabashi et al. Review of Particle Physics. *Phys. Rev. D*, 98(3):030001, 2018.

[44] Albert M Sirunyan et al. Combined measurements of Higgs boson couplings in proton–proton collisions at $\sqrt{s} = 13\,\text{TeV}$. *Eur. Phys. J. C*, 79(5):421, 2019.

[45] C. Boehm, T. A. Ensslin, and J. Silk. Can Annihilating dark matter be lighter than a few GeVs? *J. Phys.*, G30:279–286, 2004.

[46] Celine Boehm, Dan Hooper, Joseph Silk, Michel Casse, and Jacques Paul. MeV dark matter: Has it been detected? *Phys. Rev. Lett.*, 92:101301, 2004.

[47] Kim Griest and Marc Kamionkowski. Unitarity Limits on the Mass and Radius of Dark Matter Particles. *Phys. Rev. Lett.*, 64:615, 1990.

[48] K. Hamaguchi, S. Shirai, and T. T. Yanagida. Composite messenger baryon as a cold dark matter. *Phys. Lett.*, B654:110–112, 2007.
Koichi Hamaguchi, Eita Nakamura, Satoshi Shirai, and T. T. Yanagida. Decaying Dark Matter Baryons in a Composite Messenger Model. *Phys. Lett.*, B674:299–302, 2009.
Koichi Hamaguchi, Eita Nakamura, Satoshi Shirai, and Tsutomu T. Yanagida. Low-Scale Gauge Mediation and Composite Messenger Dark Matter. *JHEP*, 04:119, 2010.

[49] Hitoshi Murayama and Jing Shu. Topological Dark Matter. *Phys. Lett.*, B686:162–165, 2010.

[50] Thomas Hambye and Michel H. G. Tytgat. Confined hidden vector dark matter. *Phys. Lett.*, B683:39–41, 2010.

[51] Oleg Antipin, Michele Redi, and Alessandro Strumia. Dynamical generation of the weak and Dark Matter scales from strong interactions. *JHEP*, 01:157, 2015.

[52] Oleg Antipin, Michele Redi, Alessandro Strumia, and Elena Vigiani. Accidental Composite Dark Matter. *JHEP*, 07:039, 2015.

[53] Christian Gross, Andrea Mitridate, Michele Redi, Juri Smirnov, and Alessandro Strumia. Cosmological Abundance of Colored Relics. *Phys. Rev.*, D99(1):016024, 2019.

[54] Hajime Fukuda, Feng Luo, and Satoshi Shirai. How Heavy can Neutralino Dark Matter be? 2018.

[55] Jeremy Bernstein, Lowell S. Brown, and Gerald Feinberg. The Cosmological Heavy Neutrino Problem Revisited. *Phys. Rev.*, D32:3261, 1985.

[56] Mark Srednicki, Richard Watkins, and Keith A. Olive. Calculations of Relic Densities in the Early Universe. *Nucl. Phys.*, B310:693, 1988.

[57] Laura Lopez-Honorez, Thomas Schwetz, and Jure Zupan. Higgs portal, fermionic dark matter, and a Standard Model like Higgs at 125 GeV. *Phys. Lett. B*, 716:179–185, 2012.

[58] Michael A. Fedderke, Jing-Yuan Chen, Edward W. Kolb, and Lian-Tao Wang. The Fermionic Dark Matter Higgs Portal: an effective field theory approach. *JHEP*, 08:122, 2014.

[59] Jing-Yuan Chen, Edward W. Kolb, and Lian-Tao Wang. Dark matter coupling to electroweak gauge and Higgs bosons: an effective field theory approach. *Phys. Dark Univ.*, 2:200–218, 2013.

[60] Vardan Khachatryan et al. Constraints on the Higgs boson width from off-shell production and decay to Z-boson pairs. *Phys. Lett. B*, 736:64–85, 2014.

[61] Georges Aad et al. Constraints on the off-shell Higgs boson signal strength in the high-mass ZZ and WW final states with the ATLAS detector. *Eur. Phys. J. C*, 75(7):335, 2015.

[62] J. Aalbers et al. DARWIN: towards the ultimate dark matter detector. *JCAP*, 11:017, 2016.

[63] Giorgio Arcadi, Yann Mambrini, and Francois Richard. Z-portal dark matter. *JCAP*, 1503:018, 2015.

[64] Koichi Hamaguchi and Kazuya Ishikawa. Prospects for Higgs- and Z-resonant Neutralino Dark Matter. *Phys. Rev.*, D93(5):055009, 2016.

[65] Shigeki Matsumoto, Satyanarayan Mukhopadhyay, and Yue-Lin Sming Tsai. Singlet Majorana fermion dark matter: a comprehensive analysis in effective field theory. *JHEP*, 10:155, 2014.

[66] Clifford Cheung, Lawrence J. Hall, David Pinner, and Joshua T. Ruderman. Prospects and Blind Spots for Neutralino Dark Matter. *JHEP*, 05:100, 2013.

[67] Ken'ichi Saikawa and Satoshi Shirai. Primordial gravitational waves, precisely: The role of thermodynamics in the Standard Model. *JCAP*, 1805(05):035, 2018.

[68] A. Airapetian et al. Precise determination of the spin structure function g(1) of the proton, deuteron and neutron. *Phys. Rev.*, D75:012007, 2007.

[69] Geneviève Bélanger, Fawzi Boudjema, Andreas Goudelis, Alexander Pukhov, and Bryan Zaldivar. micrOMEGAs5.0 : Freeze-in. *Comput. Phys. Commun.*, 231:173–186, 2018.

[70] M. Ackermann et al. Searching for Dark Matter Annihilation from Milky Way Dwarf Spheroidal Galaxies with Six Years of Fermi Large Area Telescope Data. *Phys. Rev. Lett.*, 115(23):231301, 2015.

[71] Morad Aaboud et al. Search for dark matter at $\sqrt{s} = 13$ TeV in final states containing an energetic photon and large missing transverse momentum with the ATLAS detector. *Eur. Phys. J.*, C77(6):393, 2017.

[72] Morad Aaboud et al. Search for dark matter and other new phenomena in events with an energetic jet and large missing transverse momentum using the ATLAS detector. *JHEP*, 01:126, 2018.

[73] John Ellis, Andrew Fowlie, Luca Marzola, and Martti Raidal. Statistical Analyses of Higgs- and Z-Portal Dark Matter Models. *Phys. Rev.*, D97(11):115014, 2018.

[74] Christoph Bartels, Mikael Berggren, and Jenny List. Characterising WIMPs at a future e^+e^- Linear Collider. *Eur. Phys. J.*, C72:2213, 2012.

[75] E. A. Kuraev and Victor S. Fadin. On Radiative Corrections to e+ e- Single Photon Annihilation at High-Energy. *Sov. J. Nucl. Phys.*, 41:466–472, 1985. [Yad. Fiz.41,733(1985)].

[76] J. Abdallah et al. Search for one large extra dimension with the DELPHI detector at LEP. *Eur. Phys. J.*, C60:17–23, 2009.

[77] Patrick J. Fox, Roni Harnik, Joachim Kopp, and Yuhsin Tsai. LEP Shines Light on Dark Matter. *Phys. Rev.*, D84:014028, 2011.

[78] C. Patrignani et al. Review of Particle Physics. *Chin. Phys.*, C40(10):100001, 2016.

[79] Marcela Carena, Andre de Gouvea, Ayres Freitas, and Michael Schmitt. Invisible Z boson decays at e+ e- colliders. *Phys. Rev.*, D68:113007, 2003.

[80] Pisin Chen and Kaoru Yokoya. Disruption Effects From the Interaction of Round e^+e^- Beams. *Phys. Rev.*, D38:987, 1988.

[81] Michael E. Peskin. Consistent Yokoya-Chen approximation to beamstrahlung. *SLAC-TN-04-032, LCC-0010*, 1999.

[82] Asesh K. Datta, Kyoungchul Kong, and Konstantin T. Matchev. The Impact of beamstrahlung on precision measurements at CLIC. *eConf*, C050318:0215, 2005.

[83] J. Erler, S. Heinemeyer, W. Hollik, G. Weiglein, and P. M. Zerwas. Physics impact of GigaZ. pages 1389–1402, 5 2000.

[84] D. S. Akerib et al. LUX-ZEPLIN (LZ) Conceptual Design Report. 9 2015.

[85] E. Aprile et al. Projected WIMP sensitivity of the XENONnT dark matter experiment. *JCAP*, 11:031, 2020.

[86] Kim Griest and David Seckel. Three exceptions in the calculation of relic abundances. *Phys. Rev. D*, 43:3191–3203, 1991.

[87] Ken'ichi Saikawa and Satoshi Shirai. Precise WIMP Dark Matter Abundance and Standard Model Thermodynamics. *JCAP*, 08:011, 2020.

[88] Michael J. Baker and Andrea Thamm. Leptonic WIMP Coannihilation and the Current Dark Matter Search Strategy. *JHEP*, 10:187, 2018.

[89] LEPSUSYWG, ALEPH, DELPHI, L3 and OPAL experiments, note LEPSUSYWG/yy-nn.

[90] Particle Data Group 2020. Review of Particle Physics. *Progress of Theoretical and Experimental Physics*, 2020(8), 08 2020. 083C01.

[91] Georges Aad et al. Search for electroweak production of charginos and sleptons decaying into final states with two leptons and missing transverse momentum in $\sqrt{s} = 13$ TeV pp collisions using the ATLAS detector. *Eur. Phys. J. C*, 80(2):123, 2020.

[92] Georges Aad et al. Searches for electroweak production of supersymmetric particles with compressed mass spectra in $\sqrt{s} = 13$ TeV pp collisions with the ATLAS detector. *Phys. Rev. D*, 101(5):052005, 2020.

[93] John F. Gunion, Howard E. Haber, Gordon L. Kane, and Sally Dawson. *The Higgs Hunter's Guide*, volume 80. 2000.

[94] Abdelhak Djouadi. The Anatomy of electro-weak symmetry breaking. I: The Higgs boson in the standard model. *Phys. Rept.*, 457:1–216, 2008.

[95] Abdelhak Djouadi. The Anatomy of electro-weak symmetry breaking. II. The Higgs bosons in the minimal supersymmetric model. *Phys. Rept.*, 459:1–241, 2008.

[96] A.M. Sirunyan et al. Measurements of Higgs boson properties in the diphoton decay channel in proton-proton collisions at $\sqrt{s} = 13$ TeV. *JHEP*, 11:185, 2018.

[97] A. Djouadi, V. Driesen, W. Hollik, and Jose I. Illana. The Coupling of the lightest SUSY Higgs boson to two photons in the decoupling regime. *Eur. Phys. J. C*, 1:149–162, 1998.

[98] Hong-Jian He, Nir Polonsky, and Shu-fang Su. Extra families, Higgs spectrum and oblique corrections. *Phys. Rev. D*, 64:053004, 2001.

[99] W. Grimus, L. Lavoura, O.M. Ogreid, and P. Osland. A Precision constraint on multi-Higgs-doublet models. *J. Phys. G*, 35:075001, 2008.

[100] W. Grimus, L. Lavoura, O.M. Ogreid, and P. Osland. The Oblique parameters in multi-Higgs-doublet models. *Nucl. Phys. B*, 801:81–96, 2008.

[101] Riccardo Barbieri, Lawrence J. Hall, and Vyacheslav S. Rychkov. Improved naturalness with a heavy Higgs: An Alternative road to LHC physics. *Phys. Rev. D*, 74:015007, 2006.

[102] M. Cepeda et al. *Report from Working Group 2: Higgs Physics at the HL-LHC and HE-LHC*, volume 7, pages 221–584. 12 2019.

[103] Prateek Agrawal, Zackaria Chacko, and Christopher B. Verhaaren. Leptophilic Dark Matter and the Anomalous Magnetic Moment of the Muon. *JHEP*, 08:147, 2014.

[104] Takeo Moroi. The Muon anomalous magnetic dipole moment in the minimal supersymmetric standard model. *Phys. Rev. D*, 53:6565–6575, 1996. [Erratum: Phys.Rev.D 56, 4424 (1997)].